Title
Understanding the Basis of Hypoxia Induced Craniofacial Malformations in Chick Embryos

Author
Smith, Francis Joel

Publication Date
2012

Peer reviewed|Thesis/dissertation

Understanding the Basis of Hypoxia Induced Craniofacial Malformations in Chick Embryos

by

Francis Joel Smith

DISSERTATION

Submitted in partial satisfaction of the requirements for the degree of

DOCTOR OF PHILOSOPHY

in

Oral and Craniofacial Sciences

in the

GRADUATE DIVISION

of the

UNIVERSITY OF CALIFORNIA, SAN FRANCISCO

DEDICATION AND ACKNOWLEDGEMENTS

I would first like to dedicate this work to my dear mother, who (with Dad) adopted me when I was unwanted by my original parents and needed a home to grow up in with love. She, and the rest of my family, encouraged me to persevere in faith despite my adversities from living with craniofacial anomalies. I would also like to acknowledge the speech therapists who gave me the gift of speech, as well as the multitudinous surgeons and other medical specialists who reconstructed my face from practically nothing and provided me with hearing aids and other therapies I needed to lead a normal life. I would like to thank not only my family, but also my friends worldwide who have stood behind me and encouraged my perseverance to the end.

Secondly, I dedicate this work to all my mentors at King's College London and the University of California San Francisco (UCSF) for their willingness to take a chance with me and believe in me. The seed for my craniofacial research was planted when I learned of the work of Dr. Michael J. Dixon on Treacher Collins syndrome and met him in person several times. All of them have encouraged me in my pursuit of my career in craniofacial embryological research, and have seen my unique personal connection to my work. In the Department of Craniofacial Development at King's College London, Dr. Martyn Cobourne provided me with my first practical experience in craniofacial development research in his laboratory in the summer of 2006. Subsequently, Dr. Philippa ("Pip") Francis-West, also at King's, mentored and advised me in my BSc thesis project.

At UCSF, there are a number of mentors who need to be acknowledged. Dr. John S. Greenspan (a fellow King's alumnus), from the very beginning, has proven to be a great

all-round mentor and father figure. Dr. Dan Ramos believed in my ability to tackle demanding research projects and took me in as a student for my first rotation in his lab, and has been another avid fan of mine during my progress at UCSF. Being a rabid SF Giants baseball fan, he barely tolerated my St. Louis Cardinals preference, but we often enjoyed doing "scientific" business together at Giants ballgames. Dr. Rich Schneider also was a great laboratory mentor and teacher at the same time, and helped me develop my embryological techniques. He has been a valued advisor on my qualifying exam and dissertation committees. Other valued mentors on my dissertation committee have been Dr. Ophir Klein (for his craniofacial development expertise), Dr. Emin Maltepe (for his knowledge of cellular response to hypoxia), and Dr. Benedikt Hallgrimsson, of the University of Calgary, for his mentorship in the area of quantitative geometric morphometrics. Dr. Hallgrimsson saw the potential in me as a morphometrician, and graciously invited me to do a sabbatical with him for the whole of October 2010 in Calgary, and subsequently, offered me the postdoctoral fellowship in his laboratory at the conclusion of my UCSF studies. As the primary mentor for my dissertation research, Dr. Ralph Marcucio has encouraged me to think creatively and innovate independently as a researcher. In Dr. Marcucio's lab, there are two colleagues who need acknowledgement. Dr. Nathan Young capably assisted me in analyzing my morphometric data on chick embryos, and Dr. Diane Hu helped me with thorny technical issues in some of the experiments.

Francis Joel Smith

Understanding the Basis of Hypoxia Induced
Craniofacial Malformations in Chick Embryos

ABSTRACT

Craniofacial anomalies are disfiguring, debilitating birth defects that afflict a large portion of the world's population. These malformations can be caused by genetic and/or environmental factors, and one such factor, prenatal hypoxia, is of particular interest in our research on craniofacial dysmorphology. There is experimental and clinical evidence for a correlation between hypoxia and craniofacial malformations, however, the mechanisms underlying such defects are not yet understood. The goal of our research has been to understand the mechanisms whereby hypoxia causes abnormal craniofacial morphology in early embryonic development.

Chick embryos were incubated in either normoxic (21% O2) or hypoxic (7%-19% O2) conditions and collected on days 2-6 for morphological and cellular analyses. Embryos were photographed for morphological analyses, and facial shape variation was quantified via two-dimensional geometric morphometrics. 13-day embryos were cleared and stained for analysis of skeletal and cartilaginous development. Cell proliferation was assessed via BrdU staining, and apoptosis was assessed by whole-mount and section TUNEL and caspase 3 immunoassay. Embryos were examined for oxidative stress using a phospho-AMPK immunoassay.

In morphometric analyses of normal growth, older embryos (HH22-28) showed greater shape variation among embryos than younger embryos (HH16-21). All the embryos fell along a well-defined nonlinear curve of normal facial growth in relation to size, and displayed variation in relation to chronological age and discrete morphological stage. Within stages, older embryos displayed greater variation within stages than younger embryos. In studies of hypoxic embryos, their survival was reduced in a step-wise manner in comparison to normoxic control embryos. Hypoxic embryos showed a wide range of craniofacial anomalies, from mild asymmetry and eye defects to more severe frontonasal and cephalic anomalies. They also displayed delayed skull bone development, with some skeletal defects. Abnormal facial shape variation occurred in relation to centroid size and age among individuals in hypoxic groups versus the normoxic population. Hypoxia disrupted cell proliferation and caused apoptosis of neural crest progenitor cells. Hypoxic embryos also displayed increased metabolic stress response.

TABLE OF CONTENTS

DEDICATION AND ACKNOWLEDGEMENTS.....iii

ABSTRACT……..v

LIST OF FIGURES AND TABLES…….…xi

CHAPTER 1: INTRODUCTION…….1

1.1 EMBRYONIC CRANIOFACIAL DEVELOPMENT FROM NEURAL CREST…...1

1.2 CRANIOFACIAL ANOMALIES……...11

1.3 ETIOLOGY OF CRANIOFACIAL MALFORMATIONS……..14

1.4 CORRELATION OF HYPOXIA TO CRANIOFACIAL DEFECTS AND HOLOPROSENCEPHALY…….16

1.5 DELETERIOUS EFFECT OF HYPOXIA ON TISSUES……18

1.6 ADAPTATION OF CELLS TO HYPOXIA VIA HIF-1 PATHWAY…….18

1.7 HYPOXIA, HIF-1α, AND APOPTOSIS……..20

1.8 ELECTRON TRANSPORT CHAIN-DERIVED REACTIVE OXYGEN SPECIES DURING HYPOXIA……22

1.9 AMP KINASE……...24

CHAPTER 2: GOALS OF PROJECT…….31

2.1 MECHANISTIC LINK BETWEEN HYPOXIA AND CRANIOFACIAL MALFORMATIONS……31

2.2 HYPOTHESIS…….31

2.3 GOALS AND PROPOSED EXPERIMENTS……31

2.3.1 Aim 1: Link Between Cellular and Molecular Changes and Hypoxic Craniofacial Malformations.....31

2.3.1.1 Proposed Experiments Completed in Aim 1……..31

2.3.1.2 Additional Proposed but Unrealized Experiments in Aim 1……33

2.3.2 Aim 2: Relationship Between Cellular Response to Hypoxia and Malformations……34

2.3.2.1 Proposed Experiments Completed in Aim 2…….34

2.3.2.2 Additional Proposed but Unrealized Experiments in Aim 2……34

CHAPTER 3: MATERIALS & METHODS……..36

3.1 CHICK EMBRYOS……..36

3.1.1 Chronic Hypoxia……..36

3.1.2 Acute Hypoxia……..37

3.2 STATISTICAL ANALYSIS OF EMBRYONIC SURVIVAL……38

3.3 TREATMENT WITH ANTIOXIDANT……39

3.4 GROSS MORPHOLOGICAL ANALYSES……....40

3.5 ANALYSIS OF CRANIOFACIAL SKELETAL DEVELOPMENT……..40

3.6 GEOMETRIC MORPHOMETRICS……41

3.7 HISTOLOGICAL ANALYSIS……..41

3.8 ASSESSMENT OF CELL PROLIFERATION……41

3.9 ASSESSMENT OF APOPTOSIS……42

3.9.1 Whole-Mount TUNEL……42

3.9.2 Section TUNEL……42

3.9.3 Whole-Mount Syto12-GFP Assay……..43

3.9.4 Caspase 3 Assay……...43

3.10 ASSESSMENT OF AMP-ACTIVATED PROTEIN KINASE (pAMPK) EXPRESSION……44

3.11 ASSESSMENT OF HYPOXIA INDUCIBLE FACTOR-1α (HIF-1α) EXPRESSION……44

3.12 ASSESSMENT OF SONIC HEDGEHOG (*Shh*) EXPRESSION……..45

3.12.1 Embryos……45

3.12.2 *Shh* Antisense RNA Probe Synthesis……45

3.12.3 Whole-Mount *In Situ* Hybridization……45

CHAPTER 4: NORMAL FACIAL DEVELOPMENT IN THE CHICK EMBRYO.....47

4.1 SUMMARY……..47

4.2 BACKGROUND……...48

4.3 RESULTS……..49

4.3.1 Facial Shape Variation among Individuals……49

4.3.2 Normal Facial Growth Trajectory…….51

CHAPTER 5: HYPOXIC CRANIOFACIAL MALFORMATIONS IN CHICK EMBRYOS……..54

5.1 SUMMARY……..54

5.2 RESULTS……..55

5.2.1 Hypoxia Reduces Survival of Embryos……..55

5.2.2 Hypoxia Alters Craniofacial Morphology……56

5.2.3 Hypoxia Alters Craniofacial Skeletal Development……64

5.2.4 Hypoxia Leads to Abnormal Facial Shape Variation…….65

5.2.5 Cell Proliferation and Apoptosis in Hypoxic Embryos……..72

5.2.6 Metabolic Stress in Hypoxic Embryos……76

CHAPTER 6: DISCUSSION……78

6.1 NORMAL FACIAL DEVELOPMENT IN CHICK EMBRYOS FOLLOWS A CONTINUUM…….78

6.2 CRANIOFACIAL MALFORMATIONS……..80

6.2.1 Hypoxia Reduces Survival and Alters Craniofacial Morphology.....81

6.2.2 Hypoxia Delays Craniofacial Skeletal Development……..…83

6.2.3 Abnormal Facial Shape Variation and Developmental Delay in Hypoxic Embryos…….84

6.2.4 Hypoxia Increases Apoptosis and Reduces Cell Proliferation……86

6.2.5 Possible Cellular Oxidative Stress in Response to Hypoxia……87

6.2.6 Proposed Model of Hypoxic Effect on Craniofacial Morphogenesis…….90

CHAPTER 7: CLINICAL IMPLICATIONS AND FUTURE DIRECTIONS…….91

APPENDIX A: UNREALIZED EXPERIMENTS…….95

APPENDIX B: BACKGROUND AND MOTIVATION FOR MY RESEARCH…99

B.1 CONNECTION BETWEEN LIFE EXPERIENCE AND RESEARCH…….99

B.2 EDUCATIONAL AND RESEARCH BACKGROUND……....101

APPENDIX C: LABORATORY ROTATION PROJECTS……104

C.1 LABORATORY OF DAN RAMOS, OROFACIAL SCIENCES…….104

C.2 LABORATORY OF RICHARD SCHNEIDER, ORTHOPAEDIC SURGERY..107

C.3 LABORATORY OF BENEDIKT HALLGRIMSSON, UNIVERSITY OF CALGARY…….108

REFERENCES…….110

LIST OF FIGURES AND TABLES

CHAPTER 1: INTRODUCTION

FIGURE 1.1 Cranial neural crest origin and fate in chick embryos……6

FIGURE 1.2 Molecular induction of neural crest……..10

FIGURE 1.3 Treacher Collins syndrome……...12

FIGURE 1.4 Spectrum of craniofacial anomalies associated with holoprosencephaly….14

FIGURE 1.5 Holoprosencephalic malformations in an acardiac twin fetus……..17

FIGURE 1.6 Molecular adaptation to hypoxia……..19

FIGURE 1.7 Hypoxic regulation of cell death through HIF-1α.....21

FIGURE 1.8 Mitochondrial hypoxia sensing through the electron transport chain……..23

FIGURE 1.9 AMPK regulates cellular energy metabolism……..25

FIGURE 1.10 Target proteins and pathways regulated by AMPK……...27

CHAPTER 3: MATERIAL S & METHODS

FIGURE 3.1 Hypoxic incubator……37

CHAPTER 4: NORMAL FACIAL DEVELOPMENT IN THE CHICK EMBRYO

FIGURE 4.1 Principal components analysis (PCA)……..50

FIGURE 4.2 Canonical variates analysis (CVA)……..51

FIGURE 4.3 Normal growth trajectory…….52

FIGURE 4.4 Facial shape variation related to age……53

FIGURE 4.5 Facial shape variation within stages…….53

CHAPTER 5: HYPOXIC CRANIOFACIAL MALFORMATIONS IN CHICK EMBRYOS

TABLE 5.1 Hypoxia reduces embryonic survival…….56

FIGURE 5.1 Hypoxia creates abnormal craniofacial morphology (day 4)……...58

FIGURE 5.2 Hypoxia creates abnormal craniofacial morphology (day 6)……...59

FIGURE 5.3 The head, not the body, is vulnerable to hypoxia-induced malformations..60

FIGURE 5.4 Acute hypoxia (24 hour windows)……...61

FIGURE 5.5 Acute hypoxia (12 hour windows)……...62

FIGURE 5.6 Histology of normoxic and hypoxic embryos……..63

FIGURE 5.7 Hypoxia delays skull development……..65

FIGURE 5.8 Principal components analysis (PCA)…….66

FIGURE 5.9 Facial shape variation in relation to centroid size……68

FIGURE 5.10 Comparison of PC1 scores according to oxygen concentration…….69

FIGURE 5.11 Comparison of shape and centroid size scores by oxygen concentration..71

FIGURE 5.12 Developmental delay in hypoxic embryos…….72

FIGURE 5.13 Neural crest progenitor cell death in hypoxic embryos (HH9-10)…….73

FIGURE 5.14 Neuroepithelial apoptosis in hypoxic embryos (HH9-10)……..74

FIGURE 5.15 Reduced proliferation, increased activity of caspase 3 in neuroepithelial cells in hypoxic embryos (HH9-10)……...75

FIGURE 5.16 Cell proliferation and apoptosis at later stages (6 days)…….76

FIGURE 5.17 Metabolic stress in hypoxic embryos…….77

APPENDIX B: BACKGROUND AND MOTIVATION FOR MY RESEARCH

FIGURE B.1 Treacher Collins syndrome……..99

CHAPTER 1:

INTRODUCTION

1.1 EMBRYONIC CRANIOFACIAL DEVELOPMENT FROM NEURAL CREST

The development of the craniofacial region in the early embryo is a concerted effort between various tissues using molecular signals to influence each other to adopt unique fates. From gastrulation, the embryo consists of three tissue germ layers, in order from exterior to interior: ectoderm, mesoderm, and endoderm. The ectoderm gives rise to several tissues, including the neural plate (which forms the neural tube, which in turn forms the brain and spinal cord), skin, oral and nasal epithelium, external auditory canal, and tooth enamel. The head mesoderm gives rise to the craniofacial muscles. The endoderm forms the lining of the pharynx, as four pharyngeal pouches.

Of greatest interest in craniofacial development is the neural crest. During formation of the neural tube, migratory cells begin to separate from the crest of the neural tube. His [1] observed a novel mesenchymal cell population dorsal to the spinal cord, which was named the neural crest by Marshall [2]. Platt [3] first traced these cells into the embryonic branchial arches and found that they differentiated into tissues including the cartilage and odontoblasts. It was not until stable cell labeling methods became available in the late 20^{th} century that researchers came to know the true diversity of neural crest derivatives; these include not only cartilage, but bone and connective tissues, smooth muscle, and secretory cells [4]. Thus this population of cells was found to create a wider diversity of derivatives than mesoderm, effectively creating a fourth germ layer [5].

Historical evidence of differentiation of neural crest origins from mesodermal origins of craniofacial tissues exists in the literature. A classic paper by Noden [6] examined the

patterning of neural-crest-derived cranial skeletal, muscle, and connective tissues. Older models theorized that the neural-crest-derived skeletal tissues and lateral-plate-mesoderm-derived branchial arch muscles were patterned around and by the pharynx and its pouches. While some skeletal elements and other tissues may be patterned according to stimuli from surrounding epithelia, most of the evidence does not support a pre-patterning role for surface ectoderm in neural crest or mesoderm derivatives. Rather, as Noden's [6] data show, the neural crest cells have an inherent program for patterning their own derivative tissues in the branchial arches, a property established from the start of migration. Noden [6] transplated neural crest tissue from quail donor embryos into homologous regions in chick embryos, creating a "quick". Transplants of donor 1st arch neural crest cells into the 2nd and 3rd arch regions of recipient embryos led to the appearance of ectopic beak-like structures externally and duplication of external auditory meatal depressions, a complete duplicate first-arch jaw skeletal system in the 2nd arch, and ectopic first-arch muscles associated with these duplicate first-arch bones in the 2nd arch. Noden's [6] data apparently showed that patterning was inherent to the neural crest cells themselves, not the surrounding arch as previously believed. Development of muscles from paraxial mesoderm-derived mesenchyme in the arches was believed by Noden [6] to depend on patterning properties inherent in the neural crest.

However more recent research shows that branchial arch patterning is independent of the neural crest. Rather, patterning results from complex interactions between tissues in the embryonic head [7]. One important regulator of branchial arch patterning is the *Hox* family of genes. *Hoxb1* is expressed in rhombomeres r4, r7, and r8; *Hoxa2* expression runs from r2 through r8; *Hoxa3* is expressed caudally from r5; and *Hoxa4* is expressed in

r7 and r8 [8]. The neural crest that migrates from r2 to branchial arch 2 expresses *Hoxa2*, but all neural crest rostral to that point is *Hox*-negative [7], as *Fgf8* blocks *Hox* gene expression from any point rostral to the second arch. Further proof of the *Hox*-negativity of the head rostral to r2 is provided by the forced expression of *Hoxa2*, *Hoxa3*, and *Hoxa4* in chick embryos by Creuzet and colleagues [8]; when these *Hox* genes were forcibly expressed in the normally *Hox*-negative region of the head, this precluded any development of facial skeletal structures. In the case of *Hoxa2* overexpression, there was a total lack of facial cartilage or skeleton, while *Hoxa3* and *Hoxa4* overexpression led to total absence of bone, but there was some facial cartilage evident [8]. When neural crest cells were transposed into ectopic locations in the hindbrains of mouse embryos [9] and zebrafish embryos [10], some of these cells did not retain their original identity (ie, *Hox* gene expression pattern), but actually conformed to the identity of their new surrounding tissues by expressing *Hox* genes appropriate to the new locations. Branchial arch patterning can even occur, experimentally, in the absence of neural crest cells. Veitch and colleagues [11] ablated the neural tube in chick embryos (at Hamburger and Hamilton (HH) [12] stages 9-10, prior to neural crest formation) from the mesencephalon to the somite 1-4 region. These embryos expressed *Dlx2* (a marker of first branchial arch neural crest), perhaps contributed by rostral midbrain regions, but the second and third arches were crest-free (evidenced by lack of the neural crest marker HNK-1). Despite ablation, however, these embryos continued to form branchial arches and express *Bmp7, Fgf8, Pax1,* and *Shh* in their appropriate regions and amounts [11], demonstrating that branchial arch formation and patterning occurs independently of input from neural crest cells. Additionally, the skeletal elements of branchial arches are patterned by the *Dlx*

family of homeobox genes [13]; of particular interest to craniofacial developmental biology is the role of *Dlx* genes in patterning branchial arch 1 (ie, jaw) skeletal structures. For example, Depew and colleagues [14] generated double mutant mice (lacking both *Dlx5* and *Dlx6*), and found that *Dlx5/6-/-* mice had homeotic transformations of their lower jaws into mirrored duplicate upper jaws. This demonstrates that there is a "nested" pattern of expression of *Dlx5* and *Dlx6* in the jaws, influencing the patterning and organization of their skeletal elements [14].

Kontges and Lumsden [15] used the "quick" chimeric system to analyze the migration of neural crest from hindbrain rhombomeres and the midbrain to their final destinations (the arches), to define the fates of neural crest subpopulations from these regions. The midbrain, and individual hindbrain rhombomeres, each have a resident subpopulation of neural crest cells. Kontges and Lumsden [15] transplanted each rhombomere from quail donor embryos (of an early, pre-migratory stage) into the equivalent location in chick host embryos (of the equivalent stage), and used the quail-specific QcPN antibody to mark quail cells in chick hosts. A previous study found that posterior midbrain neural crest contributes to the posterior forebrain and part of the first branchial arch [15]. The authors, in their rhombomeric neural crest transplants, found discrete streams of neural crest migration from each rhombomere to the arches (Fig. 1.1). Neural crest from rhombomeres 1 and 2 (r1 and r2) flows into the first branchial arch (mandibular arch). Rhombomere 4 (r4) neural crest contributes to the second (hyoid) arch. Rhombomere 6 and 7 (r6+r7) crest migrates to the third and fourth arches. Neural crest cells are significantly depleted in r3 and r5, and those few that do survive provide only a token contribution to the second arch (Fig. 1.1) [15]. After the host embryos had received their

transplants and developed to the stage of bone and cartilage differentiation, Kontges and Lumsden [15] analyzed the skeletal structures in each arch for neural crest contributions. The first-arch skeletal structures were made up of neural crest from r1 and r2 (in the proximal elements, including proximal maxillary and mandibular bones, squamosal, and other posterior craniofacial skeleton, some middle ear bones, and cartilages), and the most distal elements (maxillary and distal mandibular bones and cartilages) were totally derived from the midbrain crest. Second-arch crest (r4) cells also contributed to the lower jaw. The second arch skeletal structures were comprised of r4 neural crest, and also had a tiny contribution from r3 and r5 crest cells (those few that did survive depletion). Crest from r3 and r5 also contributed to cranial nerves V and VII in that region. Skeletal structures in the third arch were comprised of neural crest from r6 and r7. There were sharp boundaries between the r1+r2, r4, and r6+r7 neural crest streams. Crest from r3 and r5 was restricted to r4 territory, and was excluded from the other streams. Similarly, the attachment points of skeletal muscles to their respective bony elements were derived from the same neural crest populations as the bony elements to which they were joined. Kontges and Lumsden [15] concluded that the mandibular arch skeleton has a composite architecture, being made up of neural crest cells from multiple distinct rhombomeric migratory streams that form discrete boundaries between them. Similarly, the connective tissues that join branchiomeric muscles to their respective bony elements have the same neural crest origin as their adjacent bones. Most r3 and r5 neural crest cells die off, and those few that remain migrate within the neuroepithelium to become islands of cells within second-arch structures that are mainly comprised of r4 crest cells [15].

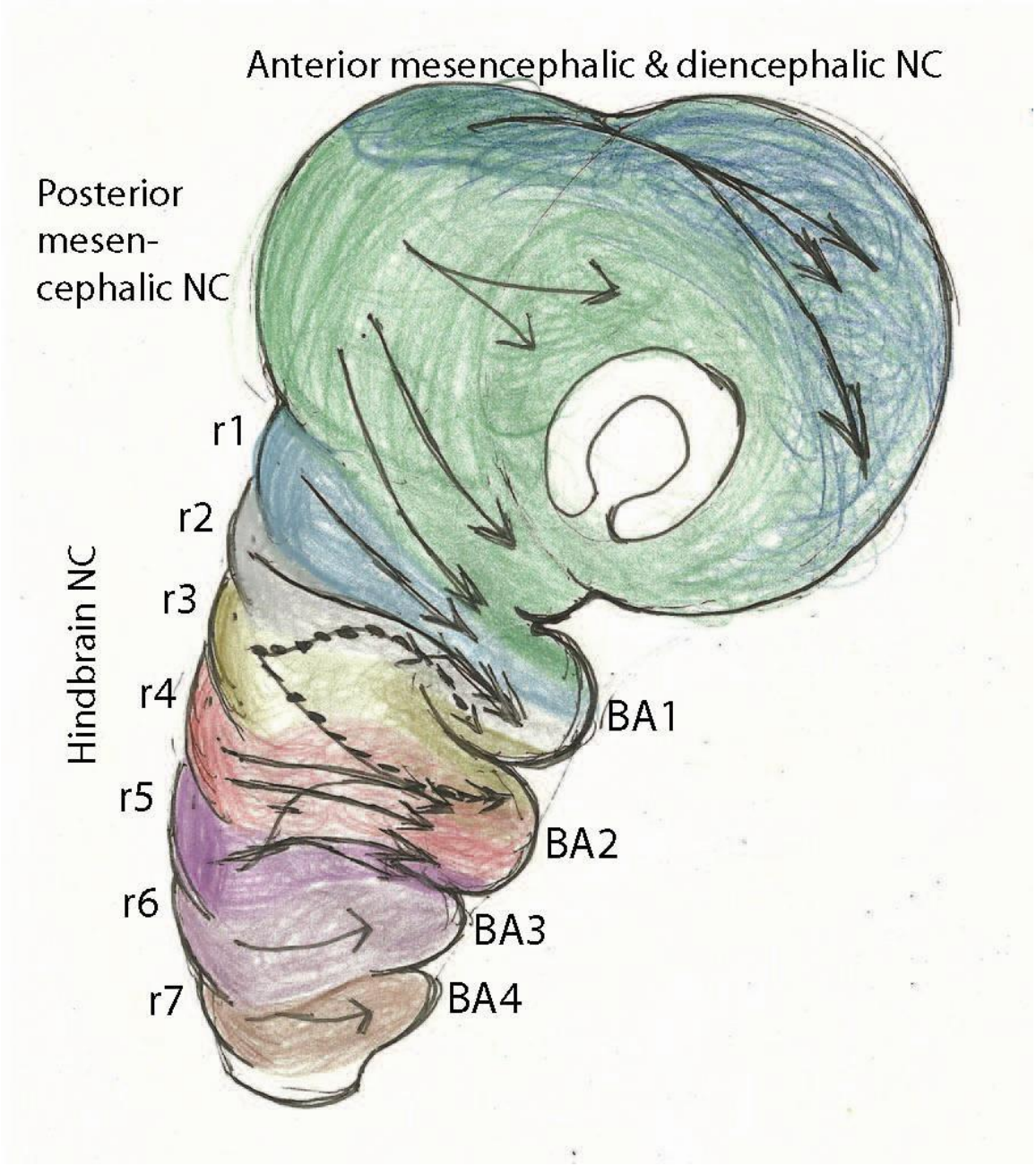

Figure 1.1: Cranial neural crest origin and fate in chick embryos. *Subpopulations of neural crest cells in early stage chick embryos originate in the midbrain and particular hindbrain rhombomeres (r1-r7) and migrate in distinct streams into the arches. (Adapted from [15])*

Even though the differentiation of neural crest-derived and mesoderm-derived craniofacial tissues has been described in detail by the experimental evidence, there has persisted some controversy about the derivation of craniofacial bones from neural crest versus mesodermal origins. For example, a discrepancy exists between the findings of two groups, Couly et al [16] and Evans and Noden [17], of exactly which parts of the avian skull originate from mesoderm versus neural crest, as is described hence.

Couly et al [16] used "quick" chimerism to analyze the origin of avian embryonic skull bones and observed that the entire prechordal skull (forward of the notochord and sella turcica) is derived from cephalic neural crest. The postchordal skull is derived from cephalic or somitic mesoderm in the ventromedial part (chordal skull) and from neural crest for the parietal bone and some of the otic capsule. The sphenoid has both neural crest and mesodermal origin (presphenoid is neural crest, postsphenoid is cephalic mesoderm). Formation of the occipito-otic part of the skull involves cooperation of somites 1-5 and hindbrain paraxial mesoderm [16]. Evans and Noden [17] fate-mapped the craniofacial neural crest and paraxial mesoderm cells in chick embryos with replication-incompetent retroviruses containing the β-galactosidase gene applied to paraxial mesoderm, crest progenitors, and at the interface between these two progenitor populations. LacZ-labeled paraxial mesoderm cells adopted diverse lineage-specific behaviors, ending up as frontal bone osteocytes, postorbital chondrocytes, endothelial cells, myocytes in oblique muscles, etc. Labeled paraxial mesoderm cells also ended up in neurocranial skeletal tissues including parietal bone, the anterior semicircular canal, etc. These cells also contributed to craniofacial skeletal muscles, including eye muscles, jaw muscles, and glottic constrictor muscles. LacZ-labeled neural crest cells ended up as

osteocytes in the supraorbital region, and contributed broadly to the frontonasal, maxillary, palatal, mandibular, and branchial arch skeletal tissues. These also contributed to corneal tissues, pyramidalis and quadratus nictitans muscles and associated connective tissues, and the aortic arches, pulmonary trunk, and truncal part of the heart's outflow tract. Double-labeling of neural crest and paraxial mesoderm resulted in staining of extraocular muscles, branchial muscles and neurocranial cartilages as having mesodermal origin, and 1st branchial arch cartilages and bones and 2nd arch cartilages as having neural crest origin. However, Evans and Noden [17] found a lack of retained nearest-neighbor relations between the progenitors of myogenic (mesodermal) and connective (neural crest) tissues. The authors identified the neural crest-mesoderm boundary at the junction of the calvarial and supraorbital parts of the frontal bone, lateral to the hypophyseal foramen, and rostral to the laryngeal cartilages. Evans and Noden [17] concluded that most of the frontal and the whole parietal bone are mesodermal in origin. Mesoderm-derived chondrocytes and intramembranous osteocytes are mostly static or move in strictly transverse directions, whilst angioblasts migrate in all directions. Myogenic mesoderm cells do not maintain constant nearest-neighbor relations with adjacent neural crest-derived cells that form connective tissues until both groups reach their final destinations in branchial arches or orbital areas.

The discrepancy in which avian skull structures derive from neural crest as opposed to mesoderm can be summarized thus. In Couly et al [16], the entire frontal, parietal, and squamosal bones are said to come from neural crest as are the bones in front of the frontal bones, but in Evans and Noden [17] only certain regions of the frontal and squamosal bones come from neural crest, while other regions of these two bones (and the whole

parietal) come from paraxial mesoderm. Another discrepancy is that Evans and Noden [17] identify not only bones, but cartilages, muscles, and other non-osseous tissues that emerge from either neural crest or mesoderm. Couly et al [16] focused almost exclusively on the bones and their origin. This latter criticism is based on the fact that nuclear marking of quail graft cells is unstable in angioblasts and other endothelial cells, so these cells cannot be detected in this method. The more recent method [17] targeted infection of neural crest and paraxial mesoderm cells with replication-incompetent retroviruses with the β-galactosidase gene, has advantages over quail-chick chimerism, in that it is less invasive and avoids species differences in developmental rates and allows whole-embryo and histological analyses, unlike "quick" chimeras.

Several molecular signaling pathways govern the induction, migration, and lineage of neural crest cells. These include the Sonic hedgehog (Shh), Wnt, and bone morphogenetic protein (BMP) cascades, among other molecules and neural crest-specific markers. Induction of the neural crest has been shown by Basch et al [18] to begin as early as gastrulation in avian embryos; the epiblast at Hamburger and Hamilton (HH) [12] stages 3-4 expresses *Pax7*. Blockage of *Pax7* translation in this region inhibits the activity of neural crest markers (Slug, Sox9, Sox10, and HNK-1), disrupting induction of the neural crest later on, thereby demonstrating the requirement for Pax7 to specify what tissue in the gastrula becomes the neural crest [18]. Subsequently, during neurulation, the posterior end of the neurula uses Fgf and Wnt signals and retinoic acid to convert the anterior neural plate border into neural crest, as observed by Villanueva et al [19] in *Xenopus laevis* embryos. Formation of the neural crest is induced by integrated Wnt, Fgf, and BMP signaling across the neural plate border and below it (Fig. 1.2) [20]. Formation

of neural crest cells is induced by horizontal signaling between the neural plate (which secretes BMP) and surrounding ectoderm (which secretes Wnt), and by vertical signaling from the paraxial mesoderm which secretes Fgf (Fig. 1.2). Garcia-Castro et al [21] perturbed Wnt signaling in chick neural crest cells *in vitro* and *in vivo* with a broad-spectrum Wnt inhibitor and found that Wnt6 is both sufficient and required to induce the formation of neural crest cells. In their recombination studies in *Xenopus* embryos, Monsoro-Burq et al [22] observed that the paraxial mesoderm induces the expression of a number of neural crest-specific genes (*Sox9, Zic5, Slug,* and *FoxD3*) in the ectoderm at the dorsolateral marginal zone (DLMZ). This process requires Fgf signaling, and Fgf8 in particular is a neural crest inducer expressed in the paraxial mesoderm [22].

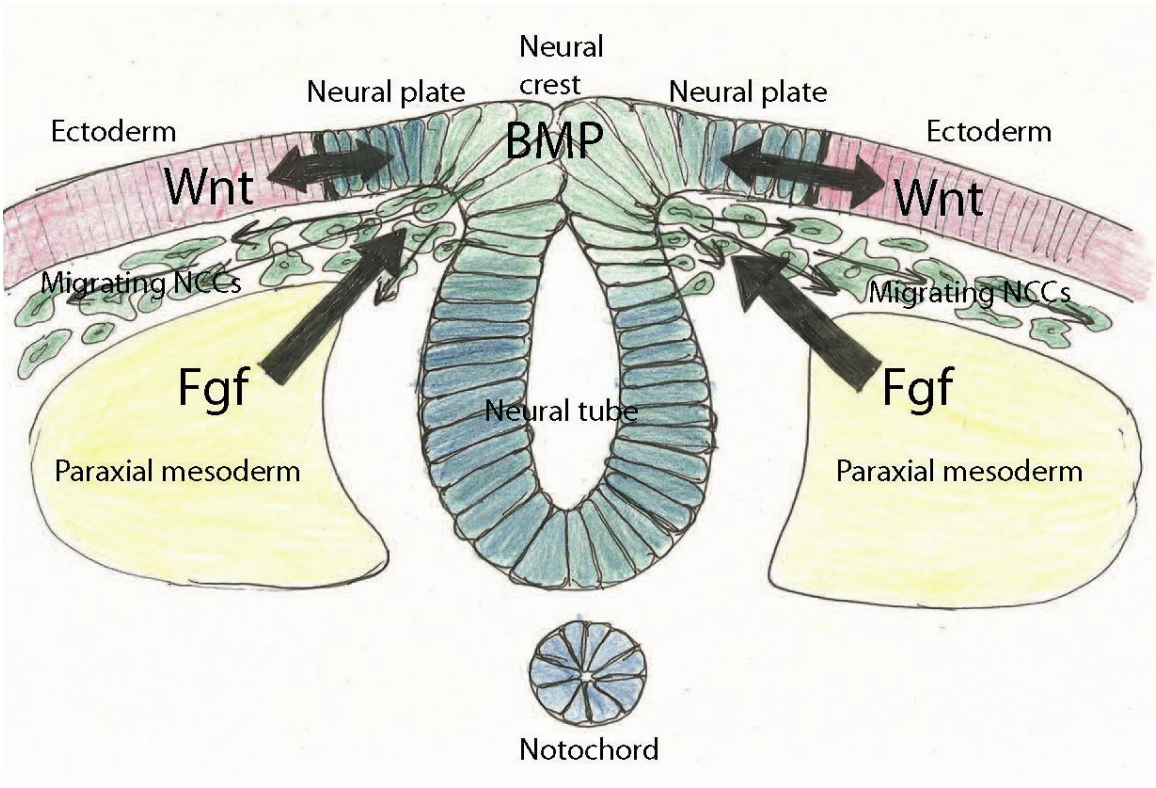

Figure 1.2: Molecular induction of neural crest. *During neurulation, the neural crest (green) is induced by three molecular signaling pathways (Fgf, Wnt, and BMP). BMP (in*

the neural crest) and Wnt (in the non-neural ectoderm) establish the boundary between the neural plate and the surrounding ectoderm. The paraxial mesoderm secretes Fgf, which also induces neural crest cell formation. (Adapted from [20])

BMP and Shh also play important roles in cranial neural crest differentiation and patterning. In their experiments with *Wnt1-Cre;Smad fl/fl* transgenic mouse embryos, Ko et al [23] proved that BMP signaling (dependent on Smad4), while not necessary for migration, is required for neural crest cell survival in the first arch, homeobox gene-mediated patterning of first-arch ectomesenchyme, and odontogenesis. Shh is a major regulator of facial patterning. Using *Wnt1-Cre:Smo n/c* transgenic mouse embryos, Jeong et al [24] found that Shh signaling in cranial neural crest cells directly regulates several *Fox* genes (expressed in the ectomesenchyme) in order to pattern the branchial arches, and that *Fox* genes mediate Shh activity during craniofacial morphogenesis.

1.2 CRANIOFACIAL ANOMALIES

Globally, 84 in 10,000 people [25] are affected by craniofacial malformations ranging from simple cleft lip and palate to complex disorders including holoprosencephaly. Two classes of disorders of particular interest are the neurocristopathies and holoprosencephaly.

Neurocristopathies are disorders of neural crest cell development, proliferation, migration, and differentiation. Since the majority of craniofacial tissues are neural crest derived, the majority of craniofacial disorders result from neural crest deficits, including the autosomal dominant Treacher Collins syndrome (OMIM 154500). First discovered in 1846 by Thomson [26], and more completely described by and named after E. Treacher Collins in 1900 [27], the syndrome is characterized by a constellation of defects of first

branchial arch derived facial structures. These include external ear malformations, atresia of the external auditory canal, middle ear defects, hypoplasia of the lower facial bones (particularly the mandible, zygomatic arches, and malar bones), eyelid defects, and cleft palate (Fig. 1.3).

Figure 1.3: Treacher Collins syndrome. *Visible characteristics include external ear defects, hypoplasia of zygomatic arches, malar bones, and mandible, and defects of the eyelids. (From personal archive)*

Dixon and colleagues localized the TCS gene *TCOF1* 6 [28, 29] and characterized its mutations [29, 30]. The *TCOF1* gene product, the nucleolar phosphoprotein treacle, functions in transcription of ribosomal RNA (rRNA) and regulates ribosome biogenesis

in a spatiotemporal manner [31, 32]. Using a *tcof1* mutant mouse model, Dixon and colleagues [31] found that haploinsufficiency of *tcof1* (and the resulting truncated treacle) results in disruption of formation of neural crest cells. The reduced proliferation leads to fewer migrating neural crest cells, leading to hypoplasia of first arch craniofacial structures [31]. Furthermore, Dixon et al [31] found significant neuroepithelial-specific apoptosis of neural crest cells, and observed that the apoptosis and reduced proliferation were consequences of a deficiency of mature ribosomes in the affected cells. Treacle is thus necessary for formation and proliferation of neural crest cells [31]. The bioenergetic stress caused by disrupted mature ribosome production in the treacle-deficient neural crest cells leads to increased stabilization of the tumor suppressor p53 [33]. The resulting apoptosis of neural crest cells occurs in a p53-dependent pathway, leading to the neurocristopathy characteristic of Treacher Collins syndrome [33].

Holoprosencephaly is a complex congenital malformation of the forebrain (prosencephalon) and face. Holoprosencephaly results from the failure of the prosencephalon to divide into two lobes. The incidence is 1:250 in early embryos and 1:16,000 live births [34]. The spectrum of cephalic malformations includes hindbrain anomalies, hemispherical fusions, and forebrain defects including aprosencephaly, microcephaly, anencephaly, and exencephaly [35, 36]. Associated facial anomalies include cyclopia, microphthalmia, anophthalmia, facial asymmetry, a single median incisor, and clefting (Fig. 1.4) [35, 36].

Figure 1.4: Spectrum of craniofacial anomalies associated with holoprosencephaly. *Malformations range from cyclopia and proboscis (the most severe form) (a, b) through hypotelorism (b-f) to a single median incisor (g) and nearly-normal appearance (h, i). (Adapted from [35])*

1.3 ETIOLOGY OF CRANIOFACIAL MALFORMATIONS

These malformations can be caused by genetic defects, environmental factors, or a combination of both, that alter cellular processes during development. For example, as previously mentioned, mutations in *TCOF1* lead to apoptosis of neural crest progenitor

cells [31, 33], causing a neurocristopathy. Alternatively, teratogenic agents, including cyclopamine, ethanol, nicotine, and other drugs can cause malformations by altering proliferation and survival of cells [37-39].

An example of a complex disorder, with teratogenic and genetic causes, is holoprosencephaly. A major gene involved in holoprosencephaly is *Sonic hedgehog (Shh)*, which encodes an intercellular signaling protein essential to development of the forebrain and face [36, 40]. In humans and mice, mutations in *Shh* lead to holoprosencephaly [41]. Human *SHH* mutations are autosomal dominant, resulting in a variable phenotype [42, 43], while mouse *Shh* mutations are autosomal recessive, resulting in cyclopia and other severe holoprosencephalic phenotypes [44]. Environmental factors known to cause holoprosencephaly include drugs like mycophenolate mofetil (MMF) [39], phenytoin [37], alcohol and cyclopamine [38].

Experimental and clinical evidence points to prenatal hypoxia as another teratogenic factor in craniofacial malformations and holoprosencephaly. Embryonic hypoxia can be caused by teratogenic drugs, including phenytoin, alcohol, and nicotine. For example, a teratogenic dose of phenytoin induces hypoxia (lasting a few hours) in rodent embryos [37], and this hypoxia leads to reduced ATP production in cells, apoptosis, cell cycle block, edema, and hemorrhage. But the major cause of damage due to hypoxia is the damage to cells upon reoxygenation due to the action of oxidative free radicals (produced by the compromised mitochondria) [37]. Phenytoin is teratogenic in that it inhibits HERG (human-ether-a-go-go) potassium channels in the embryonic heart and causes embryonic brachycardia and arrhythmia, leading to hypoxia [37]. Also, the hypoxia induced by phenytoin in rodents has led to cleft lip and maxillary hypoplasia [37].

1.4 CORRELATION OF HYPOXIA TO CRANIOFACIAL DEFECTS AND HOLOPROSENCEPHALY

Hypoxia may affect facial development by altering cellular behavior, through increased apoptosis or reduced proliferation. For example, neurocristopathies result from increased apoptosis of cranial neural crest progenitor cells [31, 33]. Conversely, defects in fibroblast growth factor (Fgf) signaling can lead to reduced cell proliferation, causing facial clefting [45, 46].

A recent clinical report suggests that hypoxia may also lead to craniofacial anomalies in humans. Siebert [47] describes a case of monochorionic, diamniotic twinning in which one twin was normal and the other twin had no heart which created hypoxia and ischemia due to reversed arterial perfusion. Structural malformations in the acardiac twin included a spectrum of anomalies that resembled holoprosencephaly [36] including: cyclopia, aprosencephaly, cystic hygroma, hypoplastic mandible, small cranium, and hypoplastic upper limbs (Fig. 1.5). The investigators suggested that hypoxia and ischemia in the acardiac twin created the holoprosencephalic phenotype due to the increased vulnerability of the head to lower levels of oxygen [47]. However, the relationship between hypoxia and holoprosencephaly was not tested directly.

Figure 1.5: Holoprosencephalic malformations in an acardiac twin fetus. *While the pump twin (A) was normal, the acardiac twin (B) displayed gross holoprosencephalic anomalies and lack of forebrain division (C, D). Adapted from [47].*

The mechanistic link between hypoxia and craniofacial malformations is not well established, because the effects of hypoxia on development are poorly understood. In the 1950s and 1960s, a number of researchers [48-56] undertook descriptive studies on the effects of hypoxia on the morphology of chick embryos. Chick embryos were made hypoxic by incubating them in an atmospheric mix of air and nitrogen, or at high altitude

[56], or shellacking the shells to prevent gaseous diffusion [49]. In all, hypoxia led to high mortality, a variety of craniofacial malformations, and in a small number of embryos, brain defects including exencephaly and anencephaly. However, these studies were descriptive and did not address the cellular or molecular mechanisms underlying the defects.

1.5 DELETERIOUS EFFECTS OF HYPOXIA ON TISSUES

Embryonic hypoxia can exert deleterious effects on the development of various tissues. Chicken embryos incubated in 15% O2 by Chan and Burggren [57] displayed shortened beaks and smaller eyes after an early period of hypoxia. Pups born from female rodents subjected to hypoxia have suffered significant cell loss (via apoptosis or necrosis) in their brain tissues in a number of studies (reviewed in [58], causing sensorineural, cognitive, behavioral, histological, and morphological deficits, demonstrating that the brain is particularly significantly vulnerable to hypoxia. Chronic hypoxia has been shown to restrict fetal growth and cause heart defects in mouse fetuses at embryonic day 12.5 (E12.5) [59]. In this study, E12.5 mouse fetuses displayed growth retardation and cardiac anomalies including myocardial thinning, detached epicardium, and smaller heart size and mass. The cardiac defects led to fetal death with signs similar to congestive heart failure. The other organs were reduced in size but apparently anatomically normal [59].

1.6 ADAPTATION OF CELLS TO HYPOXIA VIA HIF-1 PATHWAY

Cells adapt to hypoxia via the HIF (hypoxia inducible factor) pathway. HIF-1 is a dimeric transcription factor with two subunits, HIF-1α and HIF-1β. HIF-1β is always expressed at constant levels regardless of oxygen level [60, 61]. The α subunit has a brief half-life and its stability depends on the level of hypoxia in the cell. In normoxic

conditions, HIF-1α is hydroxylated by prolyl hydroxylases (PHDs) and FIH-1 and subsequently ubiquitinated by the E3 ubiquitin ligase VHL (von Hippel-Lindau protein) complex. The ubiquitinated HIF-1α is then degraded by the proteasome (Fig. 1.6). However, in hypoxic conditions, hydroxylation of HIF-1α is blocked. VHL does not bind, and HIF-1α is stabilized. HIF-1α then enters the nucleus and binds with HIF-1β to the HRE (hypoxia response element) whereby the complex regulates expression of target genes [60, 61] (Fig. 1.6).

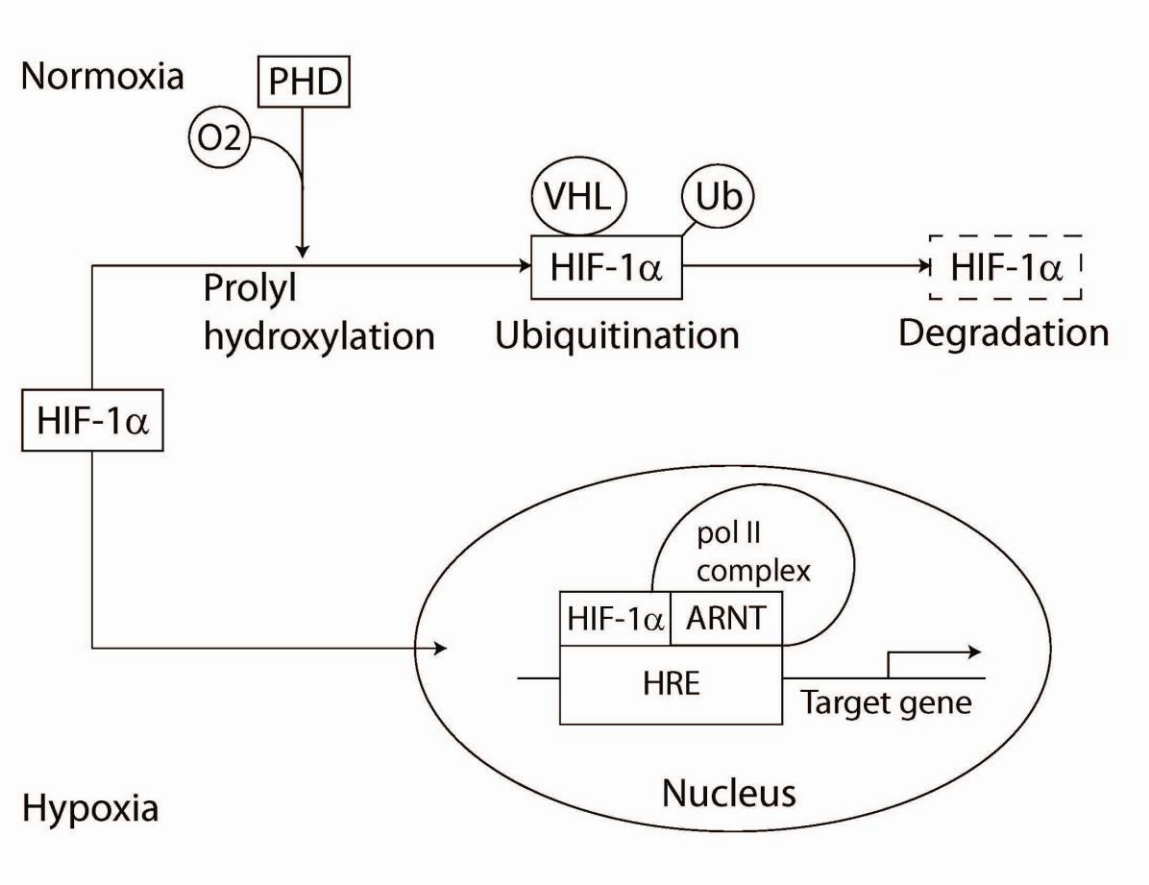

Figure 1.6: Molecular adaptation to hypoxia. *Cells adapt to hypoxia via the HIF pathway. In the presence of oxygen, HIF-1α is hydroxylated, ubiquitinated, and degraded. In the absence of oxygen, HIF-1α remains stable and activates transcription of target genes in the nucleus. (Adapted from [60])*

HIF-1α target genes function in erythropoiesis, iron metabolism, development, vasculogenesis, angiogenesis, extracellular matrix metabolism, glucose metabolism, cell proliferation, survival (normal and cancerous), and apoptosis [61, 62]. Of interest in this work is the role of HIF-1α in embryonic development. HIF-1α is important in cardiovascular development; HIF-1α-deficient mouse embryos experience cardiac malformations, poor vascular development, and embryonic lethality [63, 64].

1.7 HYPOXIA, HIF-1α, AND APOPTOSIS

Cells and tissues can only adapt to hypoxia to a certain extent. Excessive hypoxia can lead to cell death. Malhotra et al [65] used a dominant-negative HIF-1α construct and an RNA-interference-mediated knockdown of HIF-1α, as well as overexpression of HIF-1α, to determine whether hypoxia caused a HIF-1α-mediated apoptotic response in cultured cell lines. Inactivation of HIF-1α led to reduced apoptosis in response to hypoxia, while overexpression increased the number of apoptotic cells, thus demonstrating to Malhotra et al [65] that HIF-1α indeed mediates the apoptotic response to hypoxia. Three apoptotic mechanisms mediated by HIF-1α, as described by Harris [60], are as follows. First, activation of transcription of IGF-binding protein-3 (IGFBP-3) blocks IGF signaling (via PI3K and AKT) and thereby removes the inhibition of the proapoptotic protein BAD. BAD, in turn, releases cytochrome c from mitochondria. Secondly, hypoxia activates a p53-dependent mechanism that stimulates BAX to release cytochrome c (while the antiapoptotic protein BCL-2 is downregulated). Thirdly, hypoxia upregulates the proteins NIX and NIP3 in order to cause a cell death independent of either cytochrome c or caspases (Fig. 1.7).

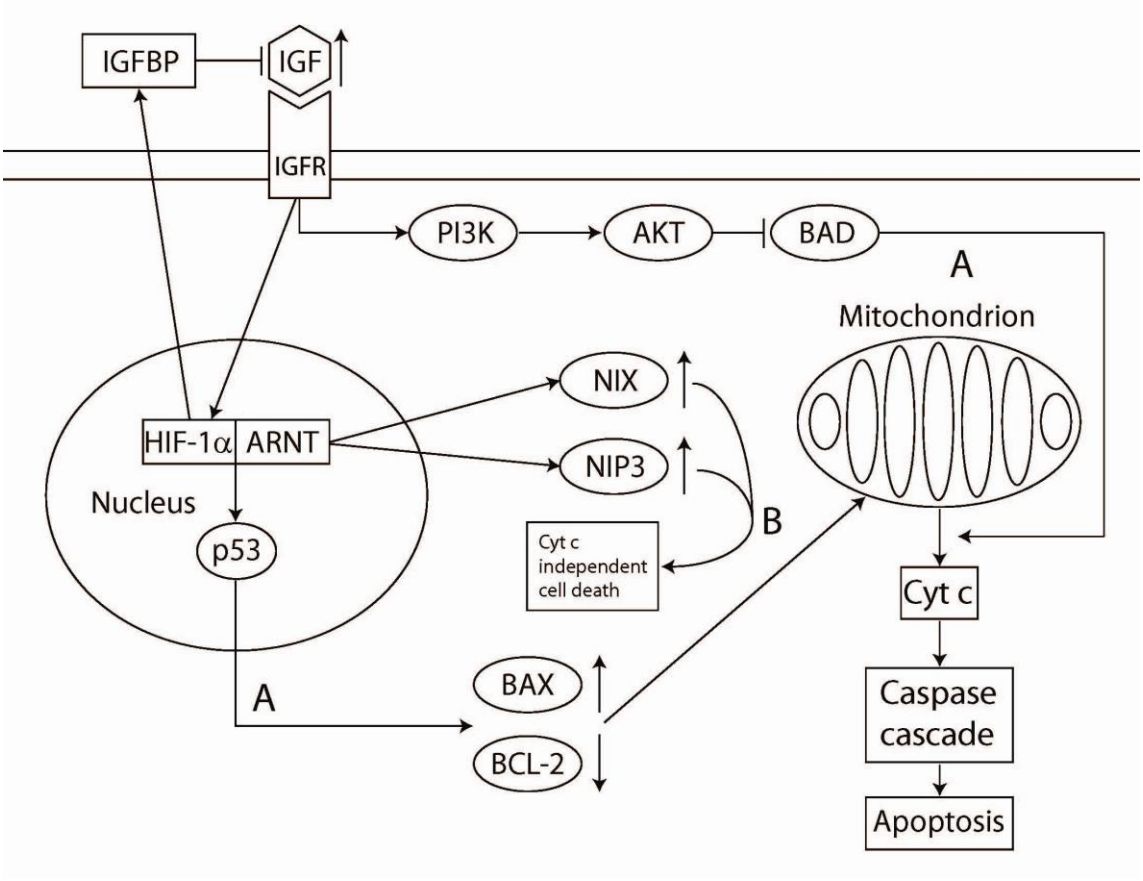

Figure 1.7: Hypoxic regulation of cell death through HIF-1α. *HIF-1α can cause apoptosis through cytochrome c release and* ***(A)*** *stimulation of the caspase cascade or* ***(B)*** *independently of cytochrome c. (Adapted from [60])*

NIP3 is a proapoptotic Bcl-2 family protein whose gene has a functional HRE in its promoter that allows it to be activated under hypoxia, as Bruick [66] found in cells cultured in prolonged hypoxia. Another proapoptotic protein, BAX, was found to be upregulated in conjunction with increased apoptosis in hypoxic cultured cell lines [65]. Shoshani et al [67] discovered a novel gene, *RTP801*, that is HIF-1α–dependent and stimulated by hypoxia to cause apoptosis in particular cell types (differentiated neurons and lung tissue in mice).

Paradoxically, while hypoxia can act through HIF-1α to cause apoptosis, it can also inhibit cell death. Ginouves et al [68] observed that in cells cultured in hypoxia, as well as in kidney tissues from mice housed in hypoxic chambers, hypoxia raises the level of PHDs and overactivates them, causing HIF-1α desensitization that protects cells from necrosis. Inactivation of PHDs in acute hypoxia, and PHD overactivation in chronic hypoxia, are apparently required for cell survival in these two conditions of hypoxia [68]. Although RTP801 is proapoptotic in mouse differentiated neurons and lung cells, it has the opposite effect in dividing neurons and cancer cells [67], demonstrating that the action of RTP801 depends on the type and state of cells.

1.8 ELECTRON TRANSPORT CHAIN-DERIVED REACTIVE OXYGEN SPECIES DURING HYPOXIA

Effects of hypoxia may be detected by a cell through byproducts of the electron transport chain (ETC). The ETC consists of five multiprotein complexes that are embedded within the inner mitochondrial membrane [69]. Complexes I and II oxidize the energy-rich molecules NADH and FADH2, respectively, and transfer the resulting electrons to ubiquinol that then shuttles them to complex III. Complex III ferries these electrons across the inner mitochondrial membrane to cytochrome c, which carries them on to complex IV. Complex IV then uses these electrons to reduce oxygen to water. Each of these steps is associated with the pumping of protons into the intermembrane space generating a proton gradient, the dissipation of which is coupled to complex V to drive the energy-intensive phosphorylation of ADP to ATP [69] (Fig. 1.8).

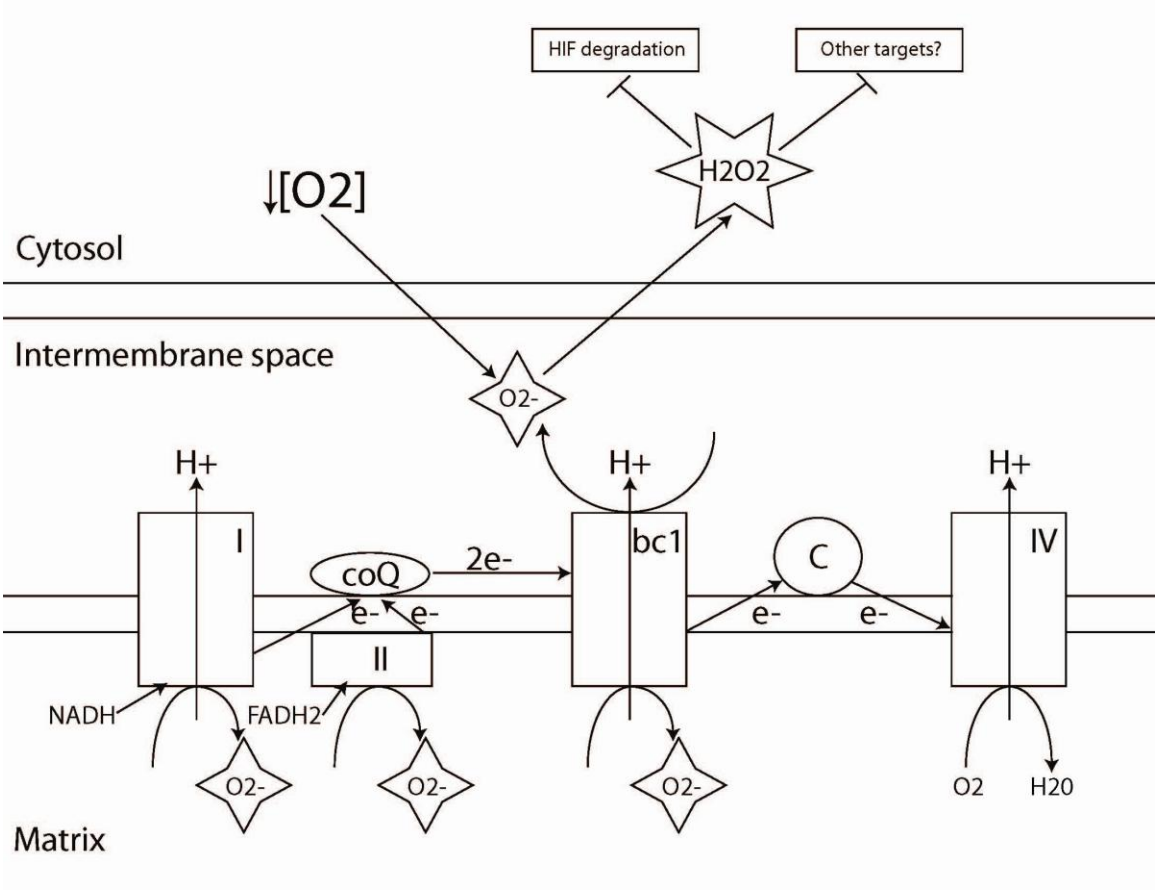

Figure 1.8: Mitochondrial hypoxia sensing through the electron transport chain. *Hypoxia increases generation of reactive oxygen species (ROS) in complex III. ROS are released into the intermembrane space and enter the cytosol. (Adapted from [69])*

Early studies with ETC inhibitors, or with cells depleted of mitochondrial DNA and hence critical electron transport chain components, laid the groundwork for more recent studies supporting a role for mitochondrial electron transport in hypoxic stabilization of HIF-1α [70]. These experiments showed that hypoxia could paradoxically trigger an increase in mitochondrial reactive oxygen species (ROS) production, and that antioxidant treatment could inhibit hypoxic HIF activation. Subsequently, it was shown that exogenous hydrogen peroxide could stabilize HIF-1α during normoxia [71]. Cells depleted of mitochondrial DNA or critical ETC components failed to produce ROS

during hypoxia [72-74].

Convincing evidence of the role of complex III-mediated ROS production in cellular oxygen sensing came from investigations using complex b mutant cybrids, generated by reconstituting mitochondrial DNA-depleted (ρ-zero) cells with either wild-type DNA or DNA containing a 4-bp deletion in the cytochrome b gene found in a patient with parkinsonism [75]. Loss of complex b renders cells incapable of respiration. However, ρ-zero cells fused to mutant cytochrome b containing cells were still capable of hypoxic HIF-1α stabilization, though not respiration, and this could be inhibited with antioxidants targeted to mitochondria (MITOQ) [76]. Therefore, cellular oxygen sensing could be uncoupled from respiration; however, mitochondrial reactive oxygen species (ROS) were still required for responses to hypoxia. These studies unequivocally demonstrated that mitochondrial ETC-derived ROS, specifically at complex III, are the key signaling molecules responsible for cellular oxygen sensing [69].

1.9 AMP KINASE

Another energy sensor that plays a role in cellular response to hypoxia is the AMP-activated protein kinase (AMPK). AMPK is a heterotrimeric serine/threonine kinase comprised of three subunits: a catalytic α subunit and two regulatory subunits (β and γ) (Fig. 1.9) [77-79]. The critical site of phosphorylation is Thr172, contained in the α subunit [77, 79].

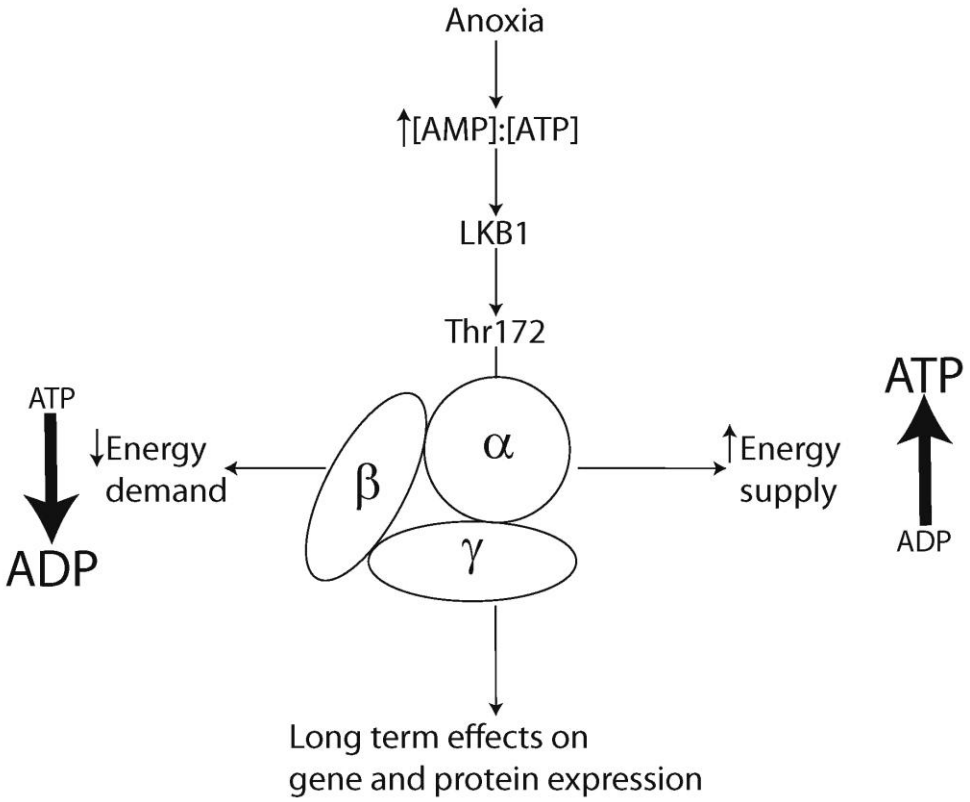

Figure 1.9: AMPK regulates cellular energy metabolism. *In response to anoxia, the [AMP]:[ATP] ratio increases, stimulating LKB1 to activate AMPK at Thr172. Activation of AMPK stimulates ATP-producing pathways to increase energy supply, while inhibiting pathways that consume ATP in order to decrease energy demand. AMPK activation in turn leads to long-term regulation of gene and protein expression. (Adapted from [79])*

To survive severe hypoxia and other metabolic stresses, the cell must sustain high levels of adenosine triphosphate (ATP), which serves as the energy currency, despite impaired mitochondrial oxidative metabolism [80]. In order to maintain a balance between supply (ie, ATP supply) and metabolic demand in the cell, AMPK is activated when the ratio of AMP to ATP increases. AMPK is activated by direct physical interaction with AMP, as well as through phosphorylation by the upstream AMPK kinase

(AMPKK) [77]. Another upstream kinase that activates AMPK is the serine/threonine protein kinase LKB1 [81]. While AMPK is allosterically activated by AMP, it is similarly antagonized by high levels of intracellular ATP, indicating competitive binding at the AMPK allosteric sites between AMP and ATP [77, 78]. AMPK is also activated by metabolic stressors that deplete cellular stores of ATP, including hypoxia and ischemia, heat shock, exercise, and metabolic toxicity [77]. Choi et al [77] also theorize that AMPK may be activated through ROS and oxidative stress. Based on prior evidence of this, Choi et al [77] examined the possible regulatory effects of hydrogen peroxide (H2O2) and oxidative stress on AMPK. The authors treated the NIH-3T3 cell line with H2O2 after temporary serum starvation. H2O2 increased AMPK activity and the AMP:ATP ratio in a dose-dependent manner [77]. The activation of AMPK was associated with increased phosphorylation of Thr172 in the α subunit. However, treatment of the cells with tyrosine kinase inhibitors (suramin, PD98509, and genistein) neither disrupted the H2O2-induced AMPK activation nor altered the AMP:ATP ratio [77], indicating that AMPK may not be a direct ROS target. Nonetheless, the AMPK cascade is highly sensitive to oxidative metabolic stress in cells [77]. More recent evidence also indicates that hypoxic AMPK activation depends on ROS but is independent of change in the intracellular AMP:ATP ratio. Emerling et al [81] subjected mouse embryo fibroblasts (MEFs) to hypoxia (1.5% or 0% O2), compared to normoxic controls, and found that AMPK was activated by the hypoxia (most notably 0% O2), regardless of the AMP level.

Downstream, AMPK activates catabolic (ATP-producing) pathways, while at the same time inhibiting anabolic (ATP-consuming) pathways [78, 79]. Anabolic pathways and genes that are blocked by AMPK participate in synthesis of lipids, fatty acids,

glycogen, and proteins, as well as lipolysis and chloride ion transport secretion [78], while catabolic pathways and gene expression activated by AMPK are involved in fatty acid oxidation, glycolysis, increased blood flow, and glucose transport (Fig. 1.10).

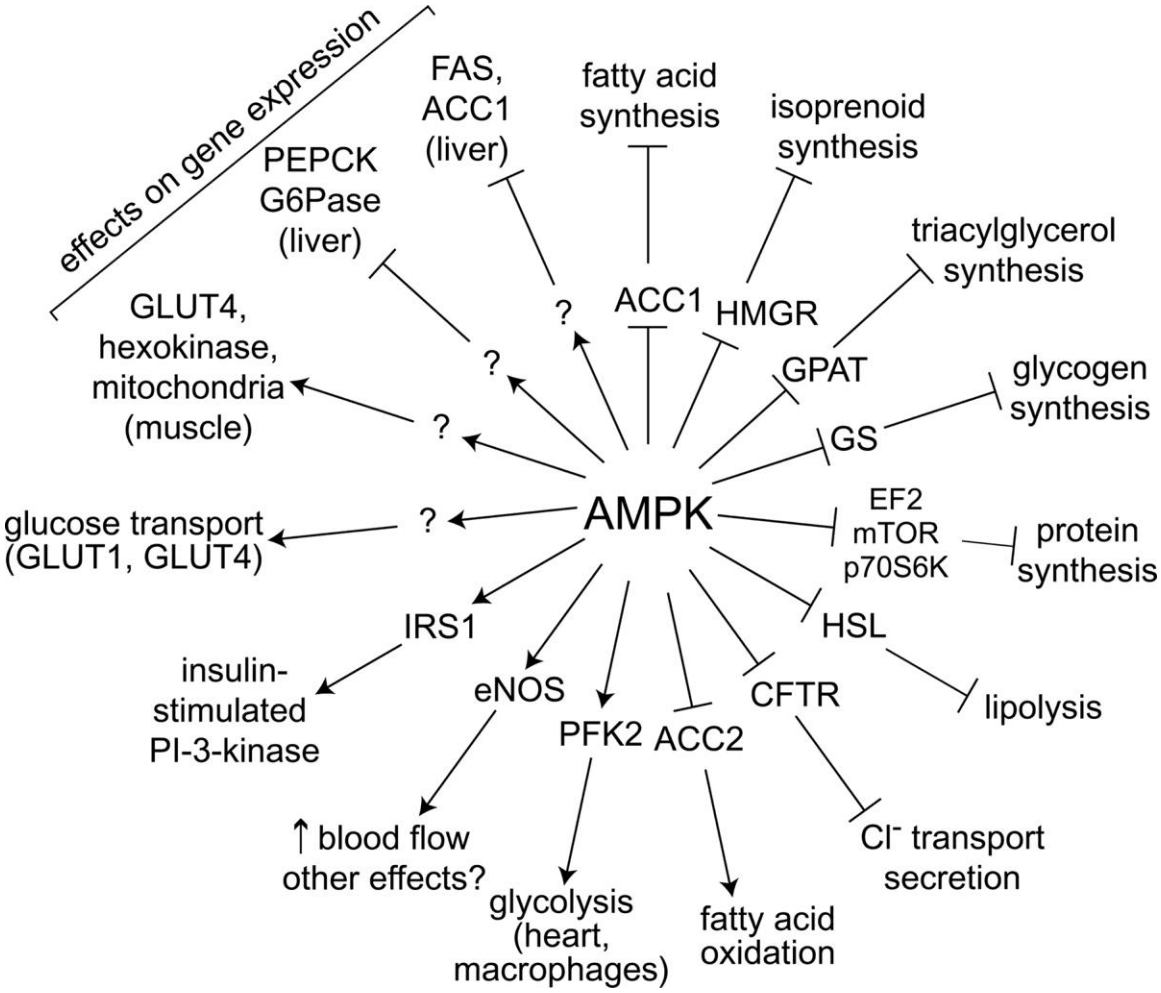

Figure 1.10: Target proteins and pathways regulated by AMPK. *AMPK activates catabolic pathways and genes involved in fatty acid oxidation, glucose transport, glycolysis, and increased blood flow. Conversely, AMPK inhibits anabolic pathways involved in lipolysis, chloride ion transport, and production of lipids, fatty acids, glycogen and proteins. (From [78])*

Under conditions of metabolic stress, AMPK activation can negatively affect cellular

growth and proliferation and can precipitate apoptosis. Jones et al [82] observed reduced proliferation, cell cycle arrest at the G1 to S transition, and increased AMPK activation in MEFs cultured in low-glucose media. The reduction in proliferation was dependent on the glucose dose, and significant apoptosis was observed in cultures totally deficient in glucose [82]. Compared to MEFs infected with an inert vector, cells infected with a vector expressing constitutively active AMPK displayed reduced proliferation, demonstrating that AMPK is sufficient to cause cell cycle arrest [82]. Jones et al [82] found that tumor suppressor p53-deficient cells infected with constitutively active AMPK failed to undergo cell cycle arrest, demonstrating a requirement for p53 to enable AMPK to induce arrest. Further, Jones et al [82] observed that p53 surprisingly enables glucose-limited cells to remain viable (while persistently arrested in the cell cycle). Long-term cell cycle arrest in viable cells is a marker of premature cellular senescence. Jones et al [82] found that cellular senescence is a process induced by AMPK and controlled by p53.

Further evidence demonstrates the ability of AMPK to stimulate apoptosis in cells under metabolic stress. AMPK has been shown to mediate apoptosis through the activation of a number of Bcl-2 family proapoptotic proteins downstream. Concannon et al [83] observed that, in the context of excitotoxic injury in neurons, prolonged AMPK activation stimulates the activity of the BH3-only protein Bim which mediates excitotoxic apoptosis. In neurotoxic apoptosis, Concannon et al [83] found that prolonged AMPK activation is sufficient to stimulate Bim expression, and that this manner of cell death depends on Bim. Another example of a proapoptotic protein that is activated by AMPK during bioenergetic stress is another BH3-only protein, Bmf [84]. Kilbride et al [84] found that in INS-1 cells treated with dominant negative HNF-1, bioenergetic stress

activated AMPK, which in turn mediated an apoptotic cascade characterized by upregulation in Bmf. Ryu et al [85] cultured rat pancreatic beta cells in anoxia; these cells subsequently experienced upregulated AMPK activity and a downstream protein (acetyl-CoA carboxylase 2), along with an increase in ROS activity. In response to treatment with constitutively active AMPK under normoxic conditions, caspase 3 was activated at a higher level, inducing apoptosis [85].

Paradoxically, activation of AMPK can also prevent apoptosis under certain conditions. Gopalani et al [86] cultured mouse splenocytes in hypoxia (0.5% O2). While sustained hypoxia normally leads to apoptosis, Gopalani et al [86] found that in these hypoxic cells, AMPK activation in concert with inhibition of cytosolic K+ efflux (by supplemental extracellular K+) actually allowed the cells to survive via prolonged cell cycle arrest rather than die. Cellular potassium homeostasis is controlled by stressors including chronic hypoxia; under conditions where the extracellular K+ concentration is restored, AMPK can operate alongside this to prevent progression to apoptosis in hypoxic stress. AMPK activation can also hinder apoptosis in certain types of cells. Nagata et al [87] treated human umbilical vein endothelial cells (HUVECs) with constitutively active AMPK under anoxic or normoxic conditions, and observed that while caspase 3 and 7 levels were increased, this increase was significantly reduced by the CA-AMPK overexpression, thereby inhibiting apoptosis. Liu et al [88] found that cultured endothelial cells (from mouse common carotid artery and bovine aortic endothelia) subjected to hypoxia and deprived of glucose showed significantly increased AMPK activity. When AMPK activity was suppressed by dominant negative AMPK or Compound C, apoptosis was significantly increased, while overexpression of

constitutively active AMPK suppressed apoptosis in these cells. When the AMPK activity increased [88], expression of pro-survival proteins (Bcl-2 and survivin) increased in the endothelial cells. The studies by Nagata et al [87] and Liu et al [88] suggest that AMPK may protect vascular endothelial cells from hypoxic or ischemic injury.

CHAPTER 2:

GOALS OF PROJECT

2.1 MECHANISTIC LINK BETWEEN HYPOXIA AND CRANIOFACIAL MALFORMATIONS

A correlation between embryonic hypoxia and craniofacial malformations, including holoprosencephaly, has been demonstrated by clinical and experimental evidence. A number of studies were undertaken in the 1950s and 1960s in which chicken embryos were incubated in hypoxia. However, the actual cellular and molecular mechanisms by which hypoxia causes these morphological defects are yet unknown.

2.2 HYPOTHESIS

Based on Siebert's [47] acardiac fetus case, and my preliminary data showing altered morphology and increased cell death and reduced proliferation in hypoxic chick embryos, it was hypothesized that hypoxia creates abnormal craniofacial morphology via HIF-1α-mediated apoptosis and decreased cell proliferation due to altered molecular signaling between the forebrain and frontonasal process in chick embryos.

2.3 GOALS AND PROPOSED EXPERIMENTS

The goals of this project were twofold. The goals are stated henceforth, and the experiments that were initially proposed (during development of the project proposal) are described for each of the two main goals or aims of the project.

2.3.1 AIM 1: LINK BETWEEN CELLULAR AND MOLECULAR CHANGES AND HYPOXIC CRANIOFACIAL MALFORMATIONS

2.3.1.1 Proposed Experiments Completed in Aim 1

The first goal was to determine the extent to which cellular and molecular changes due to hypoxia create craniofacial malformations including holoprosencephaly. To meet this first goal, morphological and morphometric analyses were proposed to examine what morphological alterations occur in hypoxic embryos, compared to normoxic control embryos and embryos with holoprosencephaly (based on observations by Siebert [47] of holoprosencephalic anomalies in an acardiac human fetus). Chick embryos were to be incubated chronically in hypoxia (at a range of oxygen levels from 9% to 19% oxygen) until collection, then examined for craniofacial defects and compared with normoxically incubated control embryos. Expected outcome measures included a dose-dependent reduction in survival and morphological alterations in hypoxic embryos. Embryos of both groups were to be imaged and analyzed via geometric morphometrics to quantify the change in craniofacial shape in hypoxic versus normoxic embryos. The purpose of this was to determine whether hypoxic embryos displayed abnormal craniofacial shape variation compared to normoxic controls.

Additional experiments were devised to assess cell proliferation and apoptosis in hypoxic embryos in comparison to normoxic embryos. To assess cell proliferation at early and later stages of development, embryos were to be sectioned and stained to detect bromodeoxyuridine (BrdU) incorporation into the DNA of dividing cells. The malformations were also hypothesized to result from apoptosis, so embryos at early and late developmental stages were to be sectioned and assayed using TUNEL to mark apoptotic cells as well as immunostained with antibodies against cleaved caspase 3 (involved as an executioner protein in the apoptotic cascade). Expected outcomes were decreased cell proliferation in hypoxic embryos, as well as increased apoptosis.

2.3.1.2 Additional Proposed but Unrealized Experiments in Aim 1

A group of embryos treated with 5E1 antibody-expressing cells (to artificially induce holoprosencephaly) were proposed to be included in the morphometrics along with the normoxic control and experimental hypoxic groups. The goal of this was to observe whether any of the hypoxic embryos displayed variation consistent with holoprosencephaly (hence the use of artificially-induced holoprosencephalic embryos). The extent to which the holoprosencephalic embryos overlapped with the hypoxic embryos in the morphospace was to be assessed, and some hypoxic embryos were expected to show variation consistent with holoprosencephaly. However this was not completed due to difficulty with injection of 5E1 antibody-expressing cells into HH9-10 chick embryos and poor survival of treated embryos.

Since the malformations observed in hypoxic embryos were thought to originate from defects in the neural crest, the migration of neural crest cells was to be traced using whole-mount staining of embryos with HNK-1, a marker for neural crest cells. Hypoxic embryos were predicted to show reduced neural crest cell migration. This was not undertaken due to lack of time.

Molecular analyses were proposed to examine expression and activity of candidate molecules involved in regulating craniofacial morphogenesis. Since craniofacial development depends on the coordinated signaling activity of morphogens including Shh, BMP, Wnt, and Fgf, sections of embryos were to be subjected to *in situ* hybridization to detect expression of *Shh, BMP2/4/7, Fgf8, Wnt9b, Ptc,* and *Gli1* in addition to immunohistochemical staining for localization of β-catenin, phospho-MEK, and HIF-1α. Real-time quantitative PCR (qPCR) was proposed to measure expression of *Shh, Gli1,*

Ptc, *BMP2/4/7*, *Fgf8*, *Wnt9b*, and *HIF-1α*. Hypoxic embryos were predicted to show disrupted signaling in one or more pathways, relative to normoxic controls. These hypoxic embryos were expected to deviate from the normal growth trajectory, falling into the morphospace occupied by hypoxic embryos. However, these molecular analyses were either unsuccessful or unable to be completed for several reasons. First, the hypoxic embryos displayed a wide variation in phenotypes, making determination of a particular target gene or pathway impossible. Secondly, technical problems were encountered during the *Shh* whole-mount *in situ* hybridization and the HIF-1α immunohistochemical analyses.

2.3.2 AIM 2: RELATIONSHIP BETWEEN CELLULAR RESPONSE TO HYPOXIA AND MALFORMATIONS

2.3.2.1 Proposed Experiments Completed in Aim 2

The second goal was to test the relationship between the hypoxia inducible factor HIF-1α, reactive oxygen species, and facial malformations. One type of experiment was designed to determine whether the effects of hypoxia could be reversed by treating hypoxic embryos with antioxidants, in order to assess the role of reactive oxygen species in these defects. At early stages, hypoxic embryos were to be treated by direct application of an antioxidant (either N-acetyl-L-cysteine (NAC) or catalase) to the head. The prediction was that the treated hypoxic embryos would show improved survival and restored morphological, cellular, and molecular activity in comparison to PBS-treated hypoxic embryos and in similarity to normoxic controls.

2.3.2.2 Additional Proposed but Unrealized Experiments in Aim 2

Gain- and loss-of-function experiments were proposed to examine the extent to which HIF-1α is necessary and sufficient to cause craniofacial dysmorphology resulting from hypoxia. To test the extent to which HIF-1α mediates hypoxic effects on craniofacial morphology, early-stage normoxic embryos were to be infected with a virus encoding a constitutively-active HIF-1α gene; infected embryos were expected to show reduced survival, developmental delay, malformations, reduced cell proliferation, increased apoptosis, and altered *Shh* expression and signaling due to interaction of HIF-1α with the *Shh* promoter [89]. To examine how necessary it is for HIF-1α to alter the craniofacial morphology of hypoxic embryos, early-stage hypoxic embryos were to be envirulated with a dominant negative *HIF-1β* lacking the DNA binding domain. These embryos were predicted to display increased survival, accelerated development, normalized morphology, as well as a restoration of normal cellular behavior and molecular signaling. All embryos in this set of experiments were to be compared morphometrically with those in the normoxic growth curve and the other hypoxic embryos. The normoxic embryos treated with the gain-of-function construct were expected to fall among the hypoxic embryos in the morphospace, and the hypoxic embryos treated with the loss-of-function construct would fall toward or within the normal growth trajectory. However, due to time constraints, neither set of experiments was carried out.

In the antioxidant-treated embryos, lactate and ROS levels were to be assessed, and were expected to be lowered. In the morphometric analyses, treated embryos would be comparable to normoxic controls. Due to loss of most embryos during antioxidant treatment, these additional analyses were not performed.

CHAPTER 3:

MATERIALS & METHODS

3.1 CHICK EMBRYOS

3.1.1 Chronic Hypoxia: Fertile White Leghorn chicken eggs (Petaluma Farms, Petaluma, CA) were incubated in a humidified chamber (Hova-Bator, GQF Manufacturing, Savannah, GA) at 37.5°C. The day on which the eggs were placed in the incubator was designated as day 0. Hypoxic conditions were generated by replacing room air in the incubator with nitrogen. The level of oxygen in the chamber was titrated down to 7%, 9%, 11%, 13%, 15%, 17%, or 19% using an oxygen sensor/controller (Proox, Biospherix, Lacona, NY) (Fig. 3.1). As a control, another group of eggs were incubated in normoxic (21% O2) conditions. Chick embryos were collected on days 2 to 6 and staged according to Hamburger and Hamilton [12]. Embryos were removed from extraembryonic membranes and sacrificed by decapitation. They were washed in 1X PBS (phosphate buffered saline), and fixed overnight in 4% paraformaldehyde in 1X PBS at 4°C.

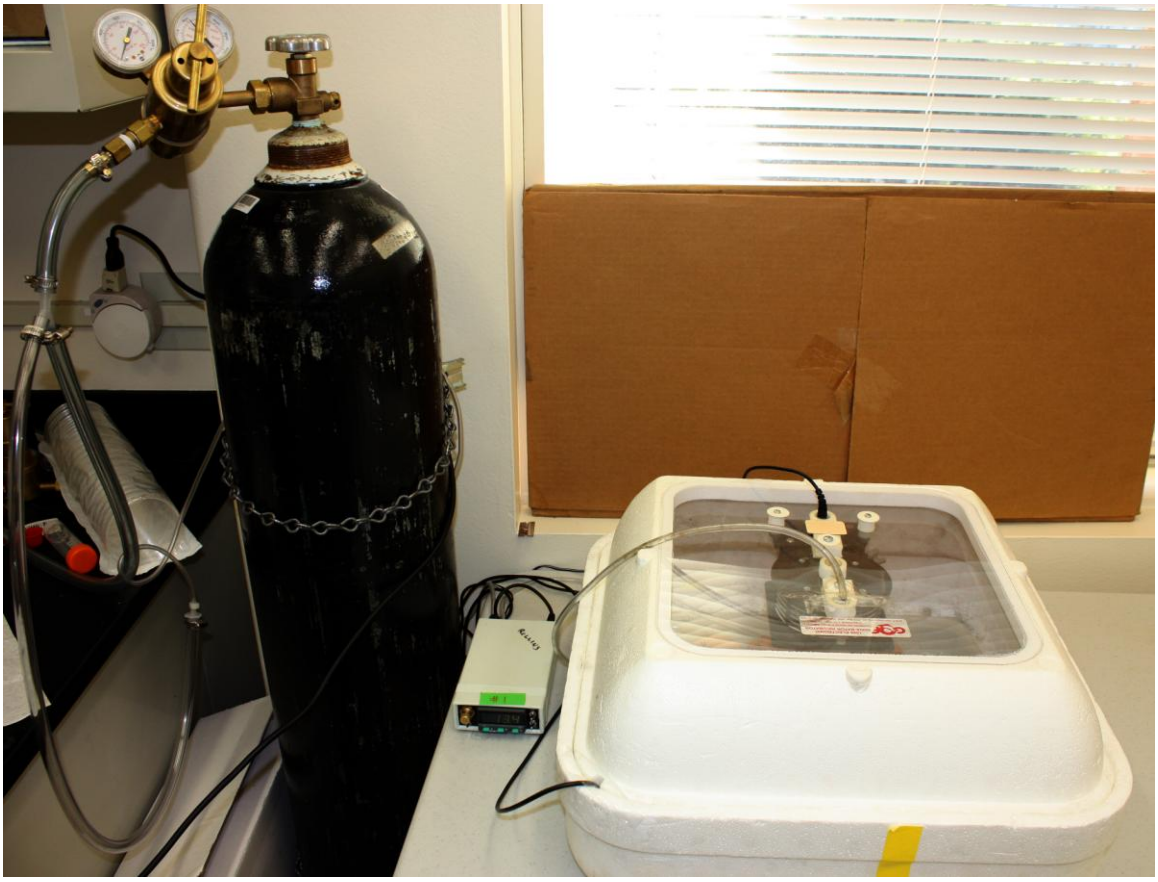

Figure 3.1: Hypoxic incubator. *Eggs are incubated in a standard humidified incubator (right), attached to a tank of nitrogen (left) via an oxygen sensor/controller (center) that controls the oxygen level in the chamber via feedback control.*

3.1.2 Acute Hypoxia: For analysis of the effects of acute hypoxia, two groups of eggs were incubated in normoxia until day 2 (HH9-10), then transferred to the hypoxic chamber, set at 9% O2. One group was incubated in hypoxia for 12 hours, and the other group for 24 hours. Subsequently, both groups were returned to the normoxic incubator until collection on day 6. The embryos were harvested and fixed as previously described.

In a subsequent experiment, five groups of eggs were incubated in 9% O2 for 24 hours on specific days and returned to normoxic incubation for the duration of the 6-day incubation period, in the following schedule. The first group was incubated from 0-24

hours in 9% O2, and transferred to normoxia for the remaining 5 days. The second group was initially in normoxia for the first 24 hours, then transferred to 9% O2 from 24-48 hours, and returned to normoxia for the remaining 4 days. The third group was incubated in normoxia for the first 48 hours, transferred to 9% O2 from 48-72 hours, and returned to normoxia for the remaining 3 days. The fourth group was incubated in normoxia for the first 72 hours, transferred to 9% O2 from 72-96 hours, and returned to normoxic incubation for the last 2 days. The final group was incubated for the first 96 hours in normoxia, 9% O2 from 96-120 hours, then normoxia for the final 24 hours before collection. All surviving embryos were collected on day 6, fixed, and prepared for imaging.

An experiment to fine-tune the critical hypoxic window within 12 hours was next undertaken. Four groups of eggs were incubated in 12-hour periods of 9% O2, between 24 and 72 hours of development, before return to normoxia for the remainder of the 6-day incubation period. All eggs were incubated together in normoxia for the first 24 hours, then transferred to 9% O2 incubation according to the following schedule. The first group was incubated in 9% O2 from 24-36 hours and returned to normoxia for the remainder of the 6-day incubation period. The second group was incubated in hypoxia from 36-48 hours before being returned to normoxia. The third group was incubated in hypoxia from 48-60 hours, and the fourth group from 60-72 hours. All surviving embryos were collected and fixed for morphological analysis on day 6.

3.2 STATISTICAL ANALYSIS OF EMBRYONIC SURVIVAL

The proportion (percentage) of survivors in each group (normoxic (21% O2) and hypoxic (7%, 9%, 11%, 13%, 15%, 17%, and 19% O2)) was noted. These survival rates

were compared using an analysis of variance (ANOVA) and a 2-tailed *t* test for significance between them. Since the survival rates were noted as proportions (binary data), the standard deviation for each group was calculated by multiplying the proportion of survivors by the proportion of dead individuals and taking the square root of this result. From this, for each group, the standard error of the mean (SEM) was computed as the standard deviation divided by the square root of the sample number of that group. The confidence interval, based on the standard α of 0.05, the sample size, and the standard deviation for each group, was calculated. A 2-tailed, 2-sample *t* test was performed to find the difference and the significance of that difference between adjacent groups, based on the null hypothesis that the difference is equal to 0. A similar 2-tailed, 2-sample *t* test was undertaken between the normoxic group and each of the hypoxic groups to determine the size and significance of the difference between the normoxic and each hypoxic group.

3.3 TREATMENT WITH ANTIOXIDANT

On day 0, before incubation in 13% O2, eggs were windowed and the blastodisc treated with either 1X PBS (as a control) or 100mg/ml N-acetyl-L-cysteine (NAC), an antioxidant. 81µl of PBS or NAC were dropped directly onto the blastodisc. After the window was closed with tape, all eggs were incubated in 13% O2 for 6 days. On each of days 1-6, the eggs were removed from the incubator, reopened, and the surviving embryos treated with PBS or NAC as described, before the eggs were returned to the incubator. On the final day, any survivors in each group, after the final treatment, were collected.

The experiment was repeated with the eggs being opened on day 1, not day 0, of incubation. Treatment was administered on days 1-6. 20µl 1X PBS or 20µl 400mg/ml NAC was placed lateral to, not directly on, the embryos. The survivors were collected on day 6.

3.4 GROSS MORPHOLOGICAL ANALYSES

Upon collection and fixation, all normoxic and hypoxic embryos were washed in 1X PBS and stained in 0.01% ethidium bromide in 1X PBS for fluorescent microphotography. Embryos were photographed (using fluorescent microscopy) for morphological analyses using a Texas Red fluorescent filter on a Leica MZFLIII dissecting microscope with a Leica LEI-750 camera (Leica Microsystems, Germany). The photographs were digitized on Adobe Photoshop imaging software (Adobe, San Jose, CA). The purpose of ethidium bromide staining and fluorescent imaging was to provide clear images with optimum contrast, for morphological visualization, assignment of cephalic and facial landmark coordinates, and geometric morphometric analysis.

3.5 ANALYSIS OF CRANIOFACIAL SKELETAL DEVELOPMENT

Eggs were incubated in the hypoxic chamber (9, 11, 13, 15, and 17% O2) for 13 days. A control group was incubated in the normoxic chamber for 13 days. Embryos were collected on day 13, sacrificed by decapitation, washed in 1X PBS, and fixed overnight in 4% PFA in 1X PBS at 4°C. The heads were washed in 1X PBS and photographed. Subsequently they were dehydrated in an ascending ethanol series and stored in 100% ethanol overnight at 4°C.

After an additional wash in 100% ethanol, the embryos were stained in alcian blue (for cartilage) for 24 hours, then washed twice in 100% ethanol. After serial rehydration,

they were trypsinized until the soft tissues were cleared of alcian blue stain. After a brief rinse in distilled water, they were stained 24 hours in alizarin red in 0.5% potassium hydroxide (for bone). The embryos were cleared in an ascending series of glycerol in distilled water to 100% glycerol, then photographed.

3.6 GEOMETRIC MORPHOMETRICS

Facial landmarks on images of embryos (normoxic and all hypoxic levels, 9% to 19% O2) were assigned via 45 fiduciary points (previously designated by Chong and colleagues [90]) in NIH ImageJ software (NIH, Bethesda, MD). These 2-dimensional landmark data were analyzed using MorphoJ morphometric software [91]. After Procrustes superimposition, principal components analysis (PCA) and canonical variates analysis (CVA) were used to analyze for facial shape variation between individuals in normoxic and hypoxic groups and between groups of embryos, respectively. Multivariate regression analyses were performed to measure craniofacial shape variation in relation to centroid size (average size of the head about a central point determined by Procrustes superimposition), stage, and age (in hours).

3.7 HISTOLOGICAL ANALYSIS

For histological analysis of forebrain and frontonasal tissues, embryos at days 4, 5, and 6 were dehydrated in a graded ethanol series and embedded in paraffin. These were sectioned at 10μm, deparaffinized, rehydrated, and stained with hematoxylin and eosin (H&E) using the protocol per Bancroft and Gamble [92] before dehydration and mounting. The stained sections were visualized with a Leica DM5000B microscope and photographed with a Leica LEI-750 camera (Leica Microsystems, Germany).

3.8 ASSESSMENT OF CELL PROLIFERATION

Normoxic and hypoxic embryos were injected, in the circulation, 20 minutes prior to harvest with bromodeoxyuridine (BrdU). These were subsequently fixed, dehydrated, embedded, and sectioned in paraffin. Sections were dewaxed and rehydrated before treatment to quench endogenous peroxidases. Staining with a biotinylated mouse anti-BrdU antibody and diaminobenzine (DAB) was performed according to the kit manufacturer's instructions (Invitrogen, Camarillo, CA) before dehydration and mounting. Sections were visualized and photographed with a Leica DM5000B microscope and LEI-750 camera (Leica Microsystems, Germany).

3.9 ANALYSIS OF APOPTOSIS

3.9.1 Whole-Mount TUNEL: To assess cell death at early stages (HH9 and 10), embryos were subjected to whole-mount TUNEL staining. Embryos were fixed, dehydrated in a graded ethanol series, rehydrated, and treated with proteinase K digestion. Subsequently they were postfixed in 4% PFA + 0.1% glutaraldehyde. The embryos were stained in TDT buffer, TDT enzyme, and AP converter from the Roche In Situ Cell Death Detection Kit, AP (Roche Applied Science, Indianapolis, IN). To enable visualization of dead cells in whole-mount embryos, they were stained with NBT and BCIP. Whole mount stained embryos were photographed on a Leica MZFLIII dissecting microscope with a Leica LEI-750 camera (Leica Microsystems, Germany).

3.9.2 Section TUNEL: Embryos (days 2 and 6) were sectioned in paraffin and TUNEL staining was performed on sections according to the TUNEL kit manufacturer's protocol (Roche Applied Science, Indianapolis, IN). After deparaffinization and serial rehydration in ethanol and water and washing in PBS, sections were permeabilized in 0.1% Triton X-100 in 0.1% sodium citrate in room temperature. After further washes in PBS, the

sections were treated with the TUNEL reaction mixture (label solution + terminal transferase enzyme) for an hour in a 37°C humidified atmosphere. After washing in PBS, sections were stained with Hoechst dye to enable visualization of all nuclei in contrast to TUNEL-stained cells before mounting. Sections were imaged by fluorescent microscopy using a Leica DM5000B microscope and LEI-750 camera (Leica Microsystems, Germany). All nuclei, being stained with Hoechst dye, were visualized in blue using the A cube. The L5 cube was used to visualize dead cells (green).

3.9.3 Whole-Mount Syto12-GFP Assay: At the same stage as the embryos assessed by whole-mount TUNEL staining, embryos were treated with the GFP-fluorescent vital dye Syto12 (Invitrogen Molecular Probes, Camarillo, CA) that specifically labels apoptotic cells. Embryos (normoxic control and 9% O2 groups) were incubated to day 2 (HH9-11). Eggs were windowed and the vitelline membrane removed from the head area of each embryo. 2μl of a 33μM solution of Syto12 in 1X HBSS was dropped directly onto the heads of the embryos. The eggs were reincubated for a further 2 hours in darkness (the flap of eggshell replaced over the window to provide darkness). The Syto12 dye was subsequently washed off the embryos with 10μl of 1X HBSS and the eggs reincubated for 30 minutes. The embryos were imaged, *in ovo*, using the GFP filter on a Leica MZFLIII dissecting microscope with a Leica LEI-750 camera (Leica Microsystems, Germany).

3.9.4 Caspase 3 Assay: To examine the activity of caspase 3 (a key executioner of the apoptotic cascade), embryos (days 2 and 6) were sectioned in paraffin. After antigen retrieval in 10mM sodium citrate buffer, they were stained with a rabbit polyclonal antibody to cleaved caspase 3 (Asp175) (1:100 in 5% goat serum in 1X TBST wash

buffer) (Cell Signaling Technology, Danvers, MA) overnight at 4°C. The primary antibody was detected using a biotinylated goat anti-rabbit secondary antibody to IgG (H+L) (1:100 in 1X TBST wash buffer). The presence of secondary antibody was detected with an avidin-biotin (ABC) reagent solution (Vector Laboratories, Burlingame, CA) and diaminobenzidine. After dehydration and washing in xylene, the sections were mounted with coverslips and visualized and photographed.

3.10 ASSESSMENT OF AMP-ACTIVATED KINASE (pAMPK) EXPRESSION

Embryos (days 2 and 6) were sectioned in paraffin. After sodium citrate buffer-assisted antigen retrieval, they were stained with a rabbit monoclonal antibody to phospho-AMP-activated kinase (pAMPK) (an important regulator of the cellular AMP:ATP ratio) (1:100 in 5% goat serum in 1X TBST) (Cell Signaling Technology, Danvers, MA) overnight at 4°C. The primary antibody was detected using a biotinylated goat anti-rabbit secondary antibody to IgG (H+L) (1:100 in 1X TBST), along with avidin-biotin (ABC) reagent solution (Vector Laboratories, Burlingame, CA) and diaminobenzidine (and hematoxylin counterstain in the 6-day embryos).

3.11 ASSESSMENT OF HYPOXIA INDUCIBLE FACTOR-1α (HIF-1α) EXPRESSION

After antigen retrieval in prewarmed 0.05% trypsin in dH2O, paraffin sections of 6-day normoxic and hypoxic embryos were blocked in 10% goat serum in PBS and stained with a rabbit polyclonal antibody to HIF-1α, 1:100 in 5% goat serum/PBS overnight at room temperature. These were subsequently washed in PBS and stained with an HRP-tagged goat polyclonal secondary antibody against rabbit IgG-H+L, 1:100 in PBS for an

hour at room temperature. After three PBS washes, the staining was detected using diaminobenzidine prior to serial dehydration and mounting.

3.12 ASSESSMENT OF SONIC HEDGEHOG (Shh) EXPRESSION

3.12.1 Embryos: Normoxic control and hypoxic embryos were collected on day 4 (HH22 in normoxia) and fixed for 2 hours in 4% PFA at room temperature. After being washed twice in 1X PBS with 0.2% Tween-20 (PBT), the embryos were dehydrated in a graded methanol series (50% methanol in PBT, then twice in 100% methanol) and stored in -20°C until used for whole-mount in situ hybridization.

3.12.2 *Shh* Antisense RNA Probe Synthesis: A plasmid containing chicken *Sonic hedgehog (Shh)* was extracted and purified from DH5α *E. coli* cells by maxipreparation. The plasmid was linearized with the restriction enzyme HindIII for 2 hours at 37°C and cleared of restriction enzyme at 55°C using proteinase K and 10% sodium dodecylsulfate (SDS). The DNA was cleaned with phenol, chloroform, and isopropanol. An antisense RNA probe was generated from the purified *Shh* template DNA using 5X transcription buffer, deoxynucleotides (dATP, dGTP, dCTP, and dUTP), digoxigenin (DIG)-labeled dUTP, and T3 RNA polymerase. DNA was removed from the probe with DNase and precipitated with tRNA, 4M ammonium acetate (NH4Ac), and ethanol.

3.12.3 Whole-Mount *In Situ* Hybridization: Embryos were rehydrated through 75%, 50%, and 25% methanol/PBT and washed twice in PBT. After treatment in 10μg/ml proteinase K and postfixation in 4% PFA + 0.1% glutaraldehyde, the embryos were incubated overnight in hybridization solution containing 1μg/ml DIG-labeled *Shh* antisense RNA probe at 65°C. Post-hybridization washes were performed with 1X MABT before incubating the embryos in 1X MABT + 2% Boehringer Blocking Reagent (BBR) + 20%

heat-inactivated lamb serum + 1:2000 AP-anti-DIG antibody overnight at 4°C. After removal of the antibody, the embryos were incubated (in light-tight conditions) in NTMT + 4.5µl/ml NBT/BCIP until staining developed (between 30 minutes and 1 day). The stained embryos were visualized and photographed on a Leica MZFLIII dissecting microscope with a Leica LEI-750 camera (Leica Microsystems, Germany).

CHAPTER 4:

NORMAL FACIAL DEVELOPMENT IN THE CHICK EMBRYO

4.1 SUMMARY

The Hamburger-Hamilton (HH) embryonic staging system was devised to classify chick embryos into discrete morphological stages of development. Earlier, chronologically-based classifications had the disadvantage of inherent morphological and size variation in embryos at any given age. Although the Hamburger-Hamilton classification relies on the use of discrete morphological characteristics in staging chick embryos, and provides a useful universal staging system for avian embryos, it does not completely eliminate the confounding factor of shape and size variation among embryos within a given stage. However such variation can still be useful in charting the growth of embryos over time along a fluid, rather than static, trajectory. To measure such variation requires a quantitative method, such as geometric morphometrics. Of significant interest is the measurement of craniofacial shape variation among embryos within stages over the course of development. The objective of this study was to chart the normal craniofacial growth trajectory of chick embryos over time. To this end, two-dimensional geometric morphometrics was used to measure the facial shape variation observed among embryos, in relation to specimen size, age, and stage. The older subgroup of embryos (HH22-28) was observed to have greater shape variation among embryos than the younger group (HH16-21). All the embryos were observed to fall along a well-defined nonlinear curve of normal facial growth in relation to size, and displayed variation in relation to chronological age and discrete morphological stage. The older subgroup of embryos displayed greater variation within stages than the younger subgroup.

4.2 BACKGROUND

Hamburger and Hamilton [12] devised a developmental staging system for chick embryos, based on discrete morphological characteristics including number of somites and shape and size of external landmarks such as limbs and branchial arches. This system was designed to overcome the disadvantages of previous classification systems that depended on chronological age, such as significant variation in embryos at any given age [12]. This classification was supplemented by another system [93], which focused on the development of the chick wing from stages HH19-36. The Hamburger and Hamilton method, with its emphasis on staging embryos based on discrete morphological landmarks, remains in universal use for staging chicks and other poultry embryos.

While the Hamburger-Hamilton staging system classifies embryos into discrete morphological stages, there is still variation among embryos at any given age (in hours or days) of development. Each stage occurs within an approximate period of hours, and each stage's period can overlap with that of the preceding or following stage, as reflected in the description of each stage [12]. Visual observation of any number of embryos within a particular stage can reveal apparent variation between them.

However, visual observation of variation between individual embryos within a discrete stage does not provide sufficient information on the significance of such apparent variation amongst the individuals. Therefore a quantitative method is required to measure the variation in shape of the embryos over time. Quantitative geometric morphometrics is performed by assigning a number of discrete morphological landmark coordinates (Procrustes coordinates) to a two- or three-dimensional image of an object, then superimposing a number of such specimen images upon each other to correct for

positional errors and to provide a true average shape [94]. Multivariate statistical procedures are performed to measure shape variation among individuals and between groups relative to any of a number of parameters including size and age.

Of particular interest is the variation in craniofacial shape during development and growth. Hallgrimsson and colleagues pioneered the use of geometric morphometrics to analyze craniofacial shape variation in normal and abnormal development and evolution of embryos and adult animals [95-100]. However there has been no attempt to trace the continuous trajectory of craniofacial growth and development. The goal of this study was to trace the normal growth trajectory of chick embryos over time using geometric morphometric analyses.

4.3 RESULTS

4.3.1 FACIAL SHAPE VARIATION AMONG INDIVIDUALS

45 craniofacial landmark coordinates were placed on two-dimensional images of embryos, according to the pattern described by Chong et al [90]. Principal components analysis (PCA) was used to find the two variables, or principal components, that accounted for the greatest variation in facial shape among individuals. The embryos were separated mainly along the PC1 axis (72.220% variance), representing change in the size of the eyes and the width of the frontonasal process, nasal pits, and maxillary processes, as well as the distance between the nasal pits. There was lesser separation along PC2 (9.373% variance), representing change in height of the nasal pits, frontonasal process, and maxillary processes (Fig. 4.1).

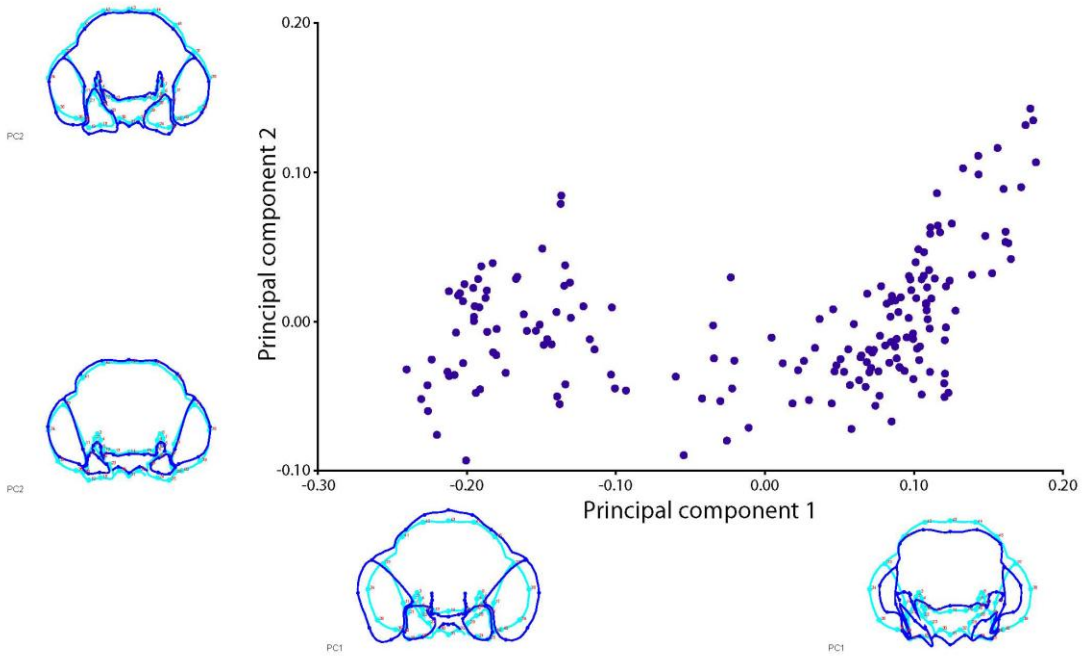

Figure 4.1: Principal components analysis (PCA). *Embryos are separated largely along axis PC1, demonstrating the greatest variation (in facial width), with the next highest variation (height of facial structures) along PC2.*

The embryos were then separated into two subgroups, younger embryos (stages HH16-21) and older embryos (HH22-28). Canonical variates analysis (CVA) was done to find the variables (or canonical variates) representing the greatest variation in embryos between the two subgroups. The older group had more variation in shape than the younger group (Fig. 4.2).

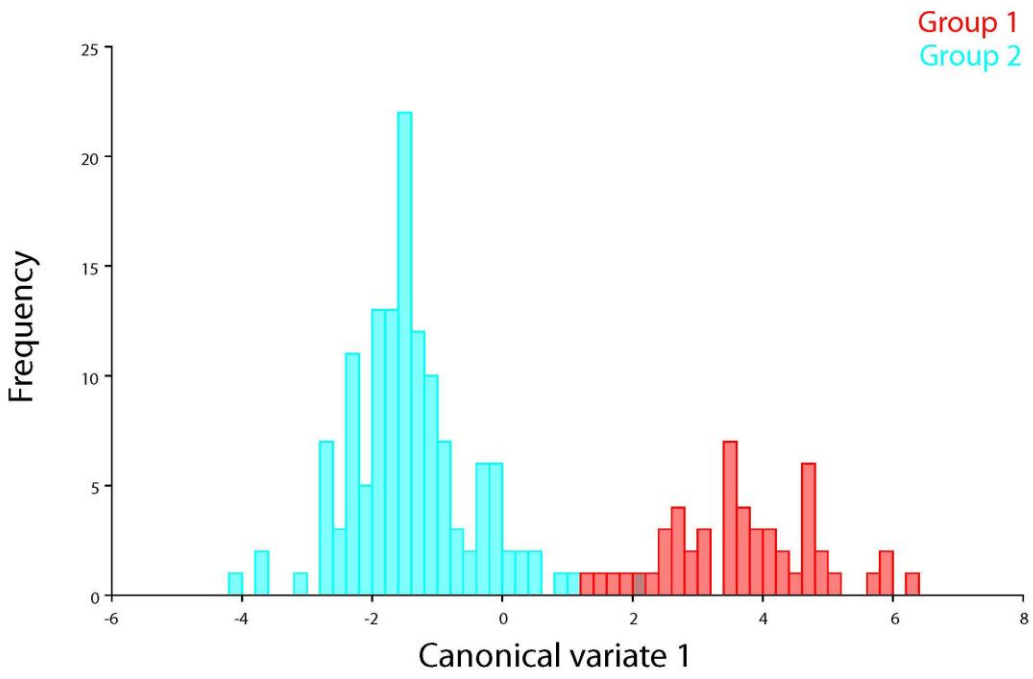

Figure 4.2: Canonical variates analysis (CVA). *Embryos within group 2 (blue) (HH22-28) demonstrate greater variation than group 1 (red) (HH16-21).*

4.3.2 NORMAL FACIAL GROWTH TRAJECTORY

Regression analysis was performed to quantify the facial shape variation in relation to centroid size. The embryos were observed to fall along a well-defined nonlinear curve of normal development in relation to centroid size (Fig. 4.3).

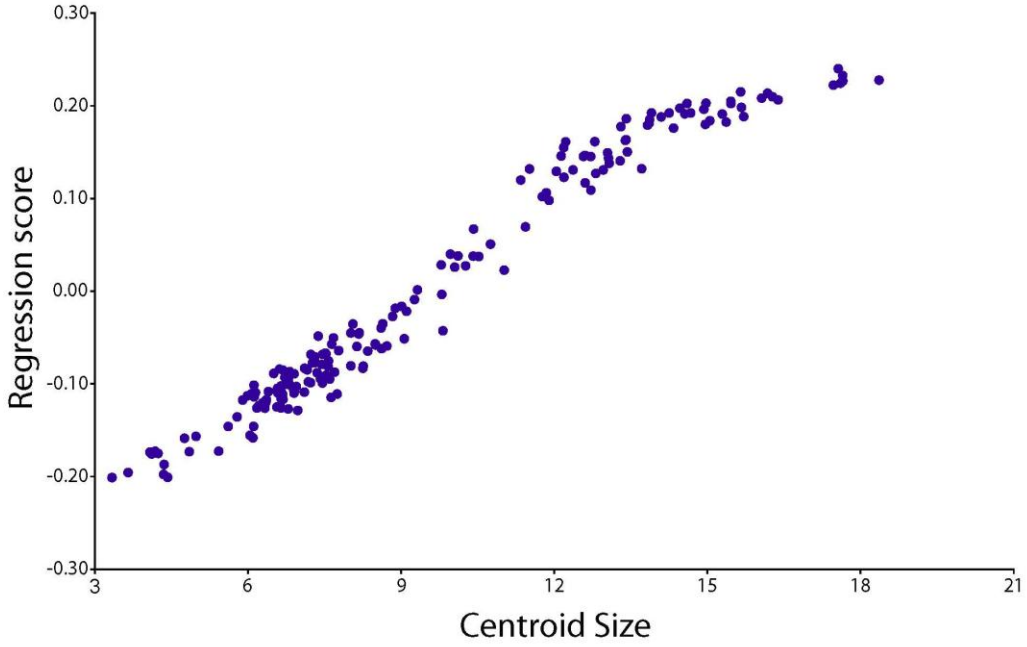

Figure 4.3: Normal growth trajectory. *Embryos display normal variation in facial shape along a growth curve in relation to centroid size.*

Regression analysis was also performed to quantify the facial shape variation between individuals in relation to age in hours and within each stage (HH). In relation to age, there appeared to be variation in facial shape (Fig. 4.4), however there was no correlation between the amount of variation and the age. Similarly, within stages, there was variation (Fig. 4.5); at stages HH20 and below, there was less variation than in stages above HH20.

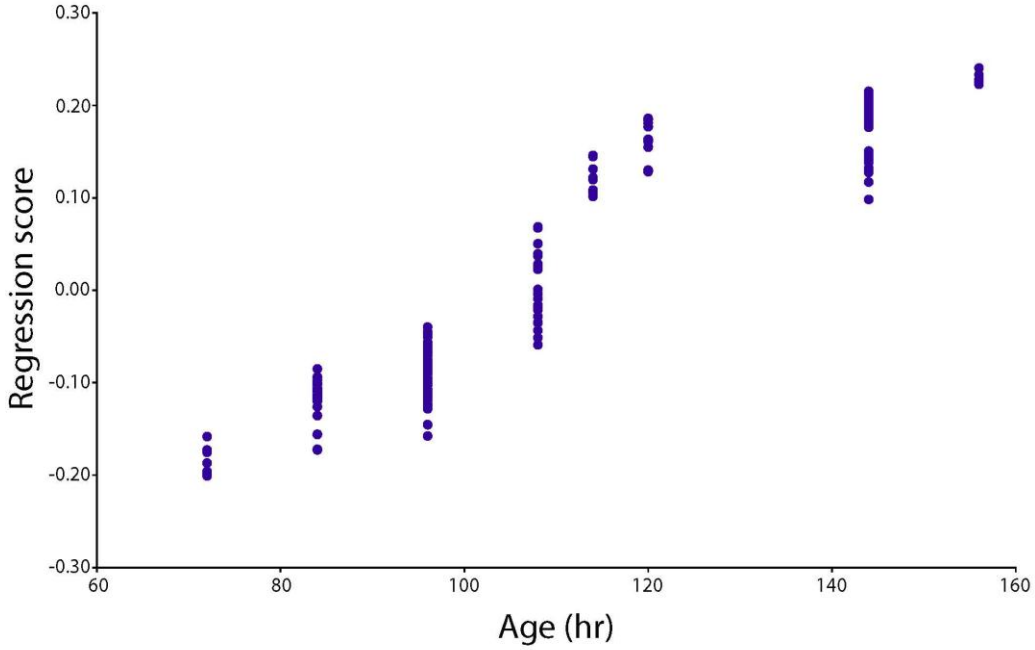

Figure 4.4: Facial shape variation related to age.

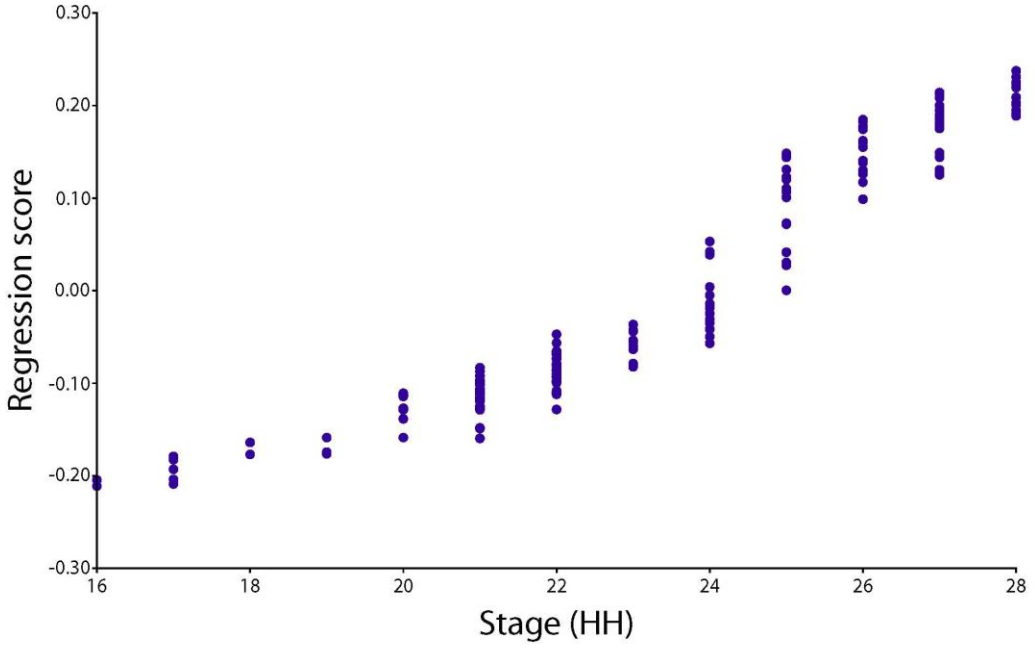

Figure 4.5: Facial shape variation within stages.

CHAPTER 5:

HYPOXIC CRANIOFACIAL MALFORMATIONS IN CHICK EMBRYOS

5.1 SUMMARY

Craniofacial anomalies can arise from genetic and/or environmental factors, including prenatal hypoxia. Recent clinical evidence correlates hypoxia to craniofacial malformations. However the mechanisms by which hypoxia mediates these defects are not yet understood. We examined the cellular mechanisms underlying malformations induced by hypoxia using a hypoxic chicken embryo model. Chicken eggs were incubated in hypoxia (7%, 9%, 11%, 13%, 15%, 17%, or 19% O2) or normoxia (21% O2). Embryos (days 3 to 6) were photographed for morphological analysis. For analysis of skeletal development, 13-day embryos were cleared and stained in alcian blue and alizarin red for cartilage and bone, respectively. Quantitative analysis of facial shape variation was performed on images of embryos via geometric morphometrics. Early stage embryos (2 days) were analyzed for apoptosis via whole-mount and section TUNEL staining and immunostained for cleaved caspase 3. Later stage embryos (day 6) were sectioned in paraffin for analysis of cell proliferation (BrdU) and apoptosis (TUNEL). Cellular response to metabolic stress was assessed by phospho-AMPK immunohistochemical staining. The survival of hypoxic embryos was reduced in a step-wise manner in comparison to normoxic control embryos. Hypoxic embryos displayed a spectrum of craniofacial anomalies, from mild asymmetry and eye defects to more severe frontonasal and cephalic anomalies. Skull bone development was delayed in hypoxic embryos, with some skeletal defects observed. Morphometrics showed abnormal facial shape variation in relation to centroid size and age among individuals in hypoxic groups

versus the normoxic population. Hypoxia disrupted cell proliferation, and in early stage embryos, caused apoptosis of neural crest progenitor cells. Hypoxic embryos also displayed increased metabolic stress response. These results indicate that hypoxia, during early embryonic craniofacial development, may induce cellular oxidative stress, leading to apoptosis of neural crest progenitor cells that are important to craniofacial morphology.

5.2 RESULTS

5.2.1 HYPOXIA REDUCES SURVIVAL OF EMBRYOS

The survival of embryos incubated in hypoxia (7, 9, 11, 13%, 15%, 17%, and 19% O_2) to day 6 was compared to that of normoxic (21% O_2) controls, in order to assess whether hypoxia increased embryonic mortality. Compared to the 93% survival rate of normoxic embryos, the survival of hypoxic embryos was reduced (Table 5.1) in a stepped pattern as follows. All hypoxic groups were significantly different from the normoxic group. There were small but significant differences in survival between the normoxic, 15%, 17%, and 19% O2 levels. The survival rates of the 9%, 11%, and 13% O2 groups were significantly lower than the higher O2 doses; there was no statistical difference in survival between the 11% and 13% O2 groups while there was a significant difference between the 11% and 9% O2 groups. All significance was $p<0.0001$. There were no survivors at 7% (ie, the nonviable level) by 6 days. Consequently there was a plateau below 15% O2, comprising the oxygen levels below that point.

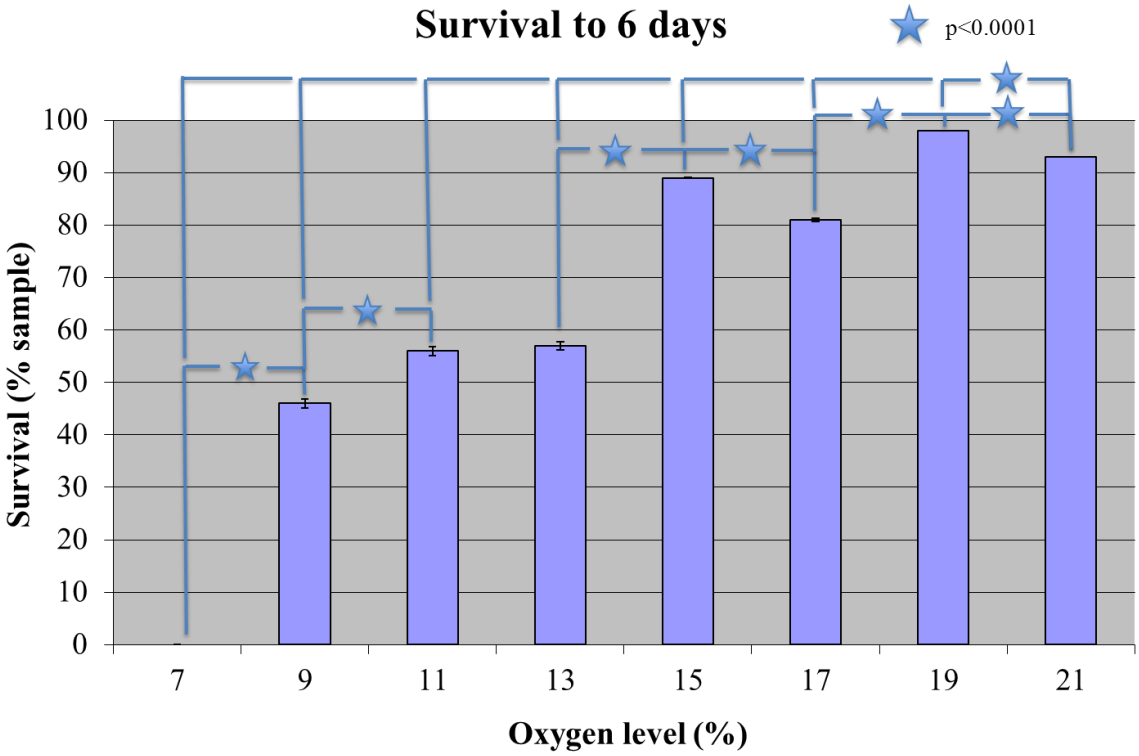

Table 5.1: Hypoxia reduces embryonic survival. *There are small but significant differences in survival between normoxia, 19%, 17%, and 15%. Survival at 13% O2 and below is significantly reduced, and 7% O2 is nonviable. Significance: p<0.0001. Sample size for each oxygen group: 7% (n=50), 9% (n=50), 11% (n=50), 13% (n=60), 15% (n=54), 17% (n=42), 19% (n=50), 21% (n=67).*

5.2.2 HYPOXIA ALTERS CRANIOFACIAL MORPHOLOGY

A morphological analysis was performed on normoxic and chronic hypoxic embryos collected on days 4 and 6 to examine the effect of hypoxia on their craniofacial morphology. Compared to normoxic embryos, hypoxic embryos exhibited developmental delay and a spectrum of cephalic and facial anomalies (Fig. 5.1 for 4-day and Fig. 5.2 for 6-day embryos). Mild defects included asymmetry of the head (Fig. 5.1B, E, F, I, J; 5.2B, E, H, I) and eye defects including unilateral or bilateral microphthalmia and

anophthalmia (Fig. 5.1B, E, F, I, J; 5.2B, E, H, I). More severe malformations included frontonasal and midline defects (Fig. 5.1C, D, G; 5.2C, F, J) and brain anomalies including anencephaly, microcephaly, and exencephaly (Fig. 5.1C, D, G; 5.2C, F, J). A minority of hypoxic embryos were sufficiently malformed to lack any recognizable facial or cephalic structures (Fig. 5.2D, G). There was no correlation between the level of hypoxia and severity of defects. While the heads of hypoxic embryos were developmentally delayed and malformed, there were no abnormalities observed with the bodies (Fig. 5.3).

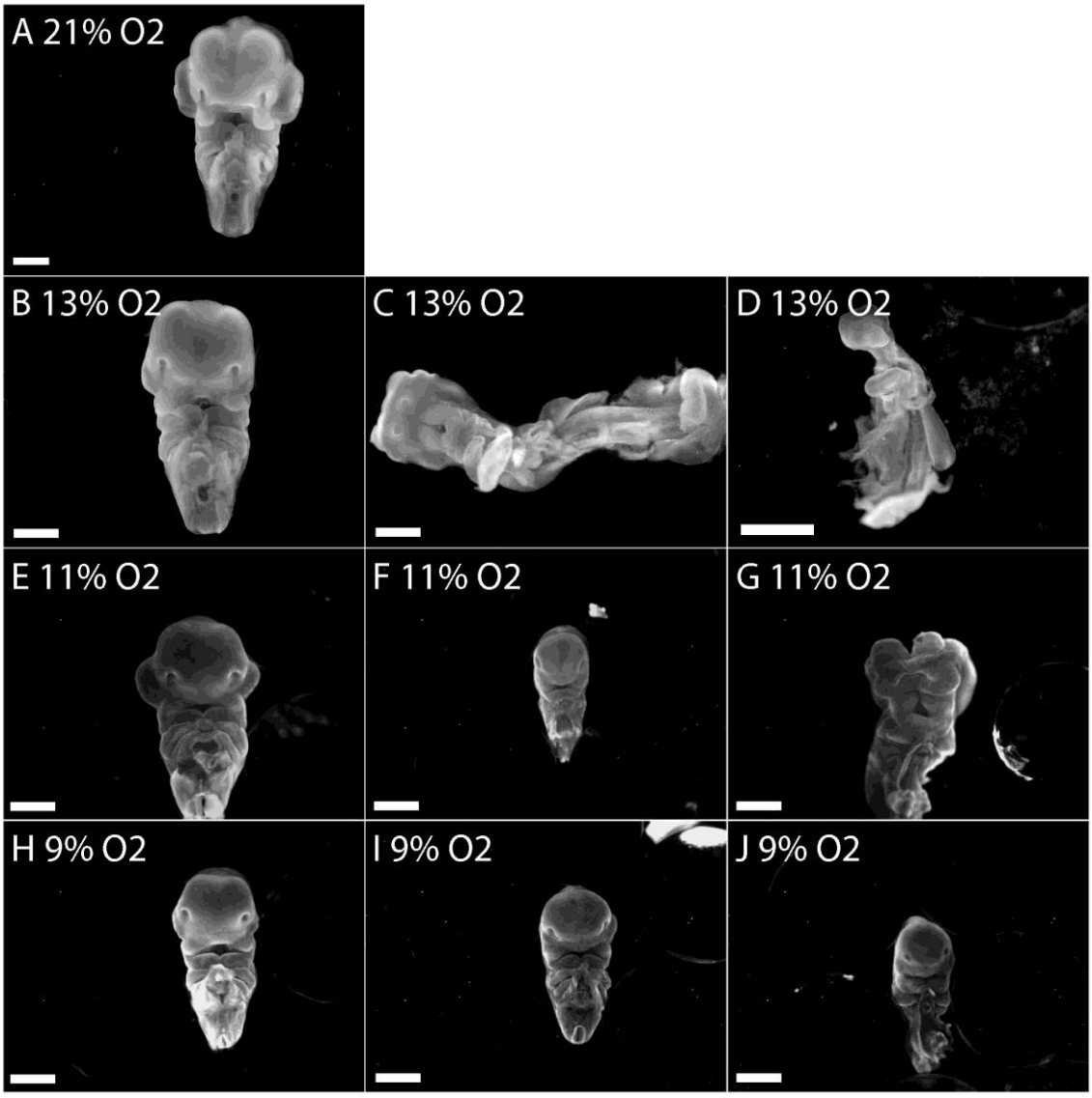

Figure 5.1: Hypoxia creates abnormal craniofacial morphology (day 4). (A) *Normoxic control, day 4,* ***(B-D)*** *13% O2,* ***(E-G)*** *11% O2,* ***(H-J)*** *9% O2.* ***(B, E, F, H, I, J)*** *Developmental delay, asymmetry, and eye defects.****(C, D, G)*** *Severe anomalies include neural tube defects and midline defects. Scale bar: 1mm.*

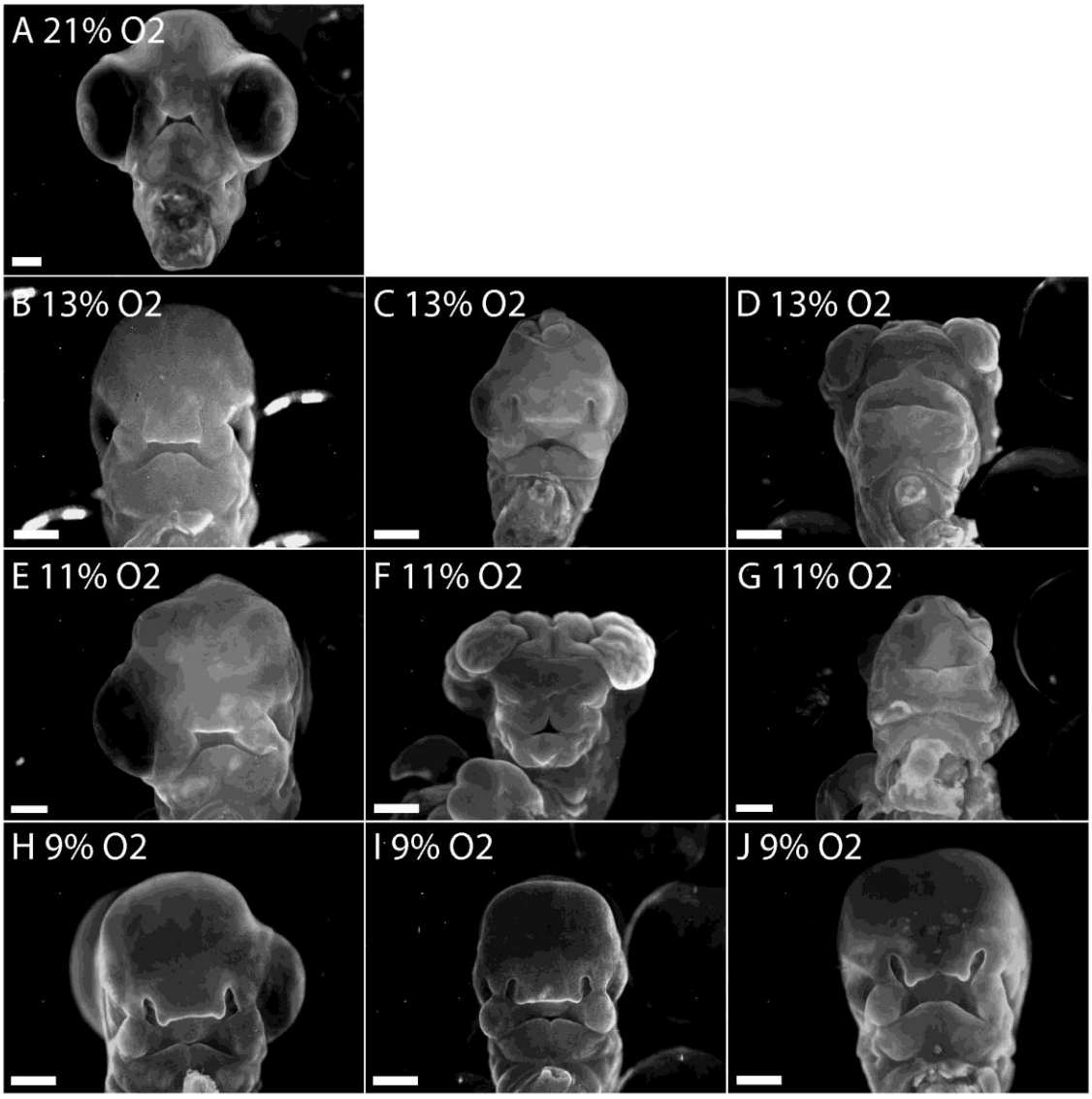

Figure 5.2: Hypoxia creates abnormal craniofacial morphology (day 6). (A) *Normoxic control, day 6,* ***(B-D)*** *13% O2,* ***(E-G)*** *11% O2,* ***(H-J)*** *9% O2.* ***(B, E, H, I)*** *Developmental delay, asymmetry, and eye anomalies.* ***(C, F, J)*** *Severe malformations include brain and neural tube defects and midline anomalies. Two embryos* ***(D, G)*** *are sufficiently malformed to lack recognizable facial landmarks. Scale bar: 1mm.*

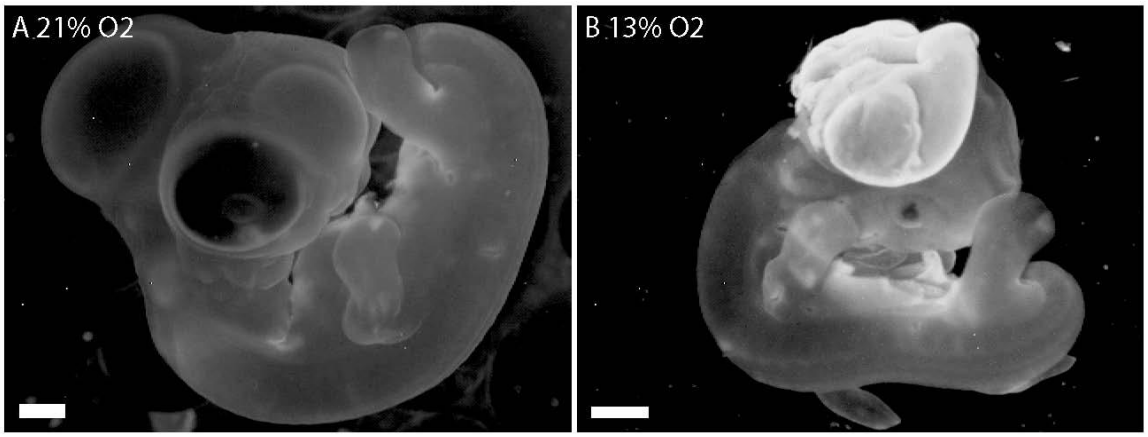

Figure 5.3: The head, not the body, is vulnerable to hypoxia-induced malformations. ***(A)*** *Normoxic control embryo, day 6. Hypoxic 6-day embryo* ***(B)*** *has normal body while head is malformed. Scale bar: 1mm.*

A similar morphological analysis was performed on acute hypoxic embryos (incubated in 9% O2 for 24 hours from 0-24 hours, 24-48 hours, 48-72 hours, 72-96 hours, or 96-120 hours of development). All acute hypoxic embryos were developmentally delayed (Fig. 5.4A-T). None of the embryos in the 0-24 hour hypoxic group were malformed (Fig. 5.4A-D). 50% of surviving embryos in the 24-48 hour hypoxic group had varying degrees of malformation (Fig. 5.4F-H), ranging from asymmetry and ophthalmic defects (Fig. 5.4F) to very severe anomalies including holoprosencephaly (Fig. 5.4G) and one was sufficiently grossly malformed as to obliterate all facial features (Fig. 5.4H). In the 48-72 hour group, 60% showed a similar range of malformations (Fig. 5.4I-L) to those observed in the 24-48 hour group. Embryos in the 72-96 hour (Fig. 5.4M-P) and 96-120 hour (Fig. 5.4Q-T) groups showed very mild (Fig. 5.4N-P; R-T) or no malformations.

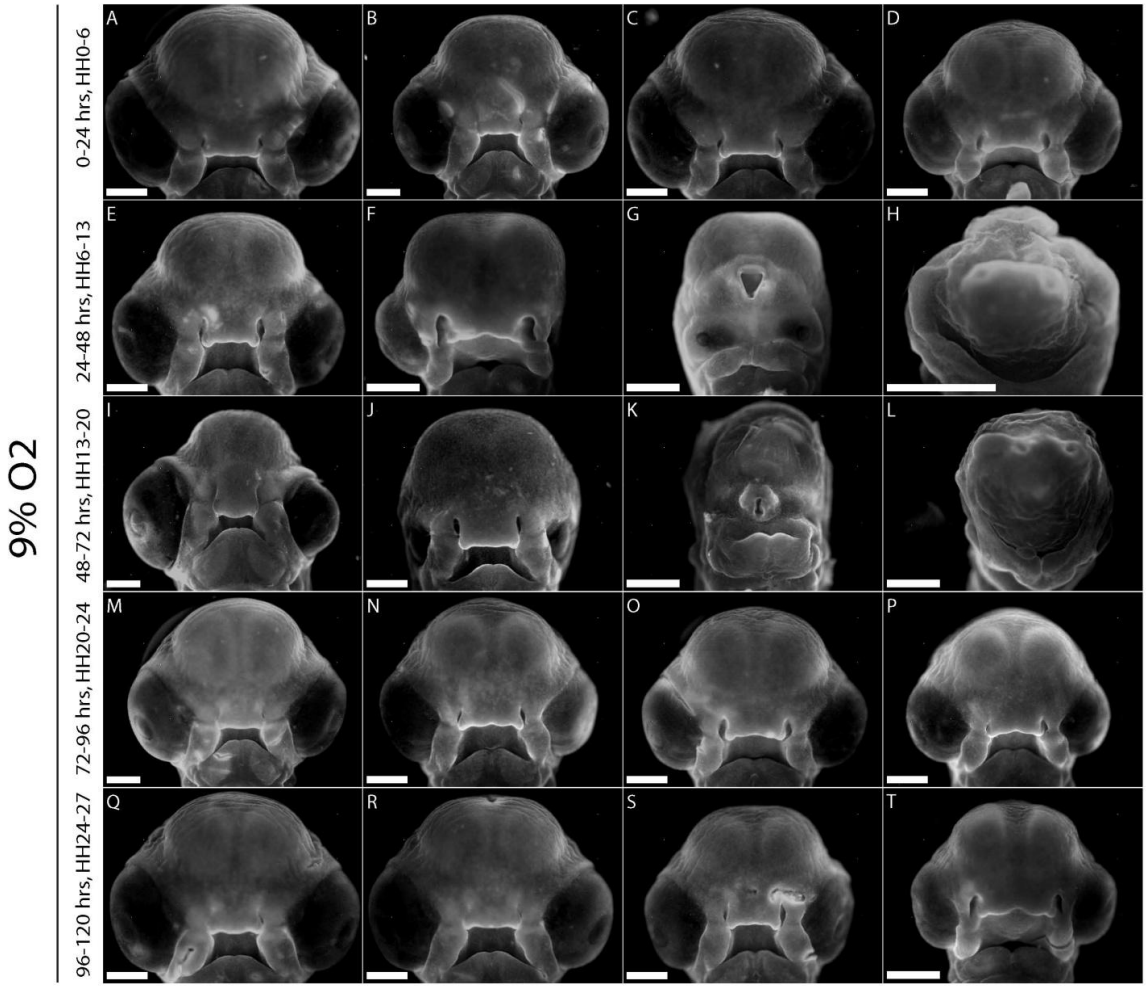

Figure 5.4: Acute hypoxia (24 hour windows). (A-D) *Hypoxic from 0-24 hours, no malformations.* ***(E-H)*** *Hypoxic from 24-48 hours. Malformations include:* ***(F)*** *left anophthalmia,* ***(G)*** *moderate holoprosencephaly,* ***(H)*** *no recognizable facial structures.* ***(I-L)*** *Hypoxic from 48-72 hours. Malformations include:* ***(I)*** *smaller left eye,* ***(J)*** *bilateral microphthalmia,* ***(K)*** *severe holoprosencephaly with proboscis,* ***(L)*** *facial obliteration.* ***(M-P)*** *Hypoxic from 72-96 hours, none severely malformed, but developmental delay is evident.* ***(Q-T)*** *Hypoxic from 96-120 hours; no malformations but developmental delay apparent. Scale bar: 1mm.*

A similar experiment was subsequently performed in which eggs were incubated in 12-hour acute hypoxic periods in 9% O2 (24-36 hours, 36-48 hours, 48-60 hours, or 60-

72 hours). All the hypoxic individuals displayed varying developmental delay (Fig. 5.5A-P). Only 35% (7 of 20) of the first group (hypoxic from 24-36 hours) survived, and exhibited mild anomalies including unilateral microphthalmia (Fig. 5.5D). The second group (hypoxic from 36-48 hours) had a better survival rate of 65% (13 of 20), but showed the most severe malformations, including unilateral microphthalmia (Fig. 5.5F), exencephaly combined with midline defects, hypotelorism, and bilateral microphthalmia (Fig. 5.5G), and facial obliteration (Fig. 5.5H). 75% (15 of 20) of the third group (48-60 hours) survived, with varying degrees of cephalic asymmetry, microphthalmia, and anophthalmia (Fig. 5.5J-L). The final group, hypoxic from 60-72 hours, had 85% (17 of 20) survival and no malformations (Fig. 5.5M-P).

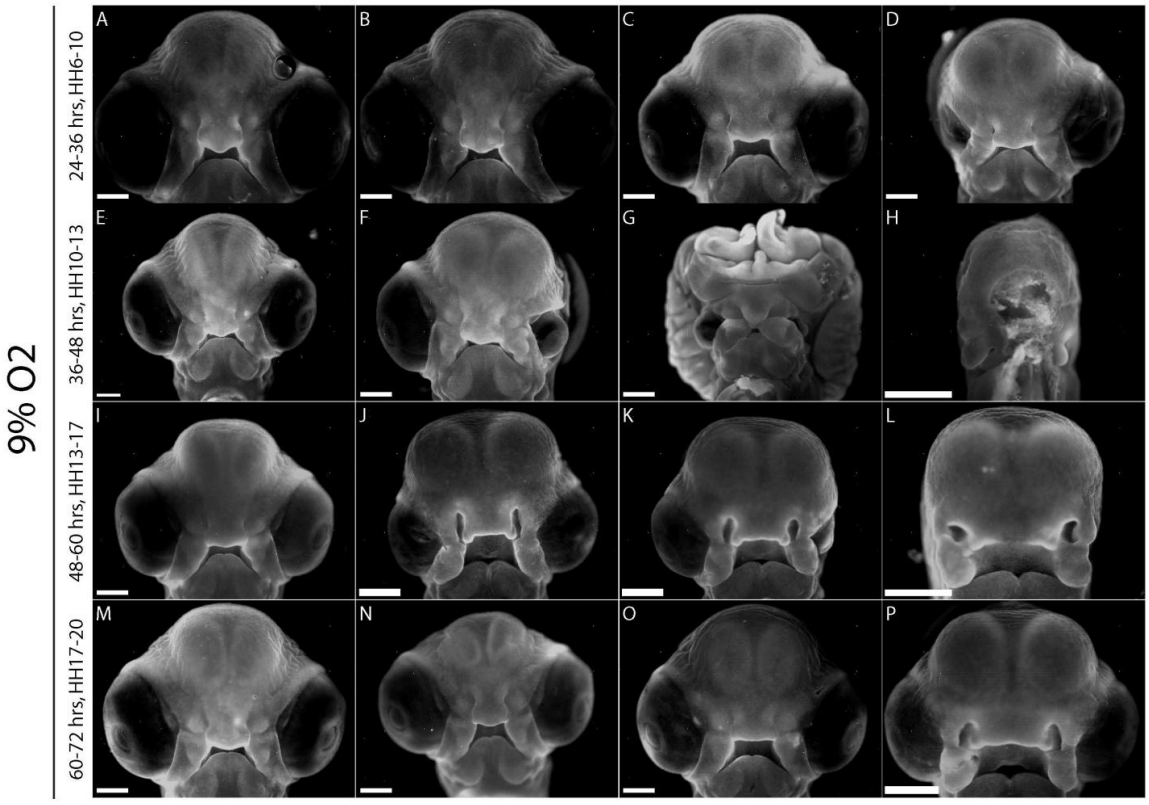

Figure 5.5: Acute hypoxia (12 hour windows). (A-D) *Hypoxic from 24-36 hours.* ***(D)*** *Right microphthalmia.* ***(E-H)*** *Hypoxic from 36-48 hours. Severe malformations:* ***(F)*** *left*

microphthalmia, ***(G)*** *exencephaly, bilateral microphthalmia, hypotelorism, and midline defects, and* ***(H)*** *lack of recognizable facial characteristics.* ***(I-L)*** *Hypoxic from 48-60 hours. Milder anomalies include asymmetry and eye defects* ***(J-L)****.* ***(M-P)*** *Hypoxic from 60-72 hours, developmental delay but no malformations. Scale bar: 1mm.*

Hematoxylin and eosin (H&E) staining revealed that normoxic embryos (Fig. 5.6A) had normal division of the forebrain and normal facial structure (Fig. 5.6B-E). Those hypoxic embryos with mild phenotypes (Fig. 5.6F) still had normal forebrain division, but displayed eye defects (eg, unilateral anophthalmia) and asymmetric facial and cephalic morphology (Fig. 5.6G-J). A minority of hypoxic embryos were severely malformed (Fig. 5.6K) and displayed gross cephalic anomalies including exencephaly with no forebrain cavity or division (Fig. 5.6L-O) along with eye and facial defects.

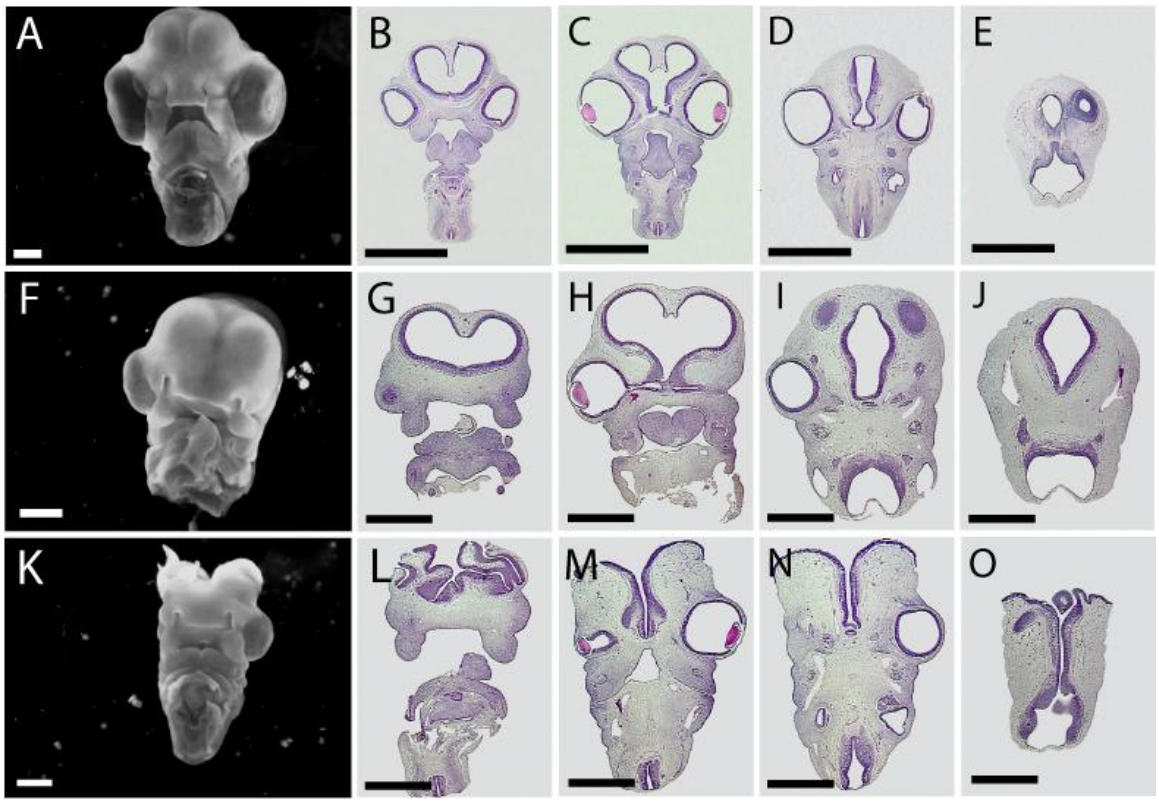

Figure 5.6: Histology of normoxic and hypoxic embryos. *A normoxic embryo* ***(A)*** *has normal forebrain division, facial tissue structure, and eyes* ***(B-E)****. A hypoxic embryo with mild anomalies* ***(F)*** *displays normal forebrain division, but shows cephalic asymmetry and left anopththalmia* ***(G-J)****. A hypoxic embryo with a severe phenotype* ***(K)*** *lacks forebrain cavity or division, and displays exencephaly and right microphthalmia. Scale bar: 1mm.*

5.2.3 HYPOXIA ALTERS CRANIOFACIAL SKELETAL DEVELOPMENT

Eggs were incubated to day 13 in either normoxia or hypoxia (9%, 11%, 13%, 15%, or 17% O2), and cleared and stained for cartilage and bone. No embryos survived at 9% O2 to day 13. Compared to the normal skull structure of normoxic embryos (Fig. 5.7A), hypoxic embryos showed reduction in ossification to varying degrees in nearly all supramandibular bones (and the frontal, jugal, and palatine to a somewhat lesser degree) (Fig. 5.7B-M), with a number of embryos displaying orbital and maxillary defects (Fig. 5.7F, H, K).

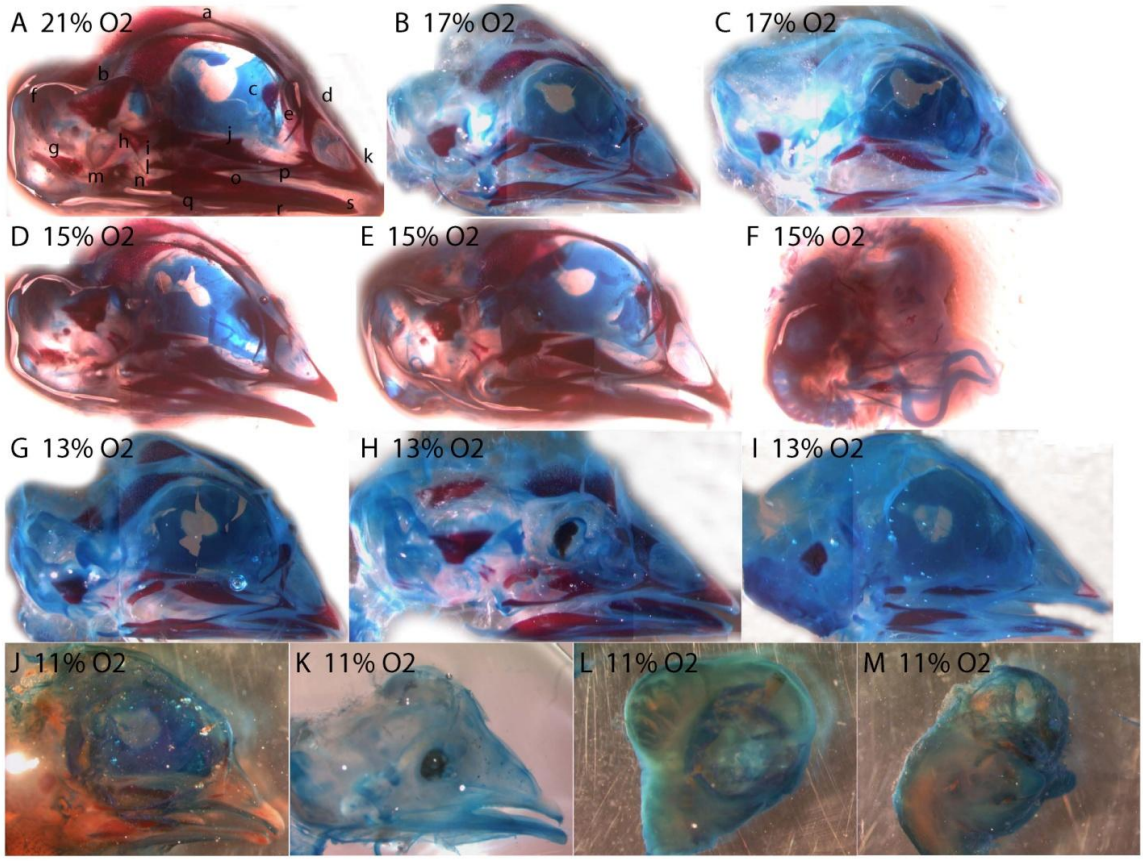

Figure 5.7: Hypoxia delays skull development. ***(A)*** *Normoxic control, 13 days.* ***(B, C)*** *17% O2.* ***(D-F)*** *15% O2.* ***(G-I)*** *13% O2.* ***(J-M)*** *11% O2. Some individuals* ***(F, H, K)*** *show skeletal anomalies including orbital defects and upper beak defects. Alizarin red (bone) and alcian blue (cartilage). Bones in* ***(A)****:* ***a*** *frontal,* ***b*** *parietal,* ***c*** *ethmoid,* ***d*** *nasal,* ***e*** *prefrontal,* ***f*** *supraoccipital,* ***g*** *exoccipital,* ***h*** *quadrate,* ***i*** *petrosal,* ***j*** *palatine,* ***k*** *premaxilla,* ***l*** *quadratojugal,* ***m*** *otic,* ***n*** *articular,* ***o*** *surangular,* ***p*** *jugal,* ***q*** *angular,* ***r*** *dentary,* ***s*** *splenial*

5.2.4 HYPOXIA LEADS TO ABNORMAL FACIAL SHAPE VARIATION

Two-dimensional geometric morphometric analysis was performed on normoxic and hypoxic embryos (in all groups from 9% to 19% O2) to determine whether hypoxia created abnormal facial shape variation. 45 craniofacial landmark coordinates were

assigned on two-dimensional images of embryos according to Chong et al [90]. After Procrustes superimposition of the landmarks on all the sampled embryos, a principal components analysis (PCA), corrected to remove size as a factor, was performed to find the two variables (principal components) that accounted for the greatest change in facial shape between individuals in the hypoxic and normoxic populations. The PCA demonstrated that while normoxic embryos were separated mainly along PC2 (size and proportionality of facial features), hypoxic embryos were differentiated along both PC2 and PC1 (shape of eyes, FNP, maxillary processes, nasal pits, and forebrain) (Fig. 5.8).

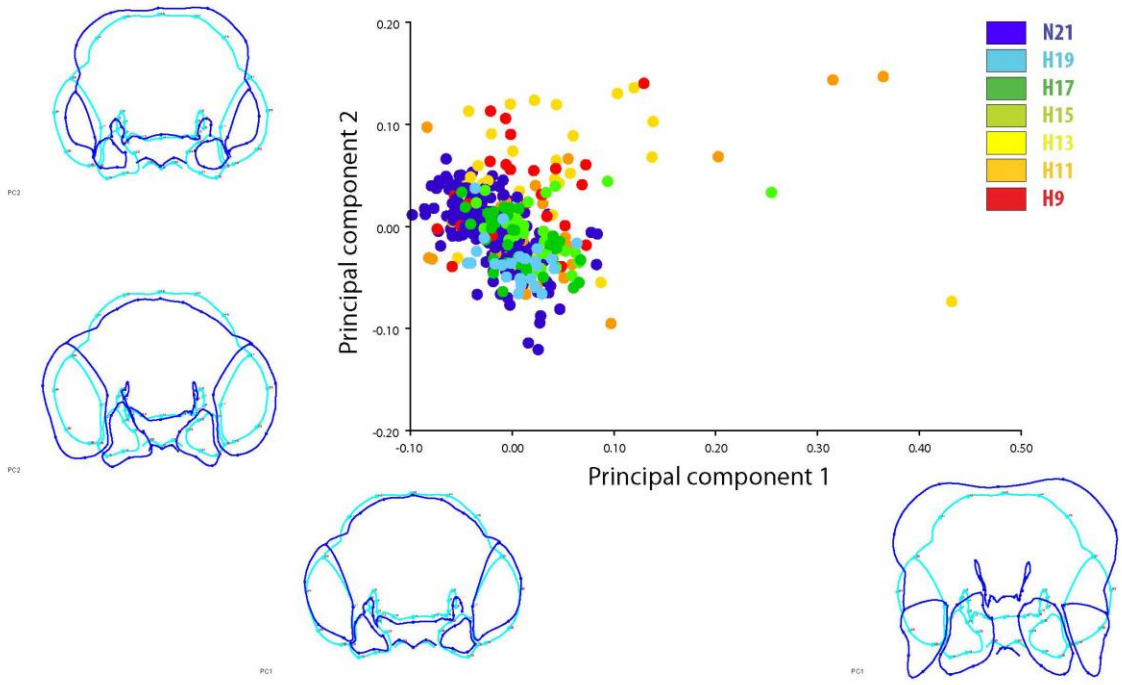

Figure 5.8: Principal components analysis (PCA). *Craniofacial shape variation along PC1 and PC2 in normoxic (purple, 21% O2) and hypoxic embryos (9%-19% O2). Normoxic embryos are separated along PC2 (change in size and proportion of craniofacial structures), while hypoxic embryos are separated along PC1 (abnormal*

shape variation in forebrain, frontonasal process, nasal pits, eyes, and maxillary processes) as well as PC2.

Regression analysis was performed to quantify the facial shape variation in hypoxic embryos (9%, 11%, 13%, 15%, 17%, and 19% O2) compared to normoxic controls in relation to centroid size and age in hours. Normoxic embryos were observed to fall along a well-defined, nonlinear curve of normal growth, representing normal facial shape variation in relation to size (Fig. 5.9), however hypoxic embryos deviated from this normal growth trajectory. While many fell along the curve, others fell off the curve (examples shown in Fig. 5.9A-G). There was a roughly dose-dependent effect of hypoxia on the position of the groups of embryos on the curve. The 19% O2 embryos did not deviate from the normoxic growth curve in either direction, and were closest to the far right end of the curve. The 17% and 15% O2 embryos deviated slightly from the curve, and rested just to the left of the 19% O2 group. The 11% and 13% O2 groups deviated the most (ie, comprised the majority of outliers) from the normal trajectory, and were more spread out along the curve. The 9% O2 embryos were distributed over most of the length of the curve, but did not show as large a deviation from the normal trajectory as did the 11% and 13% O2 embryos (Fig. 5.9).

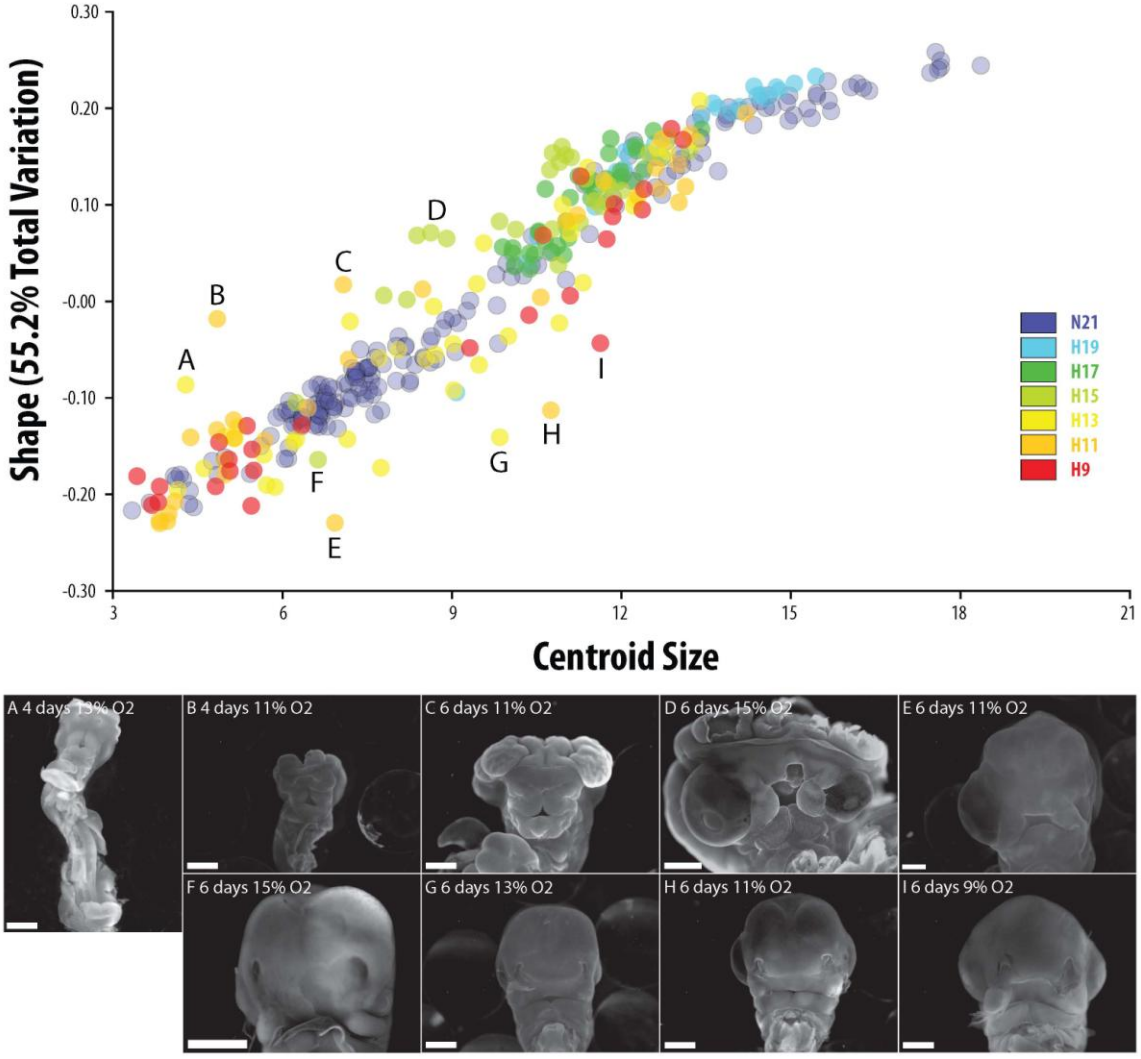

Figure 5.9: Facial shape variation in relation to centroid size. *While normoxic embryos form a normal growth trajectory, hypoxic embryos deviate from this normal growth curve. Outliers marked A-G are represented in the photos. Scale bar: 1mm.*

Next, the PC1 shape scores (residuals of shape versus age) were compared against the oxygen percentage in order to examine whether the oxygen dose affected the shape variation. The normoxic and 19% O2 hypoxic embryos were not appreciably different in shape score (Fig. 5.10). However, along the curve from 17% O2 and below, the hypoxic embryos were reduced in their PC1 shape scores compared to the 19% O2 and 21% O2 groups (Fig. 5.10). The curve leveled off between 9% and 13% O2, although there was

no appreciable difference in scores among the embryos in the 9% through 17% O2 groups (Fig. 5.10).

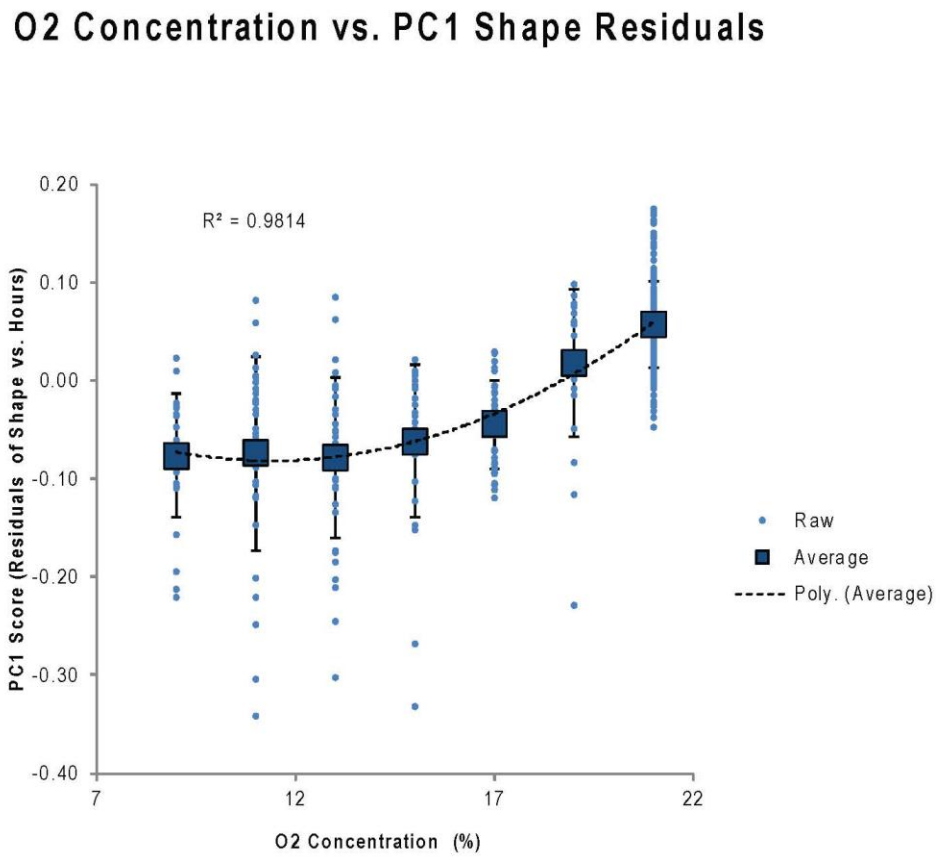

Figure 5.10: Comparison of PC1 shape scores according to oxygen concentration. *While there is no difference between the normoxic (21% O2) and 19% O2 hypoxic embryos in shape score, hypoxic embryos from 17% O2 and below have lower mean shape values than the 19% O2 and normoxic embryos.*

Further analyses were performed to compare the shape and centroid size scores versus oxygen dose at two timepoints (96 and 144 hours of incubation). The 96-hour group encompassed 9%, 11%, 13%, and 21% O2 embryos (since these were the only oxygen levels represented by embryos collected at 96 hours). The 144-hour group consisted of

the entire range of oxygen levels (9%, 11%, 13%, 15%, 17%, 19%, and 21% O2), since the additional hypoxic groups (15%, 17%, and 19% O2) comprised only 144-hour embryos (there were no 96-hour embryos from these oxygen levels). At 96 hours, the shape scores of 9%, 11%, and 13% O2 embryos were lower than those at 21% O2, describing a linear trajectory (Fig. 5.11, top left). At 144 hours, the trajectory was a more sinuous curve. The shape scores of the 21% and 19% O2 groups were not different, however, the scores of all groups at and below 17% O2 were reduced; the curve slightly leveled off (with a shallower downward slope) from 17% down to 9% O2 (Fig. 5.11, top right). At 96 hours, the centroid size scores of the 9%, 11%, and 13% O2 groups were lower than the normoxic controls; again the trajectory was linear (Fig. 5.11, bottom left). At 144 hours, the trajectory was sinuously curved. The centroid size scores of the 19% and 21% O2 groups were not different from each other, but the centroid size scores of the lower oxygen groups (17% O2 and below) were lower compared to the 19% and 21% O2 groups (Fig. 5.11, bottom right). The curve leveled off below 19% O2, forming a plateau with no further downward slope (Fig. 5.11, bottom right).

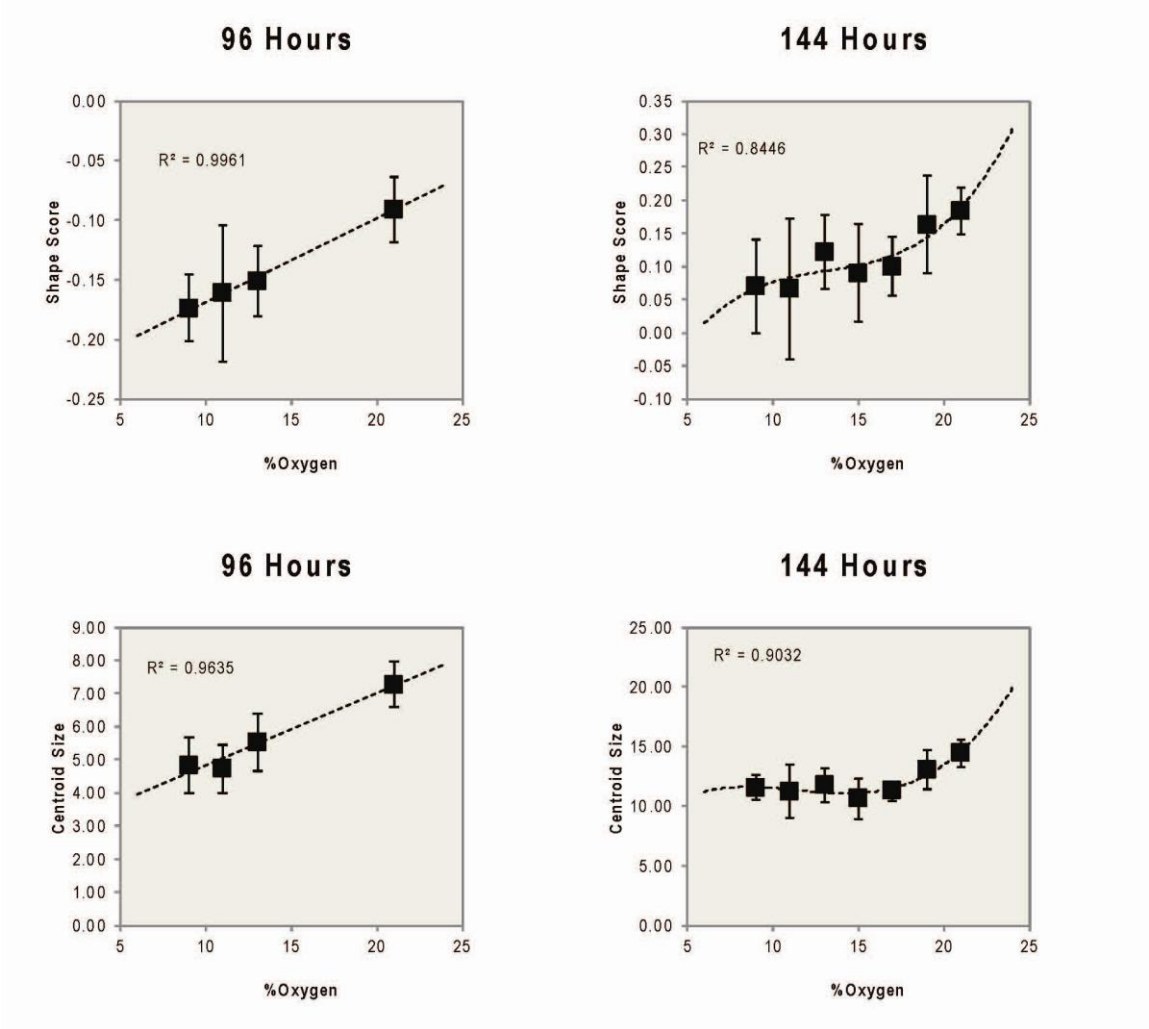

Figure 5.11: Comparison of shape and centroid size scores by oxygen concentration. ***(Top)*** *Shape scores versus oxygen concentration at 96 hours (left) and 144 hours (right).* ***(Bottom)*** *Centroid size scores versus oxygen concentration at 96 hours (left) and 144 hours (right).*

In comparison to age-matched normoxic control embryos, hypoxic embryos were developmentally delayed (Fig. 5.12). At 96 hours, there was no appreciable difference in delay between the 9%, 11%, and 13% O2 groups of embryos (these were the only hypoxic groups tested at this timepoint), although all of them were delayed behind the normoxic embryos. However, at 144 hours, the 19% O2 embryos were not delayed

relative to the normoxic controls. The other groups (9%, 11%, 13%, 15%, and 17% O2) were delayed compared to the normoxic individuals (Fig. 5.12); there was no difference between the hypoxic groups.

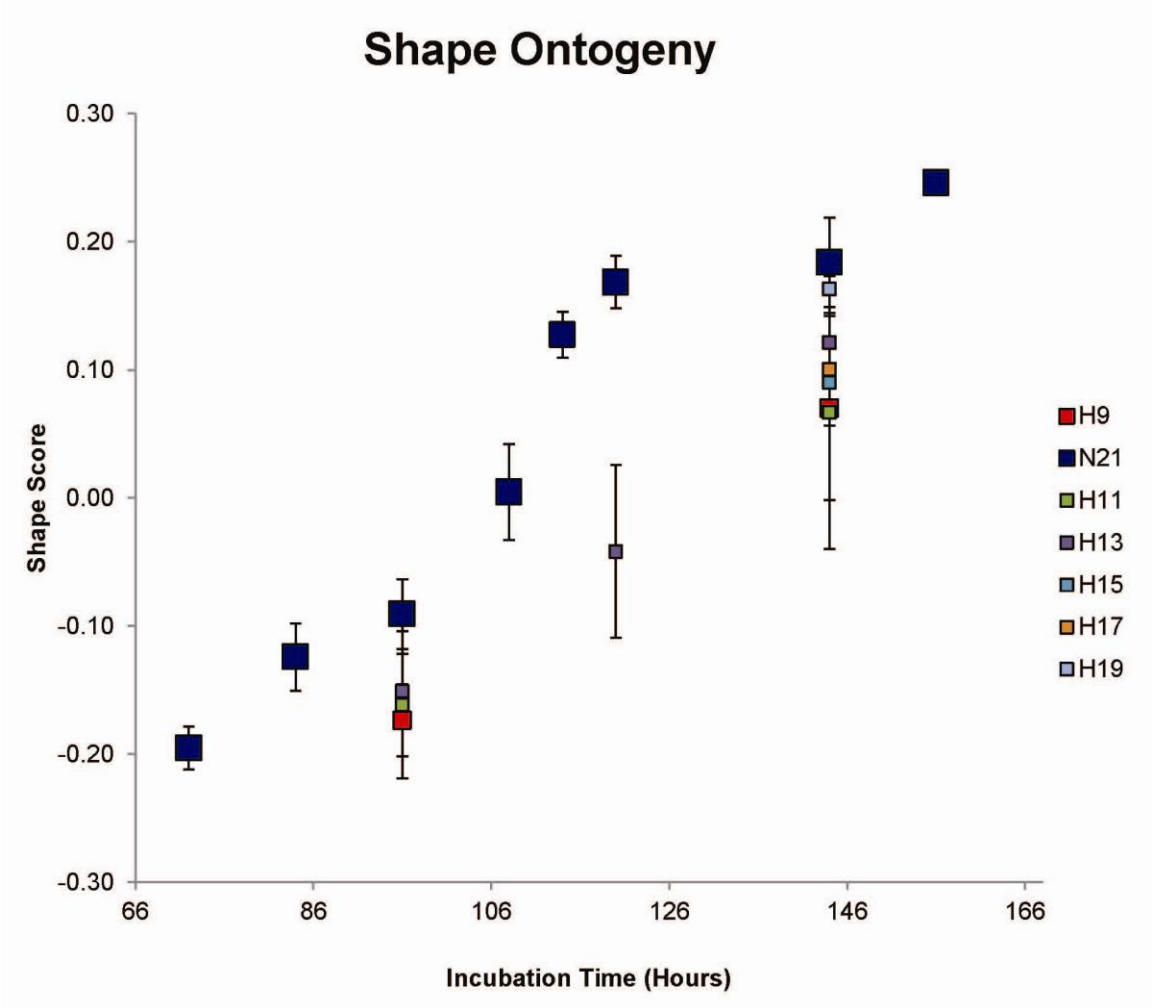

Figure 5.12: Developmental delay in hypoxic embryos. *Compared to age-matched normoxic control embryos (dark blue, 21% O2), hypoxic embryos are developmentally delayed.*

5.2.5 CELL PROLIFERATION AND APOPTOSIS IN HYPOXIC EMBRYOS

Cell behavior analyses were undertaken to explain whether the abnormal phenotypes observed in hypoxic embryos could be explained by changes in cell proliferation and

death in the cephalic and facial tissues. In early stage (HH8-10) embryos, apoptosis was analyzed via whole-mount TUNEL staining. Compared to normoxic embryos (Fig. 5.13A), which showed no apparent apoptosis, hypoxic embryos (at 13% O_2) exhibited varying amounts of neural crest progenitor cell death in the dorsal neural tube (Fig. 5.13B-F). While some showed little or no apoptosis (Fig. 5.13B, C), others displayed larger amounts of cell death in the forebrain and neural folds (Fig. 5.13D-F).

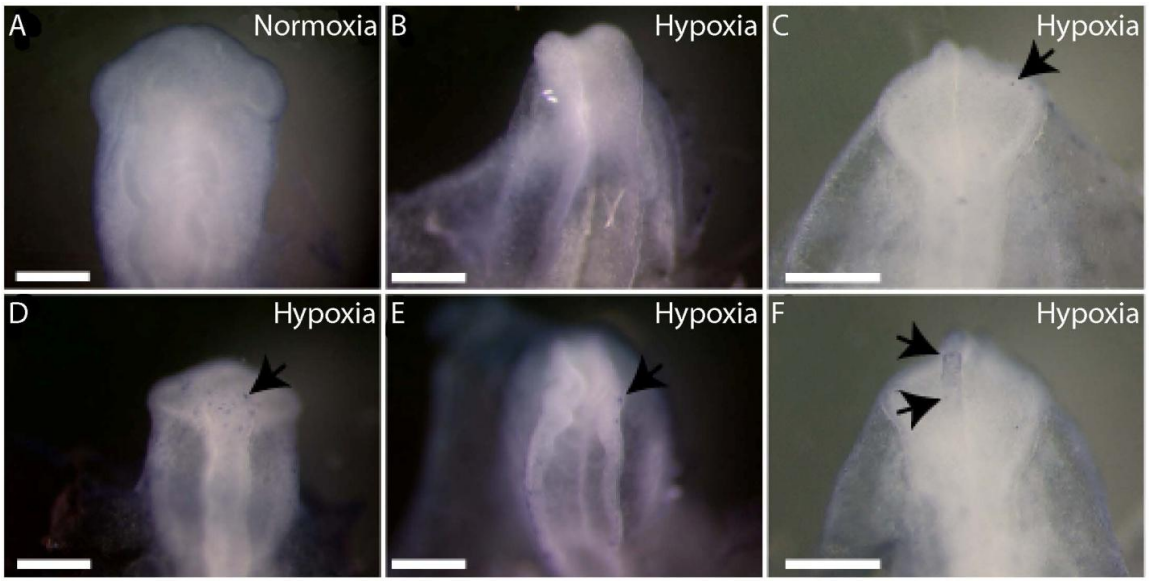

Figure 5.13: Neural crest progenitor cell death in hypoxic embryos (HH9-10). (A) *Normoxic embryo, no cell death.* ***(B, C)*** *Hypoxic embryos with little or no cell death.* ***(D-F)*** *Hypoxic embryos with significant apoptosis in forebrain and neural folds. Scale bar: 250μm.*

Since neuroapoptosis was apparent in whole-mount staining of embryos with TUNEL, embryos from the same timepoint were sectioned for fluorescent TUNEL analysis in order to confirm whether the cell death was indeed neuroepithelial in origin. Normoxic control embryos (Fig. 5.14A) displayed very little apoptosis in their neural tissues. Hypoxic embryos (Fig. 5.14B, C) showed increased cell death, particularly in the

neuroepithelial tissues in all cephalic regions (rhombencephalon, mesencephalon, and telencephalon), as well as in the ectoderm and mesoderm.

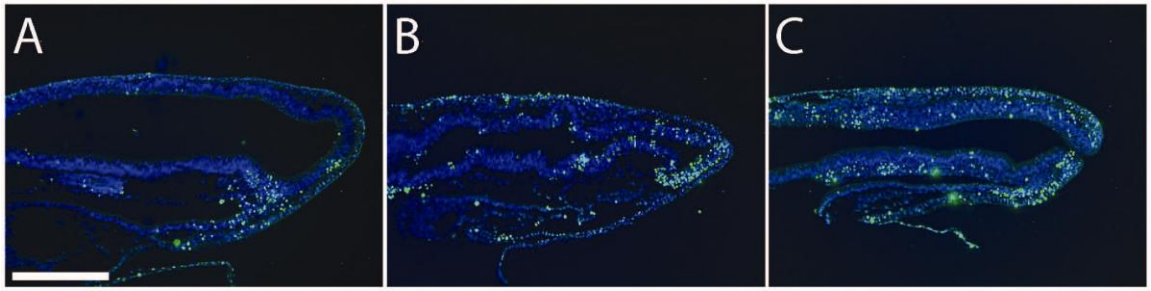

Figure 5.14: Neuroepithelial apoptosis in hypoxic embryos (HH9-10). (A) *Normoxic embryo, very little cell death in neuroepithelium.* ***(B, C)*** *Hypoxic embryos, increased apoptosis in all regions of the brain and in the ectoderm and mesoderm. Scale bar: 250μm.*

At this same timepoint, hypoxic embryos exhibited reduced cell proliferation in the neuroepithelial tissues of the head (Fig. 5.15B), compared to normoxic controls (Fig. 5.15A). To assess the presence of the cleaved form of caspase 3 (indicative of apoptosis), sections from the same embryos were stained for cleaved caspase 3. In comparison to normoxic embryos (Fig. 5.15C), hypoxic embryos (9% O2) showed more cleaved caspase 3-positive cells (Fig. 5.15D).

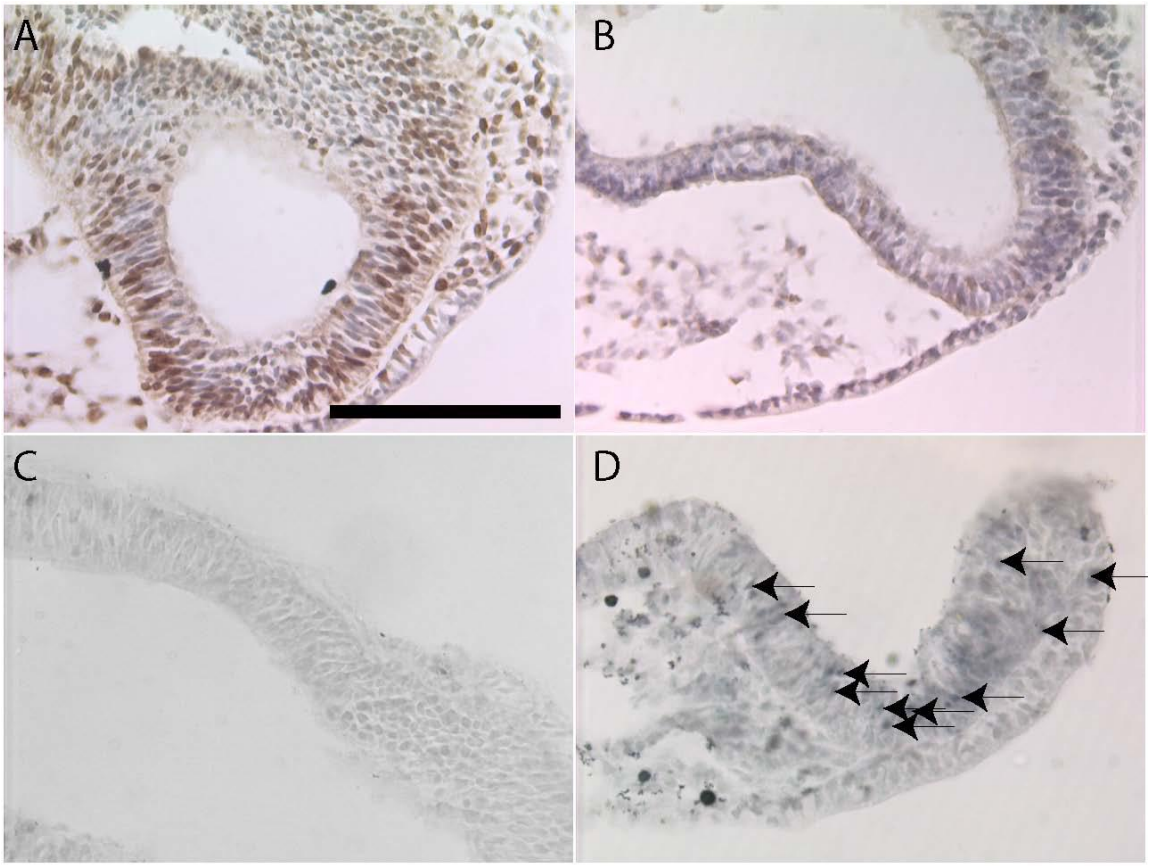

Figure 5.15: Reduced proliferation, increased activity of caspase 3 in neuroepithelial cells in hypoxic embryos (HH9-10). *Healthy proliferation of neuroepithelial cells (BrdU-positive cells) is evident in the normoxic embryo* ***(A)****, while there is reduced proliferation in the hypoxic neuroepithelium* ***(B)****. Compared to the normoxic control* ***(C)****, there are cleaved-caspase-3-positive cells present in the neuroepithelium of the hypoxic embryo* ***(D)****. Scale bar: 1mm.*

In a later stage of development (6 days), BrdU incorporation in sections of embryos was used to assess cell proliferation in frontonasal mesenchyme. Compared to normoxic 6-day embryos (Fig. 5.16A), age-matched hypoxic embryos showed reduced cell proliferation (Fig. 5.16B). Neither normoxic nor hypoxic embryos showed any evidence of apoptosis in the frontonasal mesenchyme (Fig. 5.16C, D).

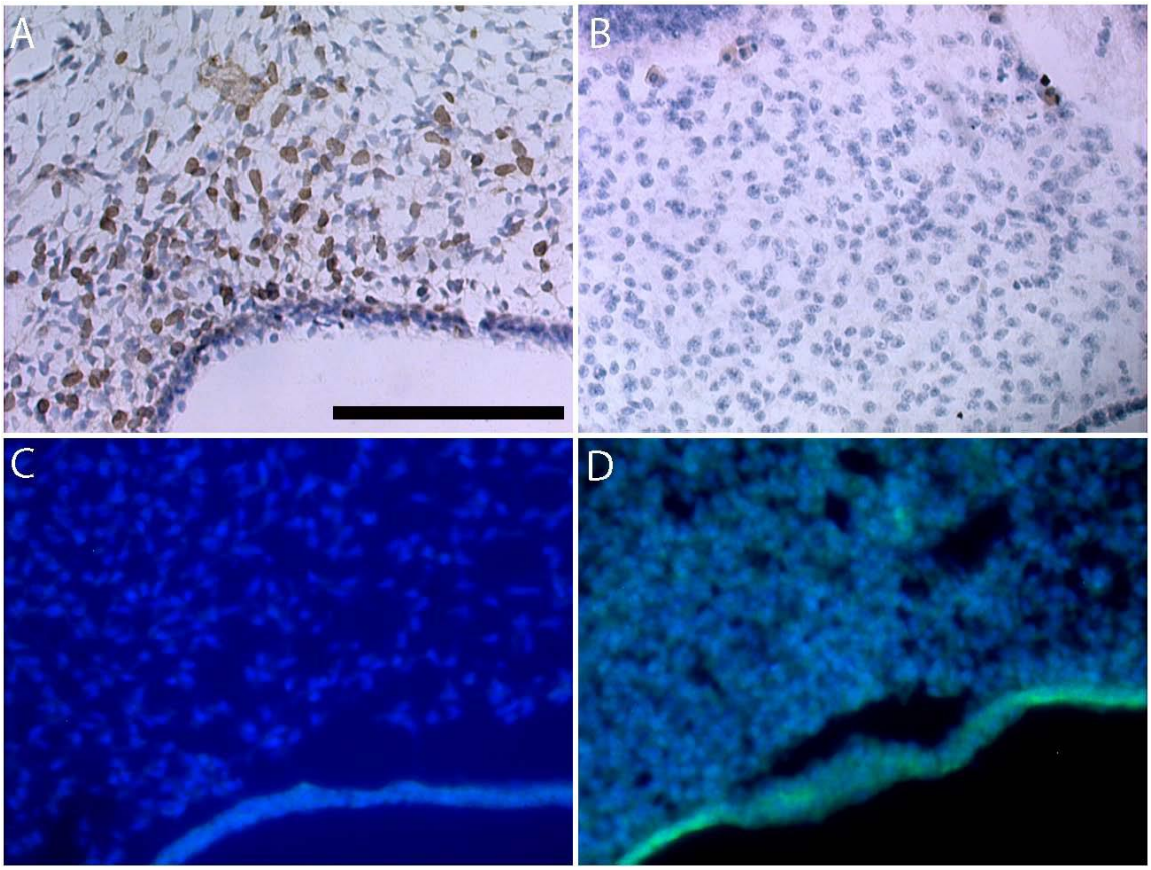

Figure 5.16: Cell proliferation and apoptosis at later stages (6 days). (A) *Large region of BrdU-positive cells in frontonasal mesenchyme of normoxic control embryo.* ***(B)*** *Lack of BrdU-positive cells in mesenchyme of hypoxic embryo. No apoptosis in frontonasal mesenchyme of normoxic* ***(C)*** *or hypoxic embryos* ***(D)****. Scale bar: 250μm.*

5.2.6 METABOLIC STRESS IN HYPOXIC EMBRYOS

Due to phenotypic variability, suggesting a generalized effect of hypoxia on craniofacial morphology, it was decided to address the possibility of cellular metabolic stress response to hypoxia. One marker of metabolic stress is the phosphorylated (activated) form of AMP-activated protein kinase (AMPK), a regulator of the ATP:AMP energy balance in the cell, activated by stressors including hypoxia. Immunohistochemistry was performed on normoxic and hypoxic embryo sections (2 and

6 days of development) using an antibody against phospho-AMPK. Although pAMPK staining was widespread in both normoxic and hypoxic embryos (Fig. 5.17A-D), we observed more cells with greater intensity of staining in the neuroepithelial tissues of hypoxic embryos at both 2 and 6 days (Fig. 5.17B, D) than in normoxic controls (Fig. 5.17A, C).

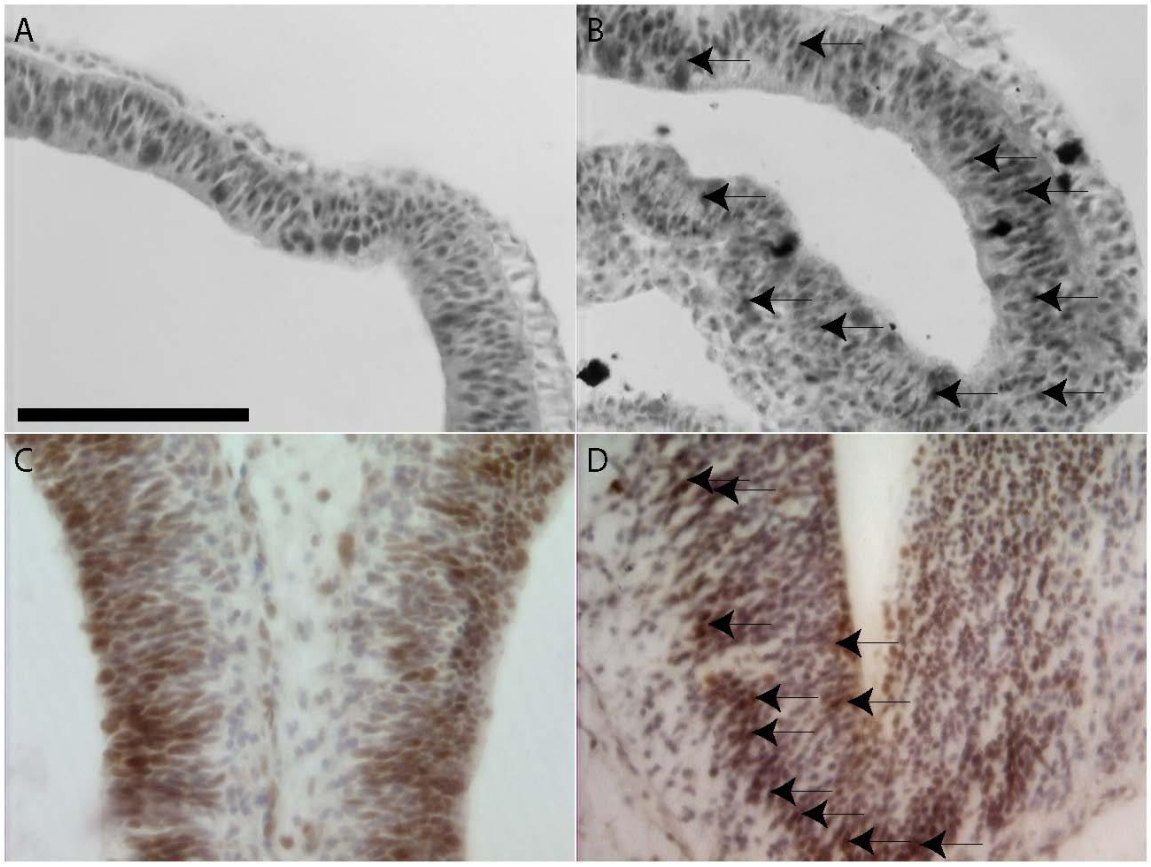

Figure 5.17: Metabolic stress in hypoxic embryos. (A, B) *2 days,* ***(C, D)*** *6 days. While pAMPK staining is widespread in both normoxic and hypoxic embryos* ***(A-D)****, there is intensified staining in the neuroepithelium of hypoxic 2-day* ***(B)*** *and 6-day hypoxic* ***(D)*** *embryos. Scale bar: 1mm.*

CHAPTER 6:

DISCUSSION

6.1 NORMAL FACIAL DEVELOPMENT IN CHICK EMBRYOS FOLLOWS A CONTINUUM

Historically, the classification of avian embryos over the course of development has relied on chronological age. However the main disadvantage of chronological staging has been the significant variation in size and shape observed among embryos within any given age. The Hamburger and Hamilton staging system was designed to classify embryos into discrete stages based on distinct morphological characteristics including somite number and size and shape of anatomical landmarks. However, Hamburger and Hamilton staging does not account for natural size and shape variation among embryos within a stage.

Of particular importance to this current work is the change in craniofacial form over the time course of development in avian embryos in normal and adverse conditions. In the study of normal craniofacial ontogeny of chick embryos, the goal was to trace the normal growth trajectory over time during chick development, in order to determine whether chick embryonic craniofacial development occurs in a continuum rather than in discrete steps. Chick embryos representative of a range of Hamburger and Hamilton stages from HH16 to HH28 were imaged, landmarked, and analyzed via two-dimensional geometric morphometrics in order to quantify the variation in craniofacial shape in relation to the centroid size, age, and HH stage of specimens. The canonical variates analysis revealed that the older group of embryos (HH22-28) had greater variation in craniofacial shape than the younger group (HH16-21). The trajectory of growth (in

relation to average size) of all the embryos was a well-defined, sinuous curve, with no plateaus or stepping. Within each stage, and in relation to age, there was apparent variation in facial shape. The variation observed within stages was greater among embryos in the older group than in the younger group.

These data demonstrate that despite the discrete nature of the morphological stages in the Hamburger and Hamilton classification, normal craniofacial development in chick embryos does not occur according to a stepped pattern. Rather, craniofacial development has been shown to proceed along a continuum; at any given timepoint (in age) or stage in development, there is appreciable variation in craniofacial morphology. Even in a group of eggs all laid or incubated at the same time, embryos do not all grow at exactly the same rate. Some will develop at a faster rate than others in the same group. It is not known what influences the differential rates of growth and development among embryos incubated for the same amount of time. The principal components analysis demonstrated that the greatest size and shape variation occurs in the width of the head and face during the course of development, particularly in the frontonasal process, nasal pits, maxillary processes, and the forebrain. To a lesser degree, normal embryonic development occurs through a change in the height of the forebrain, nasal pits, and maxillary processes.

Two-dimensional morphometrics provides only a flat representation of a three-dimensional specimen [101]. Selection and analysis of landmarks on the two-dimensional image can be hampered by errors in the positioning of the specimen during imaging and errors of facial reference landmark identification [101]. Two-dimensional images only show the length, width, and height of a specimen, and cannot possibly reflect the object's depth. Thus landmarks placed on such an image provide only a two-dimensional map of

the specimen, and cannot represent its depth. An alternative method that might be more effective is three-dimensional morphometrics [101], in which a number of landmark coordinates are placed on a manipulatable 3-dimensional microCT scanned image of a specimen and used for similar types of analyses to two-dimensional morphometrics. In this method, a much larger number of landmarks can be placed on all sides of the three-dimensional image. These landmarks form a three-dimensional topographical map of the face and brain of the embryo. This method eliminates the positional and identification errors characteristic of two-dimensional analyses while providing a more accurate, three-dimensional virtual map of the specimen. Three-dimensional morphometrics can measure the shape change laterally, coronally, and in an anterior-posterior orientation.

6.2 CRANIOFACIAL MALFORMATIONS

Craniofacial malformations are disfiguring conditions that can be caused by genetic mutations, environmental factors, or a combination of both. One particular environmental factor that is implicated in craniofacial anomalies is hypoxia during pregnancy. Despite clinical and experimental evidence of a correlation between embryonic hypoxia and craniofacial defects, the mechanisms by which hypoxia mediates craniofacial malformations are not yet understood. Based on previous experimental evidence for this correlation, as well as clinical evidence including the report of holoprosencephalic anomalies in an acardiac twin by Siebert [47], it was initially hypothesized that hypoxia-induced craniofacial malformations result from HIF-1α-mediated apoptosis and reduced cell proliferation due to altered molecular signaling between the forebrain and frontonasal regions. To address this hypothesis, the goal of this work was to examine the morphological and cellular changes present in hypoxia-induced malformations in a chick

model. Chronic hypoxic incubation of chick embryos led to poor survival, a spectrum of cephalic and facial anomalies, developmental delay, and abnormal craniofacial shape variation. Hypoxia also led to neural crest progenitor apoptosis in early stage embryos and reduced cell proliferation in early stage brain tissue and later stage frontonasal mesenchyme. Embryos also suffered metabolic stress in response to hypoxia.

6.2.1 HYPOXIA REDUCES SURVIVAL AND ALTERS CRANIOFACIAL MORPHOLOGY

The first objective was to determine whether chronic hypoxia affected embryonic survival and altered the craniofacial morphology in embryos. At first, the survival of hypoxic individuals was assessed in a limited range of oxygen levels compared to normoxic controls. Survival of hypoxic embryos at 13% was measured initially. This analysis was extended to the 9% and 11% O2 embryos when they were included in the morphological and morphometric analyses. The survival of embryos at all three hypoxic levels was reduced in relation to normoxic embryos. However this range of oxygen levels was too narrow to adequately determine whether the relationship between mortality and level of oxygen was dose-dependent. The range of oxygen levels was broadened to seek the oxygen level that was completely nonviable for embryos. The nonviable oxygen level was found to be 7%, at which no embryos survived by 6 days. The range was further expanded to fill the extant gap between 13% and 21% O2, in order to adequately describe the true relationship between hypoxia and survival. There emerged a stepped curve of survival rate versus oxygen level. There were small but statistically significant differences in survival between oxygen levels in the range of 15% to 21% O2, but at 13% O2 and below, the survival was very significantly reduced

compared to the higher levels. A plateau was observed, comprising the 13% and lower O2 concentration groups. There was a small but significant difference between the 9% and 11% O2 groups. There was no difference between the 11% and 13% O2 groups. 7% O2 was nonviable. This stepped survival pattern placed the threshold oxygen level for significantly reduced survival at 13% O2.

Among surviving chronic hypoxic embryos, there was a wide spectrum of cephalic and facial anomalies. The milder, and more common, malformations consisted of cephalic asymmetry and eye defects including unilateral or bilateral anophthalmia and microphthalmia. A small group of embryos had frontonasal anomalies including an absent midline. The most severe defects, present in a small number of individuals, were neural tube defects including anencephaly, microcephaly, and exencephaly. These disorders in some cases were combined with midline defects (including absent frontonasal process). The rarest malformations were so severe that no facial features were recognizable. The rarity of survivors with gross, severe malformations raised the possibility that the embryos that died were too severely malformed for viability in hypoxia. Hypoxia most likely exerts a selective pressure against survival of the most severely defective embryos. Among the hypoxic embryos, no correlation between severity of malformations and level of oxygen was observed. The wide variability of phenotypes indicated incomplete penetrance.

Experiments with acute hypoxia for 24 hours in embryos demonstrate a critical window of time during development in which hypoxia has the most seriously disruptive effect on morphogenesis. This window is shown to occur between 24 and 48 hours of development, the period in which the neural crest forms and neural crest cells begin to

separate. The 24-48 hour window produced the most severe anomalies, including rare cases of holoprosencephaly with a proboscis and instances of total obliteration of facial characteristics. Further experiments with acute hypoxia for 12 hours narrowed down the critical vulnerable window for hypoxia. The period of hypoxia between 24 and 36 hours of development was shown to be the critical window for survivability, as only 35% of individuals hypoxic during that period survived. The window of hypoxia between 36 and 48 hours produced embryos with the most severe malformations including neural tube defects. Later 12-hour windows of acute hypoxia produced improved levels of survival and reduced severity of malformations. These data show that the critical window for survival in hypoxia occurs between 24 and 36 hours, and the critical time period for craniofacial morphology to be affected by hypoxia is between 36 and 48 hours as shown by the maximum severity of malformations occurring during that window. The critical hypoxic window occurs during the time of neural crest development and dispersal of neural crest cells. Many craniofacial malformations and syndromes result from neurocristopathies, disorders of neural crest development, proliferation, and migration. The malformations, especially the more severe forms, observed in hypoxic embryos resemble neurocristopathies.

6.2.2 HYPOXIA DELAYS CRANIOFACIAL SKELETAL DEVELOPMENT

Since hypoxia was shown to cause craniofacial malformations in early embryos, it was hypothesized that incubation in chronic hypoxia to the range of time in which skull development occurs would produce embryos with delayed ossification and skull abnormalities. To examine the effect of hypoxia on craniofacial skeletal development, 13-day normoxic and hypoxic embryos were collected and cleared and stained for

cartilage and bone. In comparison to normoxic control embryos, hypoxic embryos showed reduced ossification roughly corresponding to the decreasing oxygen level. This delay in ossification was a generalized effect, with nearly all the bones rostral to the mandible being affected (with the palatine, jugal, and frontal bones affected to a slightly lesser degree). The mandibular bones were also truncated to a lesser degree. Within each oxygen level, there was variation in the delay of ossification. In a small number of surviving embryos, skeletal defects were observed, including orbital and maxillary malformations. The very poor survival of embryos to 13 days in severe hypoxia, along with the rarity of skeletal defects in survivors, suggests a selective pressure of hypoxia against survival of severely malformed embryos. The majority of avian skull bones are neural crest derived and are intramembranous in origin. Thus the delay in craniofacial ossification, and the presence of rare skull defects, represents the farther-reaching effects of neurocristopathy under hypoxic conditions.

6.2.3 ABNORMAL FACIAL SHAPE VARIATION AND DEVELOPMENTAL DELAY IN HYPOXIC EMBRYOS

The next step was to quantify the variation in craniofacial shape among hypoxic and normoxic embryos to examine whether there was abnormal shape change. To this end, images of embryos were analyzed via two-dimensional geometric morphometrics. While many of the hypoxic embryos were separated along the axis representing the change in the size and proportionality of their craniofacial features (as were the normoxic controls), many others were separated along a second axis, which represented extreme variation in the shape of particular facial characteristics (the forebrain, frontonasal process, maxillary processes, nasal pits, and eyes). The most extreme variation, seen in a minority of

hypoxic embryos, is apparent in frontonasal narrowing (ie, reduced distance between the nasal pits), abnormal eye morphology, extreme forebrain dysmorphology (exencephalic mushrooming), and enlarged maxillary processes, according to the PCA warped outline diagrams (Fig. 5.8). Regression analyses revealed that while many hypoxic embryos fell along the normal growth trajectory characteristic of normoxic embryos in relation to average embryonic facial size, others deviated from the normal growth curve. Such outliers likely represent embryos with malformations. There was a roughly dose-dependent pattern of deviation of hypoxic embryos from the normal growth trajectory. The 19% O2 embryos showed no visible delay or variation from the normoxic controls and did not deviate from the normal growth curve. The 15% and 17% O2 embryos were further delayed and showed little deviation from normal growth; there were a few 15% O2 embryos with severe malformations. The 13% and 11% O2 hypoxic embryos showed the widest variation; however, those incubated in 9% O2 displayed much less phenotypic variation (ie, there were very few 9% O2 survivors with severe malformations compared with those in the higher O2 levels). This may be due to the very high mortality among 9% O2 embryos, and a possible hypoxic selective pressure against the survival of those with the most severe malformations. When the facial shape scores and centroid size scores were compared against oxygen concentration, the 19% O2 and normoxic embryos were no different, however there was an appreciable decrease in these scores in hypoxic groups of embryos below 19% O2 (with a plateau occurring between 9% and 17% O2). Hypoxic embryos also exhibited developmental delay compared to age-matched normoxic control embryos.

However, with the inherent weaknesses of two-dimensional geometric morphometrics [101], the morphometric analyses performed on the normoxic and hypoxic embryos may not accurately reflect all the malformations observed in the current work. In fact, there were a number of embryos in this study that could not be landmarked or analyzed due to malformations that were sufficiently severe to obliterate all landmarks. Three-dimensional morphometric analyses [101] provide a more accurate, three-dimensional map of the specimen, avoiding the bias and other errors inherent in two-dimensional morphometrics. Two-dimensional morphometrics can only measure the shape variation in two dimensions; it cannot show the change occurring in the sagittal plane. In contrast, using three-dimensional morphometrics, it is possible to measure and analyze the true variation in craniofacial shape occurring across multiple planes in response to hypoxia.

6.2.4 HYPOXIA INCREASES APOPTOSIS AND REDUCES CELL PROLIFERATION

The next question to be addressed concerned the possible cellular mechanisms that could explain the abnormal phenotypes observed in hypoxic embryos. Whole-mount TUNEL staining at very early stages (HH9-10) showed that hypoxic embryos exhibited varying amounts of apoptosis of neural crest progenitor cells; some had little or none, while others had larger amounts of visible cell death in the forebrain and along the neural folds. Sagittal section TUNEL confirmed the neuroepithelial apoptosis by showing increased cell death in the neuroepithelium in all cephalic regions. This was further evidenced by increased levels of the cleaved form of caspase 3 observed in neuroepithelial cells, as well as reduced cell proliferation in these tissues. The variation in the amount of apoptosis seen in these early stage embryos may explain why more severe

malformations are observed in some individuals than in others. The location of the apoptotic cells, in the forebrain and neural fold/tube tissues, suggests that the abnormal phenotypes may in part be explained as neurocristopathies. Indeed, a number of embryos displayed neural tube defects including exencephaly; these defects are likely related to the severe neuroepithelial apoptosis observed in a cohort of HH9-10 hypoxic embryos. Although there was no further apoptosis apparent in later stages of development, the proliferation of frontonasal mesenchymal cells was reduced. The reduced mesenchymal proliferation may correlate to frontonasal anomalies observed in some hypoxic individuals.

6.2.5 POSSIBLE CELLULAR OXIDATIVE STRESS IN RESPONSE TO HYPOXIA

From Siebert's [47] findings of holoprosencephaly-like facial and cephalic defects in an acardiac human twin fetus, it was initially hypothesized that hypoxia led to holoprosencephaly and other craniofacial malformations via a mechanism of apoptosis in response to hypoxic disruption of molecular signaling during craniofacial morphogenesis in the embryo. Experiments to assess molecular signaling in response to hypoxia, including expression and activity of Shh, Wnt, BMP, and Fgf and their downstream targets, were proposed. *In situ* hybridization using a chick *Shh* antisense RNA probe was attempted, but was unsuccessful. However, there was too much variation in the malformations to observe any single dominant phenotype or determine whether there was a corresponding target signaling pathway for hypoxic disruption, so the other molecular signaling experiments were not performed.

This phenotypic variation indicated that chronic hypoxia has a generalized impact on craniofacial development, probably through cellular oxidative metabolic stress response to hypoxia. Sections of normoxic and hypoxic embryos were immunostained for the presence of the activated form of AMP-activated protein kinase (AMPK) which maintains the cellular energy balance in response to metabolic stressors including hypoxia. While the presence of activated AMPK was noted to be widespread particularly in the neural tissues of both normal and hypoxic embryos, staining was observed to be more intense in hypoxic neuroepithelia. Brain and neural tissues are particularly metabolically demanding and sensitive to oxidative stress. The presence of intensified AMPK in hypoxic embryonic brain and neural tissues lends support to the findings of neuroapoptosis and reduced neuroepithelial cell proliferation in early hypoxic embryos. The apoptotic and metabolic effects observed in the neuroepithelia of hypoxic embryos may explain the severe malformations, including neural tube defects, seen in a cohort of embryos.

Two other types of experiments were proposed and attempted in order to assess the molecular response of cells to hypoxia as well as the possibility of rescue of hypoxia-induced defects.

To assess cellular response to hypoxia through the HIF-1α pathway, sections of 6-day embryos (normoxic control and hypoxic) were immunostained with a rabbit polyclonal antibody to HIF-1α that was thought to be expressible in chick tissues (based on product information provided) and a secondary antibody (goat polyclonal antibody against rabbit IgG-H+L, HRP conjugated). It was expected that stable HIF-1α would be more evident in hypoxic embryos than normoxic controls. However despite repeated attempts the chick

tissues did not stain for the HIF-1α antibody. No chick-compatible HIF-1α antibody has yet been located. Contingent on the success of the immunostaining experiment, a set of experiments were proposed to examine the effects of gain of function and loss of function of HIF-1α in normoxic embryos and hypoxic embryos, respectively. The first experiment (gain of function), infecting normoxic embryos with a virus encoding a constitutively-active *HIF-1α* gene, was designed to test the extent to which HIF-1α mediates the effects of hypoxia on craniofacial morphology. Secondly, to determine whether HIF-1α is necessary for the hypoxic effects on morphology, a loss of function experiment was devised wherein hypoxic embryos would be infected virally with a dominant-negative *HIF-1α* gene lacking the DNA-binding domain. Neither experiment was carried out due to the failure of the original HIF-1α immunostaining procedure.

Experiments were also devised to examine whether the defects induced by hypoxia in chick embryos could be rescued by an antioxidant, based on prior evidence of the interaction of reactive oxygen species (ROS) with HIF-1α [71], the role of ROS in cellular hypoxia sensing [75], and previous evidence that antioxidants can reverse the effects of ROS and inhibit HIF-1α activation [76]. Initially, hypoxic embryos were treated with 5mM or 10mM N-actyl-L-cysteine (NAC) in water (or 1X PBS as a control) dropped directly on the head, daily, starting on day 2, through day 6. The NAC did not improve survival. A later experiment, in which the concentration of NAC was calculated to 10mM relative to the egg fluid volume estimate of 100ml, similarly failed to produce any results. Perhaps the treatment itself was too traumatic to the young embryos, or the concentration was too low in the initial experiments.

6.2.6 PROPOSED MODEL OF HYPOXIC EFFECT ON CRANIOFACIAL MORPHOGENESIS

A possible model for the effect of hypoxia, on the cellular level, on the craniofacial and brain development in chick embryos can be described as follows. The data show that these effects originate during the critical stage of development when the neural crest is induced, develops, and delaminates. Under hypoxic conditions, at this stage, the reduction of oxygen available to these cells triggers an oxidative metabolic stress response. This response, through the heightened activation of AMPK, leads to apoptosis in this particularly sensitive population of cells (and thus reduced proliferation). This results in a neurocristopathy, the basis for the neural tube defects and other craniofacial malformations observed (in varying degrees) among hypoxic embryos.

CHAPTER 7:

CLINICAL IMPLICATIONS AND FUTURE DIRECTIONS

Recent clinical evidence, as well as previous experimental studies, have correlated embryonic hypoxia with craniofacial and brain malformations. However, this correlation has not been further explored to date, nor are the mechanisms underlying hypoxia-induced facial and cephalic defects well understood. Therefore, the goal of this study was to examine the morphological changes and possible cellular mechanisms responsible for craniofacial anomalies caused by hypoxia.

The most important clinical implication is that prevention of pathological hypoxia during embryonic and fetal development is the most effective weapon against potential craniofacial malformations before birth. Cessation of smoking, drinking, and other drug use is an effective preventive measure. As the mechanisms behind hypoxia-induced malformations are better understood, possibilities exist for potential cellular-based and molecular therapies that can be employed during early embryonic development as malformations are detected.

The data provided by this current work indicate increased cellular death and reduced proliferation, particularly in sensitive neuroepithelial tissues, as underlying cellular mechanisms for the observed craniofacial malformations. The extreme variation in the phenotypes (and thus the lack of a predominant phenotype) precluded determination of a particular target molecular signaling pathway for hypoxic disruption. Many craniofacial anomalies can be traced back to defects in known morphogenetic signaling pathways (for example, Shh mutations cause holoprosencephaly, and Fgf defects lead to facial clefting). As a teratogen, hypoxia exerts more complicated effects on development than can be

explained by simple genetics or blamed on disruption of any one known molecular pathway.

Due to the limited timeframe and funding constraints for the project, many of the experiments initially proposed could not be undertaken. The project, as first envisioned and proposed, quickly proved to be too ambitious for the allotted time and funding. Removing these constraints, these unrealized experiments could help pinpoint the molecular mechanisms underlying hypoxic craniofacial anomalies.

First of all, a small number of my own hypoxic embryos displayed microforms of holoprosencephaly (and two showed full-on holoprosencephaly). Hence, my extant morphometric analyses should be rounded out with the addition of embryos with artificially-induced holoprosencephaly (as in the proposed 5E1 treatment, or alternatively with cyclopamine) as a control population to determine whether any of my embryos do indeed show abnormal morphological variation consistent with holoprosencephaly. This would show that holoprosencephaly, along with the other observed craniofacial anomalies, can be induced by hypoxia, as initially hypothesized.

The analyses of cell behavior (proliferation and apoptosis) that have implicated neural crest cells as the affected tissue need to be expanded to study neural crest cell migration. The HNK-1 neural crest cell marker would be a valuable tool to help determine whether any of the craniofacial anomalies observed result from neural crest migration defects.

Since the neural crest is implicated in the malformations observed in hypoxic embryos, it might not be necessary to blindly angle for candidate genes or molecular signaling pathways, as originally proposed. Rather, specific signaling pathways relevant to the neural crest need to be targeted, early in development (at the critical stage wherein

the neural crest forms and begins to disperse), for analysis. The neural crest is induced by Wnt, BMP, and Fgf signaling [20], so expression and downstream signaling analyses for these morphogens need to be undertaken. Since some of the hypoxic embryos showed microforms of (or, in two cases, complete) holoprosencephaly, the Shh pathway may have been disrupted in these holoprosencephalic anomalies, and thus bears consideration for targeted analyses of expression and signaling activity. Once the relevant molecular signaling pathways affected by hypoxia are brought to light, future therapeutics could focus on replacement of faulty genes or replenishing low levels of critical molecules in the affected pathway in the early embryo. Alternatively, after birth, tissue regeneration could be focused on jumpstarting the relevant molecular signaling mechanism.

The role of HIF-1α as a mediator of hypoxic craniofacial dismorphology needs to be examined, as originally proposed. Since HIF-1α is destabilized by oxygen in normoxic conditions, there is the necessity of devising a way to collect tissue from hypoxic embryos in a hypoxic environment to enable measurement of stable HIF-1α protein levels in these embryos. The original proposal for envirulating normoxic embryos with constitutively-active *HIF-1α* or hypoxic embryos with dominant-negative *HIF-1α* bears revisiting, in order to determine how HIF-1α mediates hypoxia-induced malformations as well as to determine the extent of the requirement for HIF-1α for hypoxic effects on craniofacial morphology. If HIF-1α is indeed found necessary and sufficient to cause malformations in embryonic hypoxia, therapeutic inhibition of the HIF pathway is a potential strategy for reversal of hypoxic malformations.

Perhaps the most promising potential therapeutic strategy (beyond prevention) is rescue of normal facial morphology by reversing or limiting the effects of oxidative stress

in hypoxic tissues in the embryo. One precedent for this is the treatment of *tcof1* mutant mouse embryos by Jones et al [33] with pifithrin-α, a p53 inhibitor, to prevent Treacher Collins syndrome malformations; pifithrin-α was shown to prevent the p53-dependent neuroapoptosis resulting from bioenergetics stress in neural crest cells of *tcof1* mutant embryos. The effects of metabolic stress on craniofacial morphology can potentially be reversed using antioxidants. Once the procedures for administering an antioxidant (ie, NAC) are optimized to prevent trauma or lethality to very young hypoxic embryos, experimental antioxidant treatment to these embryos would provide insights into the role of oxidative stress in the causation of craniofacial defects. If antioxidant rescue does indeed reverse the dysmorphological effects of hypoxia in embryos, it bears promise as an effective therapeutic strategy against these anomalies.

APPENDIX A:

UNREALIZED EXPERIMENTS

This project, as originally envisioned, was designed to include detailed analyses of the morphological, cellular, and molecular changes that could possibly explain the craniofacial malformations caused by hypoxia in chick embryos. However, due to technical difficulties, some of the experiments failed. Other experiments proved to be too ambitious to undertake within the time and budgetary limitations of the project.

The complete geometric morphometric analyses were proposed to include not only the different populations of hypoxic embryos (ie, the different oxygen levels) and normoxic control embryos, but also a second control population of embryos with artificially-induced holoprosencephaly. It was originally hypothesized that hypoxia played a role in causing holoprosencephaly and other craniofacial defects, based on a case of holoprosencephalic anomalies in an acardiac human twin, which Siebert [47] attributed to hypoxia resulting from acardia and poor oxygen perfusion in the fetus. A minority of my hypoxic embryos showed microforms of holoprosencephaly, and two individuals showed full-on holoprosencephaly including proboscis and severe hypotelorism. In order to determine whether any of my hypoxic embryos indeed displayed abnormal craniofacial shape variation characteristic of holoprosencephaly, a control group was proposed that consisted of normoxic embryos injected with cells expressing the 5E1 antibody. This antibody blocks Shh signaling, and causes holoprosencephaly. I cultured 5E1 cells from lab stocks, and attempted to inject them into HH10-11 embryos by mouth-blowing through a glass needle, but due to oral anatomical defects on my part, this proved impossible. The injection was attempted again with

nitrogen-fed picospritzer injection, and seemed to work. However many embryos were lost due to the trauma of injection. Since the treatment produced no viable results, it was next proposed to use existing specimen images from another lab colleague, landmark them, and use them instead in the morphometrics. Due to time limitations, this was not undertaken.

Analysis of cell death using TUNEL was problematic. Repeated attempts at staining with fluorescently labeled TUNEL resulted in annoying autofluorescence that created background staining, rendering any results inconclusive. Even if cells appeared positive, they were thought to be probable artifacts as a result of the autofluorescence. Whole-mount TUNEL staining in 2-day embryos produced more believable results. Finally, with the able help of one of my laboratory colleagues, the technical issues were overcome enough to obtain results from TUNEL staining sagittal sections of 2-day embryos, and her efforts were rewarded with true positive staining of apoptotic cells in the neuroepithelium of hypoxic embryos to a greater extent than in normoxic controls. These results served to confirm those from the whole-mount TUNEL experiment. Until this breakthrough occurred, alternative methods for analysis of apoptosis had been tried. Whole-mount embryos (hypoxic and normoxic) were stained *in ovo* with Syto12-GFP (a vital dye targeting apoptotic cells) on day 2 (HH9-11), reincubated in the dark for 2 hours, then photographed using the GFP fluorescent filter. The results from Syto12 also proved inconclusive due to autofluorescence. Immunostaining of sections of embryos for cleaved caspase 3 proved most successful, as no counterstaining was used so the positive cells stood out.

The original hypothesis also stated that hypoxia caused malformations via altered molecular signaling. Since craniofacial development relies on coordinated signaling through a number of pathways including Shh, Wnt, BMP, and Fgf, experiments were proposed to analyze expression and downstream signaling activity of these morphogens using *in situ* hybridization, qPCR, and immunohistochemical assays. A *Shh* antisense RNA probe was generated and purified, but repeated attempts at whole-mount *in situ* hybridization failed to generate any discernible staining and resulted instead in background staining. Meanwhile, the phenotypes of hypoxic embryos proved to be significantly variable, ranging from mild defects (cephalic asymmetry and eye defects) to more severe anomalies including frontonasal malformations, some midline and clefting phenotypes, and in rare cases, neural tube defects as well as holoprosencephaly. Some embryos were sufficiently grossly malformed to obliterate any recognizable facial features. This extreme variation in morphology precluded the determination of any single predominant phenotype, much less any predominantly-targeted molecular pathway. Thus no further signaling analyses were undertaken, as they would have proven to be blind fishing expeditions considering the limits on time and funding. A proposal for a general microarray analysis was briefly considered at first, but was similarly rejected as a potentially blind shotgun experiment.

Since it was also hypothesized that the apoptosis in hypoxic embryos was mediated by HIF-1α, I initially attempted to assess the levels of stable HIF-1α protein in hypoxic embryos compared to normoxic controls, using immunohistochemistry with a rabbit polyclonal antibody to HIF-1α, which was probably mistakenly understood to be compatible with the chick tissue (from the product information). No staining was

observed in either hypoxic or normoxic embryos. Further experiments to test the role and necessity of HIF-1α in mediating craniofacial defects were proposed. Infection of normoxic embryos with a virus encoding constitutively active *HIF-1α* was proposed to determine the extent to which it is required to mediate these anomalies. Similarly, envirulation of hypoxic embryos with dominant-negative *HIF-1α* (with no DNA-binding region) was intended to test whether HIF-1α is required to alter morphology. Due to time constraints, neither experiment was undertaken.

Antioxidant treatment to rescue the morphology and survival of hypoxic embryos was attempted, but unsuccessful. Initially, N-acetyl-L-cysteine (NAC) was diluted to 5mM or 10mM in water (from 100mg/ml stock), then applied directly to the head of early hypoxic embryos *in ovo* once daily until collection at 6 days. 1X PBS was used as a control. NAC treatment (using diluted NAC) did not improve survival, but rather killed most of the embryos, either due to trauma or excessive concentration. Subsequently, 81µl of the 100mg/ml stock of NAC was applied to the heads of embryos on day 0 just before incubation in 13% O2, then daily thereafter until collection at 6 days. The rationale was to calculate the desired concentration (5mM) relative to the 100ml estimated fluid volume of the egg, rather than standard dilution in water. Once again it proved traumatic and lethal to the embryos. The procedure was repeated, this time applying the NAC lateral to, not directly on, the embryo, starting 24 hours after the start of incubation and daily thereafter until collection on day 6. A smaller volume but identical concentration was used. The results were equally unsuccessful.

APPENDIX B:

BACKGROUND AND MOTIVATION FOR MY RESEARCH

B.1 CONNECTION BETWEEN LIFE EXPERIENCE AND RESEARCH

My research interests are inextricably intertwined with my life experience. I was born with Treacher Collins syndrome (the genetics and pathology of which are previously described in the Introduction). Among my phenotypes were cleft palate, bilateral auditory canal atresia, microtia, and absence of middle ear ossicles and eardrums. Other phenotypes included the Pierre Robin sequence (micro- and retrognathia and glossoptosis), malar hypoplasia, and absence of lower orbital rims (Fig. 34).

Figure B.1: Treacher Collins syndrome. *Photo of author (age 3) demonstrating severe craniofacial phenotype of Treacher Collins syndrome. From personal archive.*

Sequelae have included severe upper airway obstruction and sleep apnea secondary to the Pierre Robin anomalies (which have required numerous tracheotomies). Other

secondary effects include severe conductive hearing loss (requiring bone-conduction hearing aids) and a peculiar "quack-like" quality of cleft palate speech common in Treacher Collins syndrome (corrected in part by intensive speech therapy). During my lifetime, I required innumerable craniofacial reconstructive surgeries at two tertiary pediatric hospitals with interdisciplinary teams devoted to comprehensive care of craniofacial deformities. These procedures included multiple stages of otoplasty (for the microtia) and an unsuccessful attempt at canaloplasty (for the atresia). To address the maxillofacial deformities, multiple mandibular and maxillary augmentation and reconstruction procedures (the LeFort series of osteotomies) were performed, often requiring tracheotomy and intermaxillary fixation. The absent malar and zygomatic arch bones were approximated with rib grafts. The cleft palate was almost completely closed in an initial palatoplasty; however, two attempts to close the palatal fistula with tongue flaps were unsuccessful.

My multiple surgeries fostered, at a very early age, a lifelong interest in human anatomy and surgery (particularly craniofacial reconstruction). In secondary school, I was encouraged to pursue medicine as a career path by family, peers, and medical professionals who were familiar with me. Early on, I decided to focus on craniofacial anomalies. I focused my undergraduate studies on a premedical degree in biology, and subsequently pursued a master's degree in biology in an attempt to bolster my chances at acceptance into medical school.

Also in early secondary school (and through my undergraduate years) a seed was planted for my parallel interest in craniofacial embryology. I was made aware of the early research by Dixon and his colleagues to isolate and characterize the *TCOF1* gene, its

protein product treacle, and the mutations and pathology involved in Treacher Collins syndrome [28-30]. I personally met Dr. Dixon at a Treacher Collins syndrome symposium at NYU Medical Center when he presented the keynote talk there in 1997. I met him two more times in the United Kingdom.

B.2 EDUCATIONAL AND RESEARCH BACKGROUND

I received my bachelor's degree in biology (premedicine) in 1998, and subsequently, my master's degree in biology in 2001, both from Purdue University. At that time, I applied to medical schools all over the USA, UK, and Ireland, in order to pursue my career goal in medicine, specializing in craniofacial surgery. My applications to medical schools were unsuccessful, but I did secure a place in the BSc program in biomedical sciences at King's College London in 2003. I deferred entry to 2004, allowing myself a gap year to prepare for this monumental move. From 2004 through 2007, I read biomedical sciences at King's, fully intending to continue on into the medical school there. My modules at KCL included anatomy (with dissection, along with the medical students), embryology, developmental biology, genetics, molecular biology, among others. Many of these modules happened to coincide with a blossoming interest in craniofacial embryology (whose seed had been planted back in early high school).

A major shift in my career aspirations occurred in 2006, when I learned of a summer research program at King's College London's dental institute, which has a department dedicated to research in craniofacial development in the embryo. I made connections with the craniofacial development department and secured a potential summer research project with Dr. Martyn Cobourne. We successfully applied for a Wellcome Trust UK summer research grant. That summer, in the Cobourne laboratory, I gained my first practical

experience in craniofacial embryology research, and co-authored a paper on the expression of the *Scube3* epidermal growth factor-related gene in mouse embryos [102]. In this first research project, I learned techniques including generation and purification of an antisense RNA probe for *Scube3*, harvesting and preparation of mouse embryos, and whole-mount *in situ* hybridization in order to find the gene's expression pattern. This project cemented my desire to pursue a research career goal in the emerging niche field of craniofacial embryology.

In the 2006-2007 academic year, a new intercalated BSc program in craniofacial sciences was inaugurated at King's. I enrolled in it, since its focus directly coincided with my interests. I not only gained deeper scientific knowledge of the craniofacial sciences and learned many new techniques, but also learned to effectively communicate my findings through oral and poster presentations. In 2007, I joined the laboratory of Dr. Philippa Francis-West and participated in a project to analyze the regulation of craniofacial muscle development in chick embryos.

In 2007, the time came for me to choose the next step in my academic path. My mentors encouraged me to pursue a PhD in the field of craniofacial embryology. I applied for places in PhD courses at King's College London and in the United States. I secured admission offers from the University of Southern California (USC) Center for Craniofacial Molecular Biology and the University of California San Francisco (UCSF) graduate program in Oral and Craniofacial Sciences. Of these two offers, I chose the UCSF program due to the supportive atmosphere I encountered there as well as the environment of the city of San Francisco. At UCSF I have gained much valuable research experience and mentorship in my chosen field, and have gotten many opportunities to

share not only my research, but also my unique connection to my research, in presentations at scientific meetings both in the USA and overseas.

Besides my research, I continue to engage in peer mentoring and outreach in public and among the community of people with craniofacial anomalies. I attend an annual craniofacial family retreat (through the Children's Craniofacial Association), and speak about my life experience at conferences, schools, churches, and other venues when such opportunities arise. An autobiography is in progress, slated for publication in the near future.

APPENDIX C:

LABORATORY ROTATION PROJECTS

Before I began my actual dissertation research project, as a student at UCSF, I was required to undertake rotations in different laboratories focusing on different fields of research. These laboratory rotations, each lasting one academic quarter, were designed to provide exposure to fields of work that did not necessarily encompass my area of interest in craniofacial embryonic development. In each of these rotations, I was provided the opportunity not only to observe research being done by the mentor and his team, but also to gain hands-on experience as a contributor to this research. I not only gained experience and skill in laboratory skills and data analysis, but learned more of the science itself behind my work and findings. I learned the valuable skills of communicating my findings through both formal oral and graphic presentations and informal discussion. Many of my laboratory and analytical skills accompanied me to subsequent laboratory projects, but my scientific communication skills gained in these rotations have served me well in the greater scientific world. It is true that my dissertation project itself was fertilized in, and evolved from, a laboratory rotation, but generally it is not intended that these rotation experiences necessarily develop into formal thesis research.

C.1 LABORATORY OF DAN RAMOS, OROFACIAL SCIENCES

The focus of this laboratory is the interaction of human oral cancer cells with their extracellular environment. In this first laboratory rotation, I was introduced to cell culture methods, fluorescent microscopy, and immunofluorescence as a method of visualizing cellular structures and interaction with the extracellular matrix. Dr. Ramos was my main mentor in this rotation, but I also received valuable help and advice from the lab manager

(regarding sterile cell culture techniques) and a postdoctoral fellow. After learning these techniques, I was assigned my own project. I also attended weekly laboratory meetings held in collaboration with another departmental professor's lab. I had opportunities to present recent papers in a journal club format in several of these joint meetings.

The objective of my rotation project was to examine the role of emmprin in the differentiation of human oral squamous cell carcinoma (OSCC) cells. Emmprin (extracellular matrix metalloproteinase inducer) is a member of the immunoglobulin superfamily of cellular adhesion molecules. Excessively high levels of emmprin have been seen in highly metastatic and invasive cells. Emmprin causes overexpression of matrix metalloproteinases (MMPs) through homophilic, emmprin-emmprin interactions between cancer cells. To examine changes in differentiation of oral cancer cells due to overexpression of emmprin, I compared the expression of two cytoskeletal intermediate filaments between two lines of oral squamous cell carcinoma cells (SCC9), one line (SN) as the control (expressing no emmprin) and the other line (HE) overexpressing emmprin. Expression of keratin would mark cells that are fully developed and committed to epithelial type, while expression of vimentin would mark cells that are less differentiated (and likely of mesenchymal origin). Keratin expression was expected to be stronger in the control (SN) cells (with no emmprin), marking them as fully differentiated epithelial cells, compared to the HE cells (overexpressing emmprin). Vimentin expression was expected to be higher in the HE cells, marking them as less differentiated (and more mesenchymal) than the SN cells. Thus, I hypothesized that emmprin does play a role in differentiation of oral cancer cells.

Two lines of human oral squamous cell carcinoma cells were used: SCC9SN cells (with no emmprin or B6 integrin) were the control cells, and SCC9HE cells (overexpressing emmprin) were the experimental cell population. Cells from each line were cultured to confluence on coverslips at 37°C. To enable the SN cells to adhere to their coverslips (as SN cells are poorly adhesive), these coverslips were coated with 50ul of 10ug/ml collagen I. The coverslips for the HE cells were not coated, as HE cells adhere well.

I compared the expression of keratin and vimentin between the SCC9SN (control) cells and SCC9HE cells (overexpressing emmprin) by immunofluorescence using primary antibodies to cytokeratin and vimentin, respectively, and a fluorescent secondary antibody. The SCC9SN cells showed no expression of keratin at all. In stark contrast, nearly all the SCC9HE cells showed very strong expression of keratin; the fibers were clearly visible throughout the cell cytoplasm. The SCC9SN cells showed obvious vimentin expression, with visible fibers throughout the cytoplasm. However, vimentin expression was very weak or absent in the SCC9HE cells, with scattered, weak expression.

The results from these experiments were exactly the opposite of what I expected. Keratin expression was expected to be stronger in the SCC9SN cells than in the SCC9HE cells. Vimentin expression was expected to be stronger in the SCC9HE cells than in the SCC9SN cells. However, in these experiments, keratin was expressed very strongly in the SCC9HE cells, while the SCC9SN cells showed absolutely no keratin expression. Vimentin expression was very weak or absent in the SCC9HE cells, while it was strong in the SCC9SN cells. What could explain these strange results? One explanation is that

perhaps the cell lines, obtained from laboratory LN2 stores, could have been unknowingly switched or mislabeled. This might explain the reversed results for both keratin and vimentin. Another plausible explanation is that the cells, on their coverslips during the immunofluorescence procedure, dried. This is a common mishap; extreme care must be taken during washes and antibody staining to not allow the cells to dry at all (by leaving some liquid on them between washes); cells very easily and quickly dry out. Dried cells do not take up antibodies well, thus do not stain clearly. These unexpected results demonstrate the need for more precision and care in selection and keeping the cell lines unswitched, as well as extreme care in ensuring the cells remain wet during immunofluorescent procedures. From these results, I could not determine whether emmprin played a role in the differentiation of the SCC9 cells.

C.2 LABORATORY OF RICHARD SCHNEIDER, ORTHOPAEDIC SURGERY

The laboratory of Richard Schneider focuses on the regulation of craniofacial skeletal development in duck and quail embryos. Dr. Schneider is particularly renowned for his design and use of the "quck" embryo, a chimera consisting of a duck embryo with quail tissue grafted onto one side of the head at an early stage. Dr. Schneider, as my main mentor, educated me thoroughly in embryonic craniofacial tissue morphogenesis and advised me on the design for the rotation project. Other students and postdoctoral fellows in the laboratory taught me techniques including embryo collection, *in ovo* injection of drugs, and histochemical staining for bone, cartilage, and osteoclast activity. I updated my mentor and colleagues in weekly meetings on my progress and received feedback. My work contributed to research that was shared at national meetings.

The goal of the Schneider rotation project was to examine the effect of alendronate (an anti-osteoporotic drug) on mandibular and maxillary bone development in quail, duck, and quck embryos. Quail eggs were injected with alendronate on day 7 of incubation, either with single injections or double injections (at a 12-hour interval), and the embryos were collected two days later. Duck, quail, and quck embryos were also collected. Whole-mount embryos were stained for bone using alizarin red. Other embryos were embedded in paraffin, sectioned, and stained in trichrome and TRAP stains for bone and tissue analyses and for osteoclast activity.

Quail embryos treated with alendronate had elongated lower beaks, demonstrating that alendronate prevents the resorption of bone by osteoclasts. TRAP staining showed that quail mandibular bone has greater osteoclast activity (and is shorter) than the duck mandible (which has less osteoclast activity). Thus, due to greater osteoclast activity, the quail beak is shorter than that of the duck. Staining of quck sections bore this out, as the quail transplant side of the beak was shorter than the host (duck) beak side and showed higher levels of osteoclast activity.

C.3 LABORATORY OF BENEDIKT HALLGRIMSSON, UNIVERSITY OF CALGARY

Benedikt Hallgrimsson has pioneered the use of quantitative geometric morphometrics in the analysis of cranial and facial shape variation in numerous species. Using two-dimensional (photographic) images and three-dimensional micro-CT-scanned images of embryos, Dr. Hallgrimsson assigns facial and cephalic landmarks and uses multivariate statistics to analyze the change in shape over time during normal and abnormal development. Dr. Hallgrimsson has collaborated with the Marcucio lab at

UCSF, providing his expertise and assistance in their analysis of craniofacial shape variation in avian, reptilian, and other embryos. In my study of the morphological changes occurring in hypoxic chick embryos, Dr. Hallgrimsson has introduced me to geometric morphometrics as a tool to analyze whether hypoxia significantly alters craniofacial morphology in hypoxic embryos.

I spent a whole month on sabbatical in Dr. Hallgrimsson's laboratory in Calgary learning the techniques of three-dimensional morphometrics. The goal of my project was to create three-dimensional micro-CT images of duck and quail embryos in order to compare the normal developmental trajectory of the two species. The Hallgrimsson laboratory has the advantage of being equipped with the necessary micro-CT scanning equipment that the Marcucio laboratory lacks. Under the leadership of Dr. Hallgrimsson, his postdoctoral fellows guided me in the preparation of specimens for imaging, the use of the scanning equipment, and the landmarking and analysis of the images.

Duck and quail embryos, harvested in and imported from the Marcucio laboratory, were fixed in 4% paraformaldehyde in phosphate-buffered saline (PBS). The specimens were soaked in micro-CT contrast medium for an hour before being washed in PBS. Each embryo was positioned vertically in the sample scan tube, which was placed in the micro-CT scanner. After a scout view at an appropriate resolution, each embryo was scanned for 45 minutes to an hour. The three-dimensional images were imported into Amira software and landmarked. The 3-dimensional data were further analyzed by Nathan Young in the Marcucio lab. Extant two-dimensional morphometric images and files from duck and quail embryos (from the Marcucio lab) were analyzed using MorphoJ software.

REFERENCES

1. His, W., *Untersuchungen uber die erste Analge des Wirbeltierleibes. Die erste Entwicklung des Hunchens im Ei.* . 1868, Leipzig: F.C.W. Vogel.
2. Marshall, A.W., *The morphology of the vertebrate olfactory organ.* Quart. J. Micr. Science, 1879. **19**.
3. Platt, J.B., *A contribution to the morphology of the vertebrate head, based on a study of Acanthias vulgaris.* J Morphol., 1891. **5**: p. 78-112.
4. Hall, B.K., *The neural crest as a fourth germ layer and vertebrates as quadroblastic not triploblastic.* Evol Dev, 2000. **2**(1): p. 3-5.
5. Hall, B.K., *The neural crest as a fourth germ layer and vertebrates as quadroblastic not triploblastic.* Evol Dev, 2000. **2**(1): p. 3-5.
6. Noden, D.M., *The role of the neural crest in patterning of avian cranial skeletal, connective, and muscle tissues.* Dev Biol, 1983. **96**(1): p. 144-65.
7. Trainor, P.A. and R. Krumlauf, *Hox genes, neural crest cells and branchial arch patterning.* Curr Opin Cell Biol, 2001. **13**(6): p. 698-705.
8. Creuzet, S., et al., *Negative effect of Hox gene expression on the development of the neural crest-derived facial skeleton.* Development, 2002. **129**(18): p. 4301-13.
9. Trainor, P. and R. Krumlauf, *Plasticity in mouse neural crest cells reveals a new patterning role for cranial mesoderm.* Nature Cell Biology, 2000. **2**(2): p. 96-102.
10. Schilling, T.F., V. Prince, and P.W. Ingham, *Plasticity in zebrafish hox expression in the hindbrain and cranial neural crest.* Dev Biol, 2001. **231**(1): p. 201-16.
11. Veitch, E., et al., *Pharyngeal arch patterning in the absence of neural crest.* Curr Biol, 1999. **9**(24): p. 1481-4.
12. Hamburger, V., Hamilton, H.L.,, *A series of developmental stages in development of the chick embryo.* J. Morphol., 1951. **88**: p. pp. 49–92.
13. Depew, M.J., et al., *Reassessing the Dlx code: the genetic regulation of branchial arch skeletal pattern and development.* J Anat, 2005. **207**(5): p. 501-61.
14. Depew, M.J., T. Lufkin, and J.L. Rubenstein, *Specification of jaw subdivisions by Dlx genes.* Science, 2002. **298**(5592): p. 381-5.
15. Kontges, G. and A. Lumsden, *Rhombencephalic neural crest segmentation is preserved throughout craniofacial ontogeny.* Development, 1996. **122**(10): p. 3229-3242.
16. Couly, G.F., P.M. Coltey, and N.M. Le Douarin, *The triple origin of skull in higher vertebrates: a study in quail-chick chimeras.* Development, 1993. **117**(2): p. 409-29.
17. Evans, D.J. and D.M. Noden, *Spatial relations between avian craniofacial neural crest and paraxial mesoderm cells.* Dev Dyn, 2006.
18. Basch, M.L., M. Bronner-Fraser, and M.I. Garcia-Castro, *Specification of the neural crest occurs during gastrulation and requires Pax7.* Nature, 2006. **441**(7090): p. 218-222.
19. Villanueva, S., et al., *Posteriorization by FGF, Wnt, and retinoic acid is required for neural crest induction.* Dev Biol, 2002. **241**(2): p. 289-301.
20. Trainor, P.A., *Specification and patterning of neural crest cells during craniofacial development.* Brain Behav Evol, 2005. **66**(4): p. 266-280.

21. Garcia-Castro, M.I., C. Marcelle, and M. Bronner-Fraser, *Ectodermal Wnt Function As a Neural Crest Inducer.* Science, 2002. **13**: p. 13.
22. Monsoro-Burq, A.H., R.B. Fletcher, and R.M. Harland, *Neural crest induction by paraxial mesoderm in Xenopus embryos requires FGF signals.* Development, 2003. **130**(14): p. 3111-3124.
23. Ko, S.O., et al., *Smad4 is required to regulate the fate of cranial neural crest cells.* Dev Biol, 2007. **312**(1): p. 435-47.
24. Jeong, J., et al., *Hedgehog signaling in the neural crest cells regulates the patterning and growth of facial primordia.* Genes Dev., 2004. **18**(8): p. 937-951.
25. WHO, *World Atlas of Birth Defects*. 2nd edition ed. 2003 Geneva, Switzerland: Human Genetics Programme of the World Health Organization.
26. Thomson, A., *Notice of several cases of malformation of the external ear, together with experiments on the state of hearing in such persons.* Monthly J Med Sci, 1846. **7**: p. 420.
27. Treacher Collins, E., *Cases with symmetrical congenital notches in the outer part of each lid and defective development of the malar bones.* Trans Ophthalmol Soc UK, 1900. **20**: p. 190-192.
28. Group, T.C.S.C., *Positional cloning of a gene involved in the pathogenesis of treacher collins syndrome.* Nature Genetics, 1996. **12**: p. 130-36.
29. Wise, C.A., et al., *TCOF1 gene encodes a putative nucleolar phosphoprotein that exhibits mutations in Treacher Collins Syndrome throughout its coding region.* Proc Natl Acad Sci U S A, 1997. **94**(7): p. 3110-3115.
30. Marsh, K.L., J. Dixon, and M.J. Dixon, *Mutations in the Treacher Collins syndrome gene lead to mislocalization of the nucleolar protein treacle.* Hum Mol Genet, 1998. **7**(11): p. 1795-1800.
31. Dixon, J., et al., *Tcof1/Treacle is required for neural crest cell formation and proliferation deficiencies that cause craniofacial abnormalities.* Proc Natl Acad Sci U S A, 2006. **103**(36): p. 13403-8.
32. Sakai, D. and P.A. Trainor, *Treacher Collins syndrome: unmasking the role of Tcof1/treacle.* Int J Biochem Cell Biol, 2009. **41**(6): p. 1229-1232.
33. Jones, N.C., et al., *Prevention of the neurocristopathy Treacher Collins syndrome through inhibition of p53 function.* Nat Med, 2008. **14**(2): p. 125-33.
34. Dubourg, C., et al., *Holoprosencephaly.* Orphanet J Rare Dis, 2007. **2**: p. 8.
35. Muenke, M., *Holoprosencephaly as a genetic model for normal craniofacial development.* Semin Dev Biol, 1994. **5**: p. 293-301.
36. Cohen, M.M., Jr., *Holoprosencephaly: clinical, anatomic, and molecular dimensions.* Birth Defects Res A Clin Mol Teratol, 2006. **76**(9): p. 658-73.
37. Webster, W.S., et al., *The relationship between cleft lip, maxillary hypoplasia, hypoxia and phenytoin.* Curr Pharm Des, 2006. **12**(12): p. 1431-48.
38. Loucks, E.J., T. Schwend, and S.C. Ahlgren, *Molecular changes associated with teratogen-induced cyclopia.* Birth Defects Res A Clin Mol Teratol, 2007. **79**(9): p. 642-51.
39. Perez-Aytes, A., et al., *In utero exposure to mycophenolate mofetil: a characteristic phenotype?* Am J Med Genet A, 2008. **146A**(1): p. 1-7.
40. Yamada, S., *Embryonic holoprosencephaly: pathology and phenotypic variability.* Congenit Anom (Kyoto), 2006. **46**(4): p. 164-71.

41. Maity, T., N. Fuse, and P.A. Beachy, *Molecular mechanisms of Sonic hedgehog mutant effects in holoprosencephaly.* Proc Natl Acad Sci U S A, 2005. **102**(47): p. 17026-31.
42. Belloni, E., et al., *Identification of Sonic hedgehog as a candidate gene responsible for holoprosencephaly.* Nat Genet, 1996. **14**(3): p. 353-6.
43. Roessler, E., et al., *Mutations in the human Sonic Hedgehog gene cause holoprosencephaly.* Nat Genet, 1996. **14**(3): p. 357-60.
44. Chiang, C., et al., *Cyclopia and defective axial patterning in mice lacking Sonic hedgehog gene function.* Nature, 1996. **383**(6599): p. 407-13.
45. Abu-Issa, R., et al., *Fgf8 is required for pharyngeal arch and cardiovascular development in the mouse.* Development, 2002. **129**(19): p. 4613-4625.
46. Riley, B.M., et al., *Impaired FGF signaling contributes to cleft lip and palate.* Proc Natl Acad Sci U S A, 2007. **104**(11): p. 4512-7.
47. Siebert, J.R., *Cyclopia, aprosencephaly, and acardiac twinning: Is hypoxia-ischemia a unifying mechanism?* Am J Med Genet A, 2007. **143A**(24): p. 3100-6.
48. Grabowski, C.T. and J.A. Paar, *The teratogenic effects of graded doses of hypoxia on the chick embryo.* Am J Anat, 1958. **103**(3): p. 313-47.
49. Ancel, P., *[Research on the relations between the lethal effect and the teratogenic effect of oxygen deficiency in the chick embryo.].* Acta Anat (Basel), 1959. **38**: p. 147-59.
50. Nelsen, O.E., *Hypoxia and maldevelopment of early alarplate tissue in mid- and fore-brain regions of the chick embryo.* Growth, 1960. **24**: p. 361-83.
51. Grabowski, C.T., *A quantitative study of the lethal and teratogenic effects of hypoxia on the three-day chick embryo.* Am J Anat, 1961. **109**: p. 25-35.
52. Grabowski, C.T., *The Etiology of Hypoxia-Induced Malformations in the Chick Embryo.* J Exp Zool, 1964. **157**: p. 307-25.
53. Yamamoto, S. and Y. Noguchi, *Teratogenic action of hypoxia on the chick embryo. I. Malformations observed in six-day-old embryos.* Nippon Juigaku Zasshi, 1964. **26**(4): p. 181-90.
54. Grabowski, C.T. and R.E. Schroeder, *A time-lapse photographic study of chick embryos exposed to teratogenic doses of hypoxia.* J Embryol Exp Morphol, 1968. **19**(3): p. 347-62.
55. Noguchi, Y., *Teratogenic action of hypoxia on the chick embryo. II. Malformations observed in the eighteen-day-old embryo.* Nippon Juigaku Zasshi, 1969. **31**(3): p. 119-34.
56. Smith, A.H., R.R. Burton, and E.L. Besch, *Development of the chick embryo at high altitude.* Fed Proc, 1969. **28**(3): p. 1092-8.
57. Chan, T. and W. Burggren, *Hypoxic incubation creates differential morphological effects during specific developmental critical windows in the embryo of the chicken (Gallus gallus).* Respir Physiol Neurobiol, 2005. **145**(2-3): p. 251-263.
58. Golan, H. and M. Huleihel, *The effect of prenatal hypoxia on brain development: short- and long-term consequences demonstrated in rodent models.* Dev Sci, 2006. **9**(4): p. 338-349.
59. Ream, M., et al., *Early fetal hypoxia leads to growth restriction and myocardial thinning.* Am J Physiol Regul Integr Comp Physiol, 2008. **295**(2): p. R583-95.

60. Harris, A.L., *Hypoxia--a key regulatory factor in tumour growth.* Nat Rev Cancer, 2002. **2**(1): p. 38-47.
61. Ke, Q. and M. Costa, *Hypoxia-inducible factor-1 (HIF-1).* Mol Pharmacol, 2006. **70**(5): p. 1469-80.
62. Chavez, A., et al., *Mitochondria and hypoxia-induced gene expression mediated by hypoxia-inducible factors.* Ann N Y Acad Sci, 2008. **1147**: p. 312-20.
63. Iyer, N.V., et al., *Cellular and developmental control of O2 homeostasis by hypoxia-inducible factor 1 alpha.* Genes Dev, 1998. **12**(2): p. 149-62.
64. Ryan, H.E., J. Lo, and R.S. Johnson, *HIF-1 alpha is required for solid tumor formation and embryonic vascularization.* EMBO J, 1998. **17**(11): p. 3005-15.
65. Malhotra, R., et al., *Hypoxia-inducible factor-1alpha is a critical mediator of hypoxia induced apoptosis in cardiac H9c2 and kidney epithelial HK-2 cells.* BMC Cardiovasc Disord, 2008. **8**: p. 9.
66. Bruick, R.K., *Expression of the gene encoding the proapoptotic Nip3 protein is induced by hypoxia.* Proc Natl Acad Sci U S A, 2000. **97**(16): p. 9082-7.
67. Shoshani, T., et al., *Identification of a novel hypoxia-inducible factor 1-responsive gene, RTP801, involved in apoptosis.* Mol Cell Biol, 2002. **22**(7): p. 2283-93.
68. Ginouves, A., et al., *PHDs overactivation during chronic hypoxia "desensitizes" HIFalpha and protects cells from necrosis.* Proc Natl Acad Sci U S A, 2008. **105**(12): p. 4745-50.
69. Klimova, T. and N.S. Chandel, *Mitochondrial complex III regulates hypoxic activation of HIF.* Cell Death Differ, 2008. **15**(4): p. 660-6.
70. Chandel, N.S., et al., *Mitochondrial reactive oxygen species trigger hypoxia-induced transcription.* Proc Natl Acad Sci U S A, 1998. **95**(20): p. 11715-20.
71. Chandel, N.S., et al., *Reactive oxygen species generated at mitochondrial complex III stabilize hypoxia-inducible factor-1alpha during hypoxia: a mechanism of O2 sensing.* J Biol Chem, 2000. **275**(33): p. 25130-8.
72. Brunelle, J.K., et al., *Oxygen sensing requires mitochondrial ROS but not oxidative phosphorylation.* Cell Metab, 2005. **1**(6): p. 409-14.
73. Guzy, R.D., et al., *Mitochondrial complex III is required for hypoxia-induced ROS production and cellular oxygen sensing.* Cell Metab, 2005. **1**(6): p. 401-8.
74. Mansfield, K.D., et al., *Mitochondrial dysfunction resulting from loss of cytochrome c impairs cellular oxygen sensing and hypoxic HIF-alpha activation.* Cell Metab, 2005. **1**(6): p. 393-9.
75. Rana, M., et al., *An out-of-frame cytochrome b gene deletion from a patient with parkinsonism is associated with impaired complex III assembly and an increase in free radical production.* Ann Neurol, 2000. **48**(5): p. 774-81.
76. Bell, E.L., et al., *The Qo site of the mitochondrial complex III is required for the transduction of hypoxic signaling via reactive oxygen species production.* J Cell Biol, 2007. **177**(6): p. 1029-36.
77. Choi, S.L., et al., *The regulation of AMP-activated protein kinase by H(2)O(2).* Biochem Biophys Res Commun, 2001. **287**(1): p. 92-7.
78. Hardie, D.G., et al., *Management of cellular energy by the AMP-activated protein kinase system.* FEBS Lett, 2003. **546**(1): p. 113-20.

79. Carling, D., *The AMP-activated protein kinase cascade--a unifying system for energy control.* Trends Biochem Sci, 2004. **29**(1): p. 18-24.
80. Mungai, P.T., et al., *Hypoxia triggers AMPK activation through reactive oxygen species-mediated activation of calcium release-activated calcium channels.* Mol Cell Biol, 2011. **31**(17): p. 3531-45.
81. Emerling, B.M., et al., *Hypoxic activation of AMPK is dependent on mitochondrial ROS but independent of an increase in AMP/ATP ratio.* Free Radic Biol Med, 2009. **46**(10): p. 1386-91.
82. Jones, R.G., et al., *AMP-activated protein kinase induces a p53-dependent metabolic checkpoint.* Mol Cell, 2005. **18**(3): p. 283-93.
83. Concannon, C.G., et al., *AMP kinase-mediated activation of the BH3-only protein Bim couples energy depletion to stress-induced apoptosis.* J Cell Biol, 2010. **189**(1): p. 83-94.
84. Kilbride, S.M., et al., *AMP-activated protein kinase mediates apoptosis in response to bioenergetic stress through activation of the pro-apoptotic Bcl-2 homology domain-3-only protein BMF.* J Biol Chem, 2010. **285**(46): p. 36199-206.
85. Ryu, G.R., et al., *Activation of AMP-activated protein kinase mediates acute and severe hypoxic injury to pancreatic beta cells.* Biochem Biophys Res Commun, 2009. **386**(2): p. 356-62.
86. Gopalani, N.K., et al., *Cooperativity between inhibition of cytosolic K+ efflux and AMPK activation during suppression of hypoxia-induced cellular apoptosis.* Int J Biochem Cell Biol, 2012. **44**(1): p. 211-23.
87. Nagata, D., et al., *A new constitutively active mutant of AMP-activated protein kinase inhibits anoxia-induced apoptosis of vascular endothelial cell.* Hypertens Res, 2009. **32**(2): p. 133-9.
88. Liu, C., et al., *Activation of AMP-activated protein kinase alpha1 alleviates endothelial cell apoptosis by increasing the expression of anti-apoptotic proteins Bcl-2 and survivin.* J Biol Chem, 2010. **285**(20): p. 15346-55.
89. Bijlsma, M.F., et al., *Hypoxia induces a hedgehog response mediated by HIF-1alpha.* J Cell Mol Med, 2009. **13**(8B): p. 2053-60.
90. Chong, H.J., et al., *Signaling by SHH rescues facial defects following blockade in the brain.* Dev Dyn, 2012. **241**(2): p. 247-56.
91. Klingenberg, C.P., *MorphoJ: an integrated software package for geometric morphometrics.* Mol Ecol Resour, 2011. **11**(2): p. 353-7.
92. Bancroft, J.D. and M. Gamble, *Theory and Practice of Histological Techniques*. 5th edition ed. 2002: Churchill Livingstone. 796.
93. Murray, B.M. and D.J. Wilson, *A scanning electron microscopic study of the normal development of the chick wing from stages 19 to 36. A supplement to the Hamburger and Hamilton staging system.* Anat Embryol (Berl), 1994. **189**(2): p. 147-55.
94. Kristensen, E., et al., *A novel 3-D image-based morphological method for phenotypic analysis.* IEEE Trans Biomed Eng, 2008. **55**(12): p. 2826-31.
95. Gonzalez, P.N., B. Hallgrimsson, and E.E. Oyhenart, *Developmental plasticity in covariance structure of the skull: effects of prenatal stress.* J Anat, 2011. **218**(2): p. 243-57.

96. Jamniczky, H.A. and B. Hallgrimsson, *Modularity in the skull and cranial vasculature of laboratory mice: implications for the evolution of complex phenotypes.* Evol Dev, 2011. **13**(1): p. 28-37.
97. Willmore, K.E., L. Leamy, and B. Hallgrimsson, *Effects of developmental and functional interactions on mouse cranial variability through late ontogeny.* Evol Dev, 2006. **8**(6): p. 550-67.
98. Young, N.M., et al., *Comparative morphometrics of embryonic facial morphogenesis: implications for cleft-lip etiology.* Anat Rec (Hoboken), 2007. **290**(1): p. 123-39.
99. Boughner, J.C., et al., *Short-faced mice and developmental interactions between the brain and the face.* J Anat, 2008. **213**(6): p. 646-62.
100. Young, N.M., et al., *Quantitative analyses link modulation of sonic hedgehog signaling to continuous variation in facial growth and shape.* Development, 2010 **137**(20): p. 3405-3409.
101. Badawi-Fayad, J. and E.A. Cabanis, *Three-dimensional Procrustes analysis of modern human craniofacial form.* Anat Rec (Hoboken), 2007. **290**(3): p. 268-76.
102. Haworth, K., et al., *Expression of the Scube3 epidermal growth factor-related gene during early embryonic development in the mouse.* Gene Expr Patterns, 2007. **7**(5): p. 630-4.

Publishing Agreement

It is the policy of the University to encourage the distribution of all theses, dissertations, and manuscripts. Copies of all UCSF theses, dissertations, and manuscripts will be routed to the library via the Graduate Division. The library will make all theses, dissertations, and manuscripts accessible to the public and will preserve these to the best of their abilities, in perpetuity.

Please sign the following statement:

I hereby grant permission to the Graduate Division of the University of California, San Francisco to release copies of my thesis, dissertation, or manuscript to the Campus Library to provide access and preservation, in whole or in part, in perpetuity.

Francis Joel Smith
Author Signature

8/23/12
Date